Université du Québec
à Rimouski

Etude des effets des paramètres de fabrication additive et de post-traitement thermique sur la microstructure et les performances mécaniques des aciers inoxydables

Investigation, modélisation et optimisation des performances des aciers inoxydables en fonction des paramètres du procédé de fusion sélective par laser et des paramètres de post-traitement thermique

Mémoire présenté

dans le cadre du programme de maîtrise en ingénierie

en vue de l'obtention du grade de maître ès sciences appliquées (M.Sc.A.)

PAR

© ASMA MANSOURA

Décembre 2022

Composition du jury :

Véronique Dassylva-Raymond, présidente du jury, Université du Québec à Rimouski

Noureddine Barka, directeur de recherche, Université du Québec à Rimouski

Sofiène Amira, examinateur externe, Centre québecois de recherche et de développement d'aluminium

Dépôt initial le 17 Octobre 2022 Dépôt final le 15 Décembre 2022

UNIVERSITÉ DU QUÉBEC À RIMOUSKI
Service de la bibliothèque

Avertissement

La diffusion de ce mémoire ou de cette thèse se fait dans le respect des droits de son auteur, qui a signé le formulaire « *Autorisation de reproduire et de diffuser un rapport, un mémoire ou une thèse* ». En signant ce formulaire, l'auteur concède à l'Université du Québec à Rimouski une licence non exclusive d'utilisation et de publication de la totalité ou d'une partie importante de son travail de recherche pour des fins pédagogiques et non commerciales. Plus précisément, l'auteur autorise l'Université du Québec à Rimouski à reproduire, diffuser, prêter, distribuer ou vendre des copies de son travail de recherche à des fins non commerciales sur quelque support que ce soit, y compris Internet. Cette licence et cette autorisation n'entraînent pas une renonciation de la part de l'auteur à ses droits moraux ni à ses droits de propriété intellectuelle. Sauf entente contraire, l'auteur conserve la liberté de diffuser et de commercialiser ou non ce travail dont il possède un exemplaire.

A ma fille Lina

REMERCIEMENTS

Ce présent mémoire est le fruit de nombreuses heures de travail et de recherche qui a duré plus que deux années. Une période riche en apprentissage, échanges d'informations, longues recherches et dont la finalité n'aurait pas été possible sans la participation de nombreuses personnes. Je souhaite ainsi adresser mes remerciements à toutes ces personnes pour tout ce qu'ils m'ont apporté dans la réalisation de mes travaux, et dans l'aboutissement de ce modeste mémoire de recherche.

En premier lieu, je remercie M. **Noureddine Barka**, professeur en génie mécanique à l'Université du Québec à Rimouski, pour ses encouragements et son accompagnement en tant que directeur de recherche. Sa disponibilité ainsi que ses judicieux conseils m'ont énormément aidé dans l'avancement et l'orientation de mes travaux de recherche. Une reconnaissance particulière pour son énergie, sa passion à la recherche et sa quête insatiable de l'innovation qui m'ont fourni une source de motivation pour surmonter les difficultés et atteindre mes objectifs.

Je tiens ensuite à remercier M. **Sasan Sattarpanah Karganroudi**, professeur à l'Université du Québec à Trois-Rivières, pour l'aide qu'il a fournie et les connaissances qu'il a sues me transmettre. Son expérience et sa vision de la recherche ont contribué à alimenter ma réflexion.

Mes sincères gratitudes vont également vers mes anciens et nouveaux collègues du Laboratoire de matériaux, produits et procédés de pointe, spécialement M. Herinandrianina Ramiarison, Mme Narges Omidi et M. Asim Iltaf pour leur aide à mener les travaux expérimentaux.

En dernier lieu, j'adresse ma reconnaissance particulière à mon conjoint et à mes parents. Leur amour, leurs efforts, leur soutien et leurs encouragements m'ont beaucoup

motivé lors de la réalisation de ce travail de recherche. Leur présence au cours de mon parcours était très précieuse ; j’avoue que, sans eux, je n'en serais pas là aujourd'hui.

Enfin, je voudrais exprimer ma profonde gratitude à toutes les autres personnes qui, même sans être citées personnellement, par leurs conseils et leurs diverses compétences, ont tout autant contribué à la réalisation de ce mémoire.

RÉSUMÉ

Les aciers inoxydables sont parmi les alliages les plus appréciés pour la fabrication additive vu leurs propriétés attrayantes et leur large gamme d'applications. En raison de l'histoire thermique compliquée et de taux de refroidissement élevé, la fusion sélective au laser (SLM) a introduit une microstructure hors équilibre, qui contrôle le comportement mécanique. De plus, un choix inapproprié des paramètres de fabrication conduit à la formation de défauts et affecte la qualité de la pièce finale. Cette étude vise à fournir une compréhension approfondie de la corrélation entre le processus, la microstructure et les propriétés de l'acier inoxydable fabriqué par SLM afin de mieux contrôler et optimiser ces propriétés. La première partie de ce mémoire présente une revue de littérature de la microstructure, du comportement mécanique, de la résistance à la fatigue, ainsi que de la résistance à la corrosion des aciers inoxydables fabriqués par SLM. Cette revue met en évidence la capacité du procédé SLM à produire des composants en acier inoxydable de haute performance et souligne les perspectives et les limites dans ce domaine. Le but de la deuxième partie est d'élucider l'influence des paramètres de procédé sur la densité, la rugosité de surface et les propriétés mécaniques de l'acier inoxydable 316L fabriqué par SLM. Une méthodologie systématique basée sur la méthode de Taguchi, l'analyse de variance et la méthode de surface de réponse a été utilisée pour déterminer les facteurs significatifs et développer des modèles prédictifs pour les variables de réponse en fonction de ces facteurs. La troisième partie utilise une approche similaire pour étudier l'influence des paramètres de post-traitement thermique sur la microstructure et la microdureté des aciers inoxydables 15-5 PH. Les résultats de ce projet de recherche peuvent être utilisés comme outils de conception pour prédire et optimiser avec précision les performances des aciers inoxydables fabriqués par SLM.

Mots clés : Fabrication additive, Fusion sélective au laser, Acier inoxydable, Taguchi, ANOVA

ABSTRACT

Stainless steels are among the most popular alloys for additive manufacturing owing to their attractive properties and their wide range of applications. Because of the complicated thermal history and high cooling rate, Selective Laser Melting (SLM) introduced a unique out-of-equilibrium microstructure, which controls the mechanical behavior. Moreover, inappropriate choice of processing parameters leads to defect formation and affects final part quality. This study aims to provide a deep understanding of the correlation between process, microstructure, and properties of SLM processed stainless steel in order to better control and optimize these properties. The first part of this thesis presents a review of the microstructure, mechanical and fatigue behavior, as well as corrosion resistance of stainless steels manufactured using SLM. This review highlights the capability of the SLM process to produce high-performance stainless steel components and sheds light on the perspectives and limitations in this field. The purpose of the second part is to elucidate the influence of process parameters on density, surface roughness, and mechanical properties of SLM-processed 316L stainless steel. A systematic methodology based on Taguchi design, Analysis of Variance, and Response Surface Method has been employed to determine the significant factors and develop predictive models for response variables with respect to these factors. The third part uses a similar approach to investigate the influence of post-heat treatment parameters on the microstructure and microhardness of 15-5 PH stainless steels. The findings of this research can be used as design tools to accurately predict and optimize the performance of SLM-processed stainless steels.

Keywords: Additive Manufacturing, Selective Laser Melting, Stainless steel, Taguchi, ANOVA

TABLE DES MATIÈRES

LISTE DES TABLEAUX

LISTE DES FIGURES

LISTE DES ABRÉVIATIONS, DES SIGLES ET DES ACRONYMES

AM	Fabrication additive
ANOVA	Analyse de la variance
ASTM	American Society for Testing and Materials
ASS	Acier inoxydable austénitique
BIJ	Projection de liant
BCC	Structure cubique centrée
CAD	Conception assistée par ordinateur
DED	Dépôt de matières sous flux d'énergie dirigé
DMLS	Frittage direct de métal au laser
EBM	Fusion par faisceau d'électrons
EBSD	Diffraction d'électrons rétrodiffusés
EDS	Spectroscopie à rayons X à dispersion d'énergie
FCC	Structure cubique à faces centrées
HCF	Fatigue mégacyclique
HIP	Pressage isostatique à chaud
L-PBF	Fusion au laser sur lit de poudre
OM	Microscope optique

RSM	Méthode des surfaces de réponses
SEM	Microscope électronique à balayage
PH	Durcissement par précipitation
SS	Acier inoxydable
SLM	Fusion sélective au laser
XRD	Diffraction des rayons X

LISTE DES SYMBOLES

E (J/mm^3)	Densité d'énergie
El. (%)	Allongement à la rupture
H (mm)	Espacement des hachures
H	Dureté
HRC	Dureté Rockwell
HV	Dureté Vickers
Hz	Hertz
P (W)	Puissance laser
R^2	Coefficient de détermination
Ra (µm)	Rugosité
RD (%)	Densité relative
t (µm)	Épaisseur de couche de poudre
UTS (MPa)	Résistance à la rupture
V(mm/s)	Vitesse de balayage
wt. %	Pourcentage de masse
YS (MPa)	Limite élastique

INTRODUCTION GÉNÉRALE

1. CONTEXTE GENERAL

La fabrication additive, également connue sous le nom d'impression 3D, est une technologie émergente, qui a attiré l'attention pour sa capacité unique à produire des composants presque finis, géométriquement complexes, sans qu'un outillage spécifique à la pièce ne soit nécessaire. La fabrication additive est particulièrement adaptée à la production de petite série, la réduction de poids, la personnalisation des pièces et l'intégration fonctionnelle [1, 2]. De plus, cette technique a rendu possible la simplification de l'assemblage des composants, en fusionnant différentes pièces en un seul bloc [3].

En raison du degré de développement acquis dans plusieurs domaines connexes, les procédés de fabrication additive, qui existent depuis près de 30 ans, ne sont plus aujourd'hui réservés au prototypage rapide. Ces technologies ont déjà été largement adoptées dans différentes industries telles que l'industrie aérospatiale [4], biomédicale [5, 6], automobile [7] etc., pour leur capacité à produire des composants de haute performance avec des géométries complexes qui sont impossibles à fabriquer par les méthodes conventionnelles. Plusieurs procédés de fabrication additive sont disponibles pour la fabrication des métaux, tels que la projection de liant, la fusion sur lit de poudre, l'extrusion de matière, la stratification de couches, le dépôt de matières sous flux d'énergie dirigé, etc.

La fusion sélective au laser (SLM) est l'un des procédés de fabrication additive les plus utilisés vu son aptitude à construire des objets avec une haute résolution et une grande précision dimensionnelle et géométrique [8]. Comme son nom l'indique, ce processus de fusion sur lit de poudre utilise un faisceau laser pour fondre et fusionner une poudre métallique couche par couche pour créer une pièce tridimensionnelle, ce qui offre

l’opportunité d’adapter la microstructure et les propriétés mécaniques de la pièce selon le besoin. Jusqu'à présent, plusieurs études ont été menées pour évaluer la faisabilité de la fusion sélective laser pour une variété de matériaux. Yap et al. [9] ont examiné l’état de l’art des différents matériaux utilisés dans le processus SLM ainsi que leurs applications. Ils ont signalé que l’imprimabilité de la plupart des matériaux d'ingénierie tels que l'aluminium, les aciers, les superalliages à base de cobalt et de nickel et les alliages de titane a été étudiée et validée.

Les aciers inoxydables sont aujourd'hui utilisés dans presque toutes les industries imaginables en raison de leur combinaison particulière de propriétés, à savoir leur excellente résistance à la corrosion, leur large gamme de niveaux de résistance et de ténacité, leur résistance à la chaleur, et leur biocompatibilité. Les aciers inoxydables austénitiques et ferritiques sont utilisés dans des environnements extrêmement corrosifs tels que les industries chimiques, pétrochimiques, marines et médicales, tandis que les aciers inoxydables martensitiques et les aciers à durcissement par précipitation sont utilisés dans l’industrie aérospatiale, de la défense et de l'outillage où une haute résistance mécanique et une dureté élevée sont nécessaires.

Actuellement, la fusion sélective laser est déjà utilisée pour la production des aciers inoxydables. Cependant, elle fait face encore à des défis majeurs qui limitent sa large adoption en industrie. En effet, la présence de défauts internes tels que la porosité, le manque de fusion, les fissures, en plus des contraintes résiduelles et de la microstructure hétérogène résultant de la charge thermique répétitive et du taux de refroidissement rapide du procédé empêchent l'obtention des propriétés mécaniques souhaitées [10]. Vu les phénomènes physiques complexes et le grand nombre de paramètres interagissant lors de la fusion et la solidification du lit de poudre, il est essentiel qu'une compréhension globale du processus soit développée pour optimiser les performances des pièces fabriquées par SLM.

De nombreuses études ont été consacrées à comprendre l'effet des paramètres du procédé afin de développer des conditions de traitement permettant d'obtenir des pièces sans défauts avec de bonnes propriétés mécaniques. Yadroitsev et al. [11] ont étudié les effets des

paramètres de procédé tels que la puissance du laser, la vitesse de balayage et l'épaisseur de la couche de poudre sur la formation de pistes uniques. Ils ont montré qu'en choisissant une fenêtre technologique optimale et une stratégie de balayage appropriée, il est possible de fabriquer des pièces très complexes avec des propriétés mécaniques comparables à celles du matériau corroyé. Gu et al. [12] ont étudié l'effet de la densité d'énergie (en faisant varier la puissance du laser et la vitesse de balayage) sur la porosité et la microstructure des pièces en acier 17-4 PH fabriqués par SLM. Cette étude a rapporté que même à une densité d'énergie constante avec des puissances laser et des vitesses de balayage différentes, il y avait une variation significative des pourcentages de porosité. Zhao et al. [13] ont évalué l'effet des paramètres de processus sur les phases présentes, la densité et la dureté de l'acier inoxydable 420 et ont affirmé que les pièces fabriquées répondent aux exigences de l'application de moules à injection avec une densité relative de 99 % et une dureté de 50,7 HRC, malgré la présence de l'austénite résiduelle. Ghayoor et al. [14] ont examiné le rôle de la densité d'énergie volumétrique sur l'évolution microstructurale, la texture et les propriétés mécaniques des pièces en acier inoxydable 304L fabriquées par fusion sélective au laser. La densité relative et la dureté du matériau ont été négativement affectées en diminuant la densité d'énergie. Sun et al. [15] ont démontré qu'une puissance laser plus élevée de 950 W et une stratégie de multi-balayage peuvent être utilisées pour contrôler la structure cristallographique et la taille des grains afin d'augmenter à la fois la résistance mécanique et la ductilité.

Cependant, il demeure difficile de sélectionner les paramètres optimaux qui permettent de fabriquer des pièces avec les propriétés requises en l'absence d'une modélisation concrète de la relation entre ces deux derniers. De plus, même avec des paramètres optimisés, les caractéristiques mécaniques des pièces imprimées telles que construites restent parfois insatisfaisantes. Ainsi, certaines techniques de post-traitement, telles que le traitement thermique et le pressage isostatique à chaud, ont été étudiées pour homogénéiser la microstructure et améliorer les performances mécaniques. Snehashis et al. [16] ont comparé les propriétés mécaniques de traction des pièces en acier inoxydable 15-5 PH fabriquées par SLM avec et sans traitement thermique. Ils ont trouvé que le post-traitement améliore la

résistance à la traction et la ductilité à la fois. Tascioglu et al. [17] ont étudié l'effet de la variation de la température de traitement thermique sur la microstructure, la microdureté et la résistance à l'usure de l'acier inoxydable 316L fabriqué par SLM. Selon cette étude, l'augmentation de la température du traitement thermique a entraîné une diminution à la fois de la porosité et de la dureté tandis que la microstructure est devenue plus homogénéisée. Yadollahi et al. [18] ont signalé que l'orientation de fabrication et les traitements thermiques ont une influence sur les phases microstructurales de pièces fabriquées en acier inoxydable 17-4 PH, ce qui engendre différentes propriétés mécaniques. Sarkar et al. [19] ont étudié l'effet du traitement thermique sur les propriétés mécaniques et de corrosion du 15-5PH produit par SLM. Les résultats expérimentaux ont montré que différents traitements de vieillissement affectent la taille et la forme des précipités riches en Cu et la quantité d'austénite résiduelle, entraînant des différentes résistances mécaniques et résistances à la corrosion.

2. PROBLEMATIQUE

La recension de la littérature au sujet de la fusion sélective laser des aciers inoxydables permet de constater que ce procédéoffre des opportunités prometteuses pour adapter la microstructure de l'acier inoxydable selon son application et produire des pièces de hautes performances avec des géométries complexes [20, 21]. Cependant, les phénomènes physiques complexes et les cycles thermiques subis par le matériau en solidification constituent des défis majeurs. Une meilleure compréhension des relations entre le processus, la microstructure et les propriétés sera importante pour éviter les défauts courants et assurer la reproductibilité. La connaissance de l'état de l'art des aciers inoxydables fabriqués par SLM est nécessaire pour l'avancement et l'élargissement de l'utilisation de cette famille d'alliages dans le procédé SLM.

Malgré les nombreuses investigations sur l'influence des paramètres du procédé sur la microstructure et les performances des pièces fabriquées par SLM, la plupart d'entre elles se concentrent sur l'influence de la densité d'énergie sur la qualité des pièces. Cependant, le

SLM est un processus multifactoriel complexe, qui est régi par plusieurs paramètres. Cette densité d'énergie quoiqu'elle combine dans sa formule les paramètres les plus importants, n'est pas toujours indicative. De plus, les simples corrélations tirées des résultats expérimentaux sans analyse systématique ne seraient pas efficaces pour l'optimisation du procédé. D'un autre côté, l'analyse et l'optimisation de tous les facteurs en menant des expériences conventionnelles peuvent être exhaustives et peu pratique en raison du grand nombre d'expériences requises [22]. Ceci souligne le besoin d'adopter des techniques de conception d'expériences (DOE) telles que la méthode Taguchi et des approches d'analyse statistique telle que l'analyse de variance (ANOVA) et la méthode de surface de réponse (RSM) qui sont connues pour être des moyens puissants pour déterminer la relation entre les paramètres de procédé et les performances caractéristiques à travers un nombre réduit d'expériences [23]. Cette approche a été très peu utilisée pour optimiser la fabrication des aciers inoxydables via fusion sélective au laser [24, 25]. La revue de littérature révèle l'absence de modèles de prédiction explicites et efficaces des propriétés mécaniques et physiques des aciers inoxydables fabriqués par SLM en fonction des paramètres du procédé et de leurs interactions.

D'autre part, la fabrication de certaines classes d'aciers inoxydables tels que les aciers duplex et les aciers martensitiques durcis par précipitation par SLM a engendré des changements majeurs sur leur microstructure et leurs compositions de phases, ce qui affecte leurs propriétés mécaniques. De l'austénite résiduelle a été observée dans les aciers martensitiques à durcissement structural avec des fractions différentes [26, 27]. LeBrun et al. [28] ont étudié l'effet de l'austénite résiduelle sur les propriétés mécaniques de l'acier inoxydable 17-4 PH produit par SLM. Ils ont constaté que la résistance à la traction et la dureté diminuent avec l'augmentation de la fraction volumique de l'austénite résiduelle, tandis que la ductilité est améliorée. Cependant, ces aciers sont souvent utilisés pour leur haute résistance mécanique. L'optimisation des paramètres du procédé SLM, dans ce cas, s'avère incapable de contrôler efficacement la microstructure et l'équilibre de phases régies par la solidification rapide et les cycles thermiques répétitifs au cours de l'impression.

De nombreuses études existantes ont démontré l'importance du traitement thermique pour réduire ou éliminer l'austénite résiduelle présente dans les aciers martensitiques à durcissement par précipitation fabriqué par SLM comme l'acier 15-5 PH ou 17-4P H. Pour ce type d'acier, un traitement de vieillissement est nécessaire pour engendrer la précipitation du cuivre afin de durcir le matériau. Le processus standard comporte trois étapes ; un traitement de mise en solution à une température élevée (entre 930 et 1070°C) pour 30 minutes, un refroidissement rapide et un durcissement par vieillissement à des températures situées entre 480 °C et 620 °C pour une à quartes heures [29]. Li et al. [30] ont étudié l'effet de l'augmentation de temps de traitement de mise en solution sur l'évolution de la microstructure et les propriétés mécaniques de l'inox 17-4 PH produit par SLM. Ils ont trouvé qu'un traitement de mise en solution de 1 heure offre la meilleure combinaison de résistance mécanique et de ductilité. La revue de littérature dans ce sujet prouve que le traitement thermique de cette nuance d'acier combine plusieurs défis et offre ainsi un terreau fertile pour le progrès technique et scientifique en raison des caractéristiques microstructurales uniques résultantes du procédé SLM. Les comportements de recristallisation et de précipitation non usuelles que présentent les aciers inox à durcissement structural fabriqués par SLM nécessitent des traitements thermiques plus adaptés. L'optimisation des paramètres de traitements thermiques, telle que le taux de refroidissement après mise en solution, la durée de vieillissement, et la température de vieillissement par approche statistique pour obtenir des propriétés mécaniques personnalisées et orientées vers l'application des aciers inox à précipitation fabriquées par SLM n'a pas encore été explorée.

3. OBJECTIFS

L'objectif de ce mémoire est d'offrir une meilleure compréhension et un contrôle des propriétés mécaniques et physiques des aciers inoxydables fabriqués par fusion sélective au laser avec et sans post-traitement thermique en fonction des différents paramètres intervenants afin de pouvoir les prédire et les optimiser. Pour atteindre ces objectifs, il est nécessaire de passer par des sous-objectifs qui correspondent à des étapes spécifiques du projet de recherche.

Le premier objectif est de mener une revue de littérature approfondie qui a pour but de comprendre le procédé de fusion sélective au laser et son application aux différentes nuances d'aciers inoxydables. Cette revue offre un aperçu complet de l'évolution de la microstructure des aciers inoxydables fabriqués par SLM avec et sans post-traitement, ainsi que les performances mécaniques, la résistance à la fatigue et la résistance à la corrosion qui en résulte. De plus, la recension de la littérature permet de mettre l'accent sur les lacunes à combler dans ce sujet, afin de mieux diriger les travaux futurs.

Le deuxième objectif est l'étude des effets des paramètres de fusion sélective au laser, à savoir la puissance du laser, la vitesse de balayage et l'espacement des hachures, sur la densité, la rugosité, la dureté et les propriétés mécaniques de traction de l'acier austénitique 316L. L'approche systématique basée sur des outils de planification d'expériences et d'analyses statistiques permet d'établir des modèles de prédiction de ces performances en fonction des paramètres d'entrée afin d'identifier la combinaison optimale qui peut fournir les propriétés requises selon l'application visée de l'acier.

Le troisième objectif vise à étudier l'influence des paramètres de traitement de durcissement par précipitation, notamment le taux de refroidissement, la durée du vieillissement et la température du vieillissement, sur la microstructure et la microdureté de l'acier inoxydable 15-5PH fabriqué par fusion sélective au laser. Les résultats présentés peuvent être utilisés pour sélectionner un post-traitement thermique approprié pour obtenir une dureté maximale de l'acier martensitique 15-5 PH.

4. METHODOLOGIE

La première phase de ce travail consiste à étudier l'état de l'art dans le domaine de la fusion sélective au laser des aciers inoxydables. Dans un premier temps, le procédé ainsi que ces principaux paramètres et les problèmes de fabrication les plus connus sont expliqués. Une recherche bibliographique exhaustive est menée pour chaque classe d'acier selon leur composition de phase (austénitique, martensitique, ferritique et duplex). Les résultats pertinents sur la microstructure, les propriétés mécaniques, la fatigue et la résistance à la

corrosion avec et sans traitement sont synthétisés et analysés. Enfin, les défis et les lacunes de la recherche scientifique dans ce domaine sont identifiés afin de mieux orienter les futures recherches.

La deuxième phase vise à déterminer les effets des paramètres du procédé de fusion sélective au laser sur les performances de l'acier inox 316L. Pour atteindre cet objectif, trois paramètres parmi les paramètres les plus importants étudiés dans la littérature, ainsi que leurs plages de variations, sont choisis, à savoir la puissance du laser, la vitesse de balayage et l'espacement des hachures (écart entre deux vecteurs successifs balayés au laser). L'impression des pièces est faite selon un plan d'expérience Taguchi avec trois paramètres à trois niveaux, soit neuf combinaisons au total. La microstructure et la porosité sont examinées sur des échantillons polis par microscopie optique. Les mesures de rugosités et de microdureté et les tests de tractions sont menés dans les laboratoires du département de mathématiques, informatique et génie à l'UQAR. Les résultats expérimentaux sont ensuite analysés avec le logiciel MINTAB afin d'établir l'analyse de variance ANOVA, les équations de régressions et les surfaces de réponse (RSM). Cette analyse permet de déterminer l'ordre d'importance des paramètres et leurs interactions sur les réponses mesurées et développer des modèles de prédictions empiriques pour chaque propriété en fonction des facteurs d'entrées. Enfin, les paramètres optimaux sont localisés à partir des tracés de contours de la méthode RSM.

La dernière phase de ce projet est orientéé vers l'optimisation du traitement de durcissement par vieillissement de l'acier inoxydable 15-5 PH fabriqué par SLM. La méthode de Taguchi est utilisée pour définir le plan expérimental. Les facteurs pris en compte sont : la solution de trempe, la température de vieillissement et le temps de vieillissement. Avec trois niveaux pour chaque facteur, neuf combinaisons sont examinées, et comparées à l'échantillon à l'état non vieilli. Des mesures de microdureté sont menées. L'évolution microstructurale est analysée à l'aide de la microscopie optique et de la microscopie électronique à balayage pour mettre en évidence la précipitation du cuivre et comprendre la corrélation entre la microstructure et la dureté. ANOVA est utilisée pour évaluer l'effet de

chaque facteur de traitement thermique sur la microdureté. La combinaison optimale des paramètres de durcissement par vieillissement est sélectionnée sur la base de la méthode de surface de réponse. Un modèle de régression qui prédit la dureté en fonction de la température et la durée de vieillissement est ajusté aux données expérimentales. Des tests de tractions sont effectués sur des échantillons vieillis selon la combinaison optimale pour valider les résultats obtenus.

5. ORGANISATION DU MEMOIRE

Ce mémoire de recherche est divisé en trois chapitres qui traitent les objectifs susmentionnés. Le premier chapitre se présente sous la forme d'un article de revue de littérature dédié à la compréhension approfondie du procédé de fusion sélective au laser et son application aux aciers inoxydables. Dans un premier temps, une description du procédé et de ces principaux paramètres ainsi que les défauts de fabrication les plus intrigants est présentée. Ensuite, les résultats pertinents des travaux de recherches existants sur les caractéristiques microstructurales et mécaniques ainsi que la résistance à la fatigue et à la corrosion des nuances d'aciers inoxydables les plus utilisés en fusion sélective au laser sont synthétisés.

Le deuxième chapitre traite l'étude des effets de paramètres de procédé de fusion sélective au laser sur les performances de l'acier inoxydable 316L. Cette étude porte sur la prédiction et l'optimisation de la densité, la rugosité, la microdureté et les propriétés mécaniques de traction en fonction des paramètres du procédé.

Le dernier chapitre aborde l'étude de l'influence des paramètres de traitement thermique de vieillissement par durcissement sur la microstructure et la microdureté de l'acier inoxydable 15-5 PH. Une analyse microstructurale accompagnée d'une analyse statistique des mesures de microdureté met en évidence l'effet de la variation de la température et de la durée de vieillissement sur les caractéristiques microstructurales et par la suite sur la dureté de cette nuance d'acier.

CHAPITRE 1
FUSION SELECTIVE AU LASER DES ACIERS INOXYDABLES : UNE REVUE DU PROCESSUS, DE LA MICROSTRUCTURE ET DES PROPRIETES

A. Mansoura[1], N. Omidi[1], N. Barka[1], S.S. Kangranroudi[2]

[1] Université du Québec à Rimouski, Québec, Canada

[2] Université du Québec à Trois-Rivières, Québec, Canada

1.1 RESUME EN FRANÇAIS DU PREMIER ARTICLE

La fabrication additive métallique est une méthode révolutionnaire pour la production de pièces industrielles. La fusion sélective au laser (SLM) est l'une des technologies de fabrication additive les plus couramment utilisées pour fabriquer des composants métalliques de hautes performances. Les aciers inoxydables font partie des alliages les plus appréciés pour la fabrication additive en raison de leur disponibilité sous forme de poudre, de leur faible coût, de leurs propriétés mécaniques, ainsi que de leur résistance à la corrosion. Vu les cycles de chauffage et de refroidissement répétitifs et rapides, le procédé SLM engendre une microstructure particulière, hors d'équilibre, qui à son tour contrôle les propriétés mécaniques. Comprendre l'interrelation entre le procédé, la microstructure et les propriétés qui en résultent est essentiel pour faire progresser et étendre l'utilisation des composants en acier inoxydable fabriqués par SLM. Cet article de revue de littérature éclaire les principes du processus de fusion sélective au laser, les paramètres clés et les défauts couramment rencontrés. Une discussion détaillée de la microstructure, du comportement mécanique (c.-à-d. dureté, propriétés de traction et de fatigue) et de la résistance à la corrosion des aciers inoxydables produits par SLM est également présentée. Cela comprend les nuances d'aciers inoxydables austénitiques, martensitiques, à durcissement structural, duplex et ferritiques. L'effet de divers post-traitements est brièvement synthétisé. Cette revue met en évidence la

capacité du procédé SLM à produire de l'acier inoxydable avec des performances satisfaisantes, qui peuvent dépasser celles des matériaux obtenus par des procédés de fabrication conventionnelle. Les défis et les lacunes de la recherche dans ce domaine sont identifiés dans la dernière section.

Cet article, intitulé « *Selective Laser Melting of Stainless Steels: A Review of Process, Microstructure and Properties* », a été soumis au journal *Materials & Design*. En tant que première auteure, j'ai conduit l'essentiel de la recherche bibliographique, et rédigé la majorité des parties. Narges Omidi, deuxième auteure, a contribué à la revue de la littérature et la synthèse sur les aciers ferritiques et duplex. Le professeur Noureddine Barka, troisième auteur, a fourni l'idée originale, et a révisé l'article. Sasan Sattarpanah Kangranroudi, quatrième auteur, a également contribué à la révision de l'article.

1.2 SELECTIVE LASER MELTING OF STAINLESS STEELS: A REVIEW OF PROCESS, MICROSTRUCTURE AND PROPERTIES

1.2.1 Abstract

Metal Additive Manufacturing (AM) is revolutionizing the production and use of materials. Selective Laser Melting (SLM) is one of the most common AM technologies used to fabricate high-performance metal components. Stainless Steels (SSs) are among the most preferred alloys for additive manufacturing due to their availability in the powder form, their low cost, their mechanical properties, as well as their corrosion resistance. Due to the complex thermal history and rapid solidification, SLM process introduced a peculiar microstructure, out-of-equilibrium, which in turn control the mechanical properties. Understanding the processing-microstructure-property relationship is essential to advancing and extending the use of SLM-fabricated stainless steel components. This review paper enlightens the basics of the selective laser melting process, the key processing parameters and the commonly encountered defects. A detailed discussion of the microstructure, mechanical behavior (i.e. hardness, tensile and fatigue properties), and corrosion resistance of SLM manufactured stainless steels is also provided, along with the effect of various post-process treatments. This includes austenitic, martensitic, precipitation hardening, duplex, and ferritic stainless steel grades. This review highlights the capability of the SLM process to produce stainless steel with satisfactory performance, which may exceed that of conventionally processed materials. Challenges and research gaps in this field are identified in the final section.

Keywords: metal additive manufacturing, selective laser melting, stainless steel, review, microstructure, mechanical properties

1.2.2 Introduction

Metal additive manufacturing technologies have emerged recently but have very quickly drawn a lot of attention thanks to their very attractive set of properties and

advantages. Their common feature is the build-up of parts by the deposition of material layer upon layer, based on 3D model data, achieving in that way a near-net shape, as opposed to traditional subtractive manufacturing methods [31]. This unique feature allows flexibility in design and geometry, elimination of expensive part-specific tooling costs, short lead-time, part-customization, functional integration, weight reduction, and cost-efficiency [32, 33]. These advantages are particularly relevant to the replacement and customization of high-performance components for aerospace, medical, energy, and automotive applications [3].

Growing interest in the field of metal additive manufacturing has led to the development of several processing systems. The existing metal AM techniques are usually categorized in terms of the material feedstock into three classes: (1) powder-bed systems, (2) powder-feed systems, (3) wire-feed systems. Selective laser melting (SLM) is one of the powder-bed fusion processes that uses a laser beam as an energy source to selectively melt metal powder [8]. SLM is considered the most versatile AM process because it can process a wide spectrum of materials including Fe-based alloys, Ti-based alloys, Ni-based alloys, Al-based alloys, Co-based alloys, Cu-based alloys, composites, and ceramics [9].

Stainless steels are nowadays utilized across nearly every imaginable industry due to the attractive combination of excellent corrosion resistance, wide range of strength and toughness levels, heat resistance, biological cleanability, and biocompatibility. These properties have made stainless steel the material of choice for a board range of applications [34]. Austenitic and ferritic stainless steels are used in extremely corrosive environments such as the chemical, petrochemical, marine and medical industries [5, 35] , whereas martensitic and precipitation hardened stainless steels are used in of aerospace, defense, and tooling industries where high hardness and strength are required [36, 37].

Stainless steel was one of the first metals introduced in metal additive manufacturing systems, and it is now frequently processed using selective laser melting [38]. Its popularity in SLM is due to its widespread supply chain in powder form, its low cost relative to other common alloys, along with its outstanding mechanical and physical properties. A growing amount of research has been undertaken in the field of SLM of stainless steels during the past

few decades [39]. The finding shows promising opportunities for tailoring stainless steel microstructure and producing high-performance parts with complex geometries [20, 21]. However, the complex physical phenomena and thermal cycling experienced by the material powder are still challenging. A better understanding of process-structure-property relationships will be important to avoid common defects and achieve reproducibility. The knowledge of the current state of stainless steel components processed by SLM is required for the advancement and enlargement of stainless steel use in the SLM process.

This review aims to provide readers with a thorough understanding of the selective laser melting process and its application to stainless steels. The core of the article focuses on the microstructure, the mechanical and fatigue properties, as well as corrosion resistance of stainless steels processed by SLM. A comparison with conventionally produced material properties is made to shed light on the opportunities and challenges present in the field of SLM of stainless steels. Furthermore, the effects of post-process treatments on SLM processed stainless steels are reported. Relevant reviews exist in the literature [39-41]; most of them deal with different additive manufacturing processes of steels in general. A recent review by Zitelli et al. [2] went through stainless steel grades produced by laser powder bed fusion. However, they did not underline the structure-property relationships, and the reported proprieties were limited to microstructure and mechanical properties. This paper fills the gap by providing a more complete insight into the microstructural evolution and its effect on mechanical, fatigue, and corrosion performances of SLM stainless steels.

To allow the reader to gain a structured overview of SLM process and its application to stainless steels, this paper is organized as follows: The first section describes the working principal of the SLM process, critical processing parameters, and common process-induced defects. The second section seeks to critically examine the microstructure, mechanical behavior (i.e. hardness, tensile strength, and fatigue properties), as well as corrosion properties, of each stainless steel class (i.e. austenitic, martensitic/precipitation hardening, duplex, and ferritic) where enough data is available in the literature. The last section

highlights the summary and provides an outlook on unexploited potential in the field of SLM processing of stainless steels.

1.2.3 Selective laser melting process

1.2.3.1 Process Description

Selective laser melting (SLM), also referred to as direct metal laser sintering (DMLS), is a laser powder bed fusion process (L-PBF) used to produce objects from powdered materials using a laser beam that selectively fuses or melts the regions of a powder bed, layer by layer, in an enclosed chamber, as defined by ASTM F2792 standard [42]. The working principle of SLM is schematically illustrated in Fig. 1.1. Before the production stage, the CAD data file has to be processed by specific software to create support structures when needed and slice the 3D model into layers. The generated data is then uploaded to the SLM machine. The building process starts with spreading a layer of metal powder of a predefined thickness on the build platform using a coating mechanism. A moving laser beam, with a fixed scan speed, scans the powder constituting the cross sectional area of the sliced part model. The laser beam is directed in the X and Y directions with two high-frequency scanning mirrors. The laser energy should be high enough to permit full melting of the powder particles to form near-dense metal components. Once the laser scanning is completed, the build platform is lowered along the Z-axis to allow the deposition of a new layer of metal powder. The last two steps are repeated for each subsequent layer until the entire part is built [43]. After completing the process, loose powder is vacuumed and the solidified part is removed from the substrate plate. The scanning process takes place in a building chamber filled with an inert gas like Argon or Nitrogen at oxygen levels below 500 ppm to prevent the oxidation [44]. Pre-heating of the substrate plateform or the entire building chamber can help to reduce thermal residual stresses and produce crack-free parts [45].

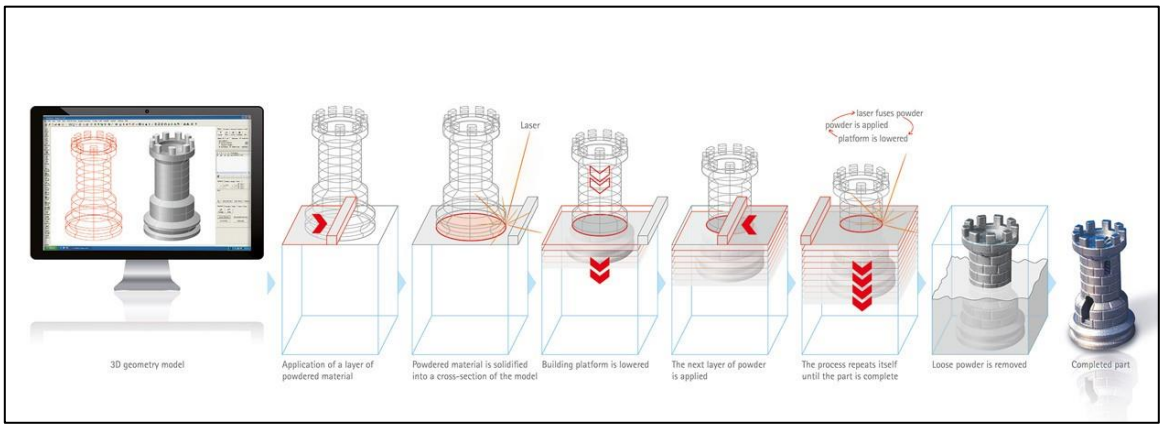

Figure 0.1. Functional principle of Selective Laser Melting process [46].

1.2.3.2 Process Parameters

In SLM process, the formation of a fully dense product with well-overlapped continuous scan tracks involves a large number of parameters and complex physical phenomena [11]. Some of the primary processing parameters are given in Fig. 1.2. The literature on process optimization focuses mostly on laser power (P), scan speed (v), hatch spacing (h), and layer thickness (t). These parameters can be combined to define the volumetric energy density (E) according to equation (1) [47]:

$$E = \frac{P}{v\,h\,t} \tag{1}$$

The units of E, P, v, h and t are $\mathrm{J/mm^3}$, W, $\mathrm{mm/s}$, mm and mm respectively. The melt pool dimensions, including melt pool length, melt pool width, and melt pool depth, are greatly affected by the applied laser energy density. It has been reported that increasing the energy density increases all three melt pool dimensions [48]. As shown in Fig. 1.3, the final part is a stack of layers superimposed along the building direction; each layer is composed of micron-sized scan tracks overlapping horizontally. An inappropriate combination of process parameters affects the melt pool characteristics and leads to defect formation such as lack-of-fusion, balling, keyholing, and surface roughness [49].

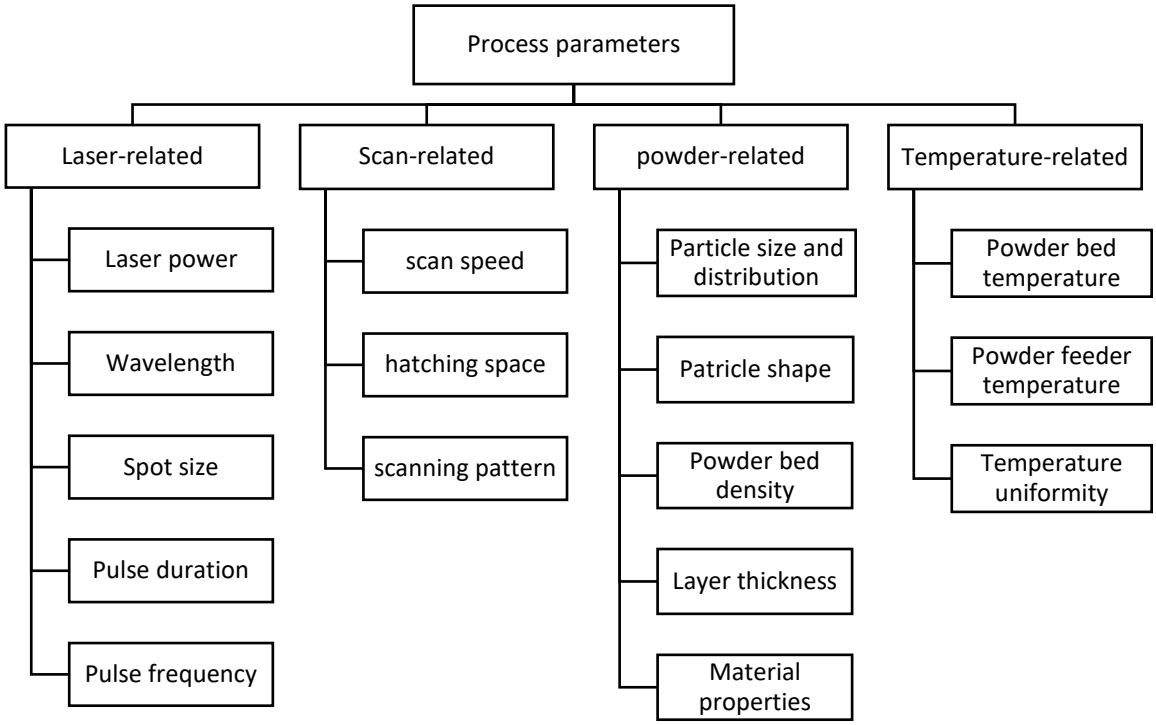

Figure 0.2. The principal process parameters in SLM process [50].

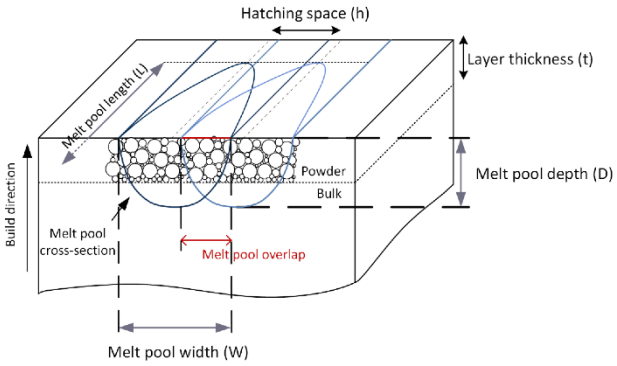

Figure 0.3. Schematic illustration of melt pool geometric characteristics [51].

The scanning strategy, which is the geometrical pattern followed by the energy beam, has a significant influence on the temperature gradient, thermal history, and densification

behavior of the build part [52, 53]. It has been shown that appropriate selection of the scanning strategy can reduce the amount of porosity, achieve more isotropic material by eliminating the fibrous texture, decrease residual stress and improve surface roughness [54, 55]. Scanning strategies with shorter scan vectors, interlayer rotation, and laser re-melting usually result in better performances. Some of the most known scan strategies are illustrated in Fig. 1.4.

In addition to the most critical SLM process parameters, feedstock powder features such as powder morphology and size distribution are also important parameters to be considered in the SLM process as they strongly influence laser energy absorption, powder flowability, and thermal conductivity of the powder bed. Smooth flowability and high packing density of powders are desirable features to guarantee successful material deposition as well as part densification during the SLM process [56].

Extensive research has been conducted so far to optimize process parameters and achieve high densification levels [25, 35, 49, 57], as it is the key factor to attaining good mechanical, fatigue, and corrosion properties.

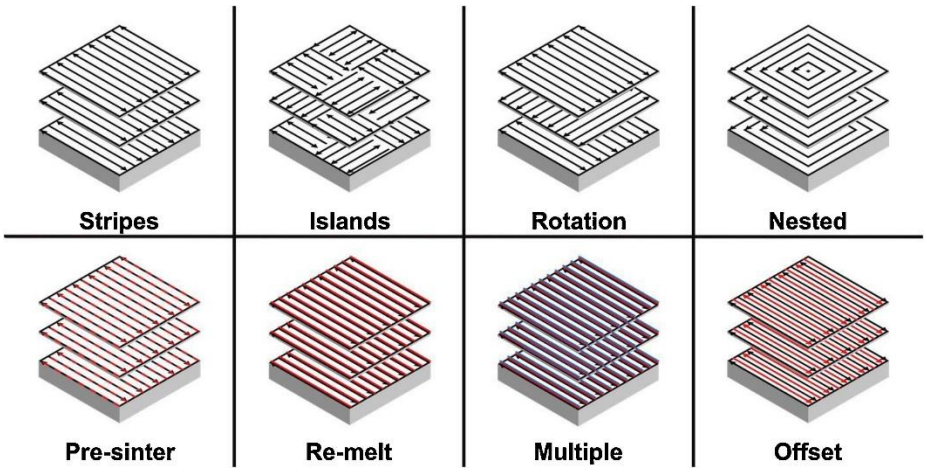

Figure 0.4. Examples of commonly used scan strategies in SLM process. Reprinted with permission from Ref. [58]

1.2.3.3 Defects in selective laser melted parts

Despite the unique capabilities of the SLM process, defects remain a critical issue that is frequently encountered in metal AM components. These flaws adversely affect material properties and may lead to early failure as they act as stress concentrators under applied loads. This section describes the formation mechanisms and mitigation strategies of some of the most challenging issues in SLM-fabricated stainless steel components. Other defects such as surface roughness, vaporisation of alloying elements, spatter and denudation, etc. exist; describing all of these in detail would lengthen this review excessively. The reader is referred to other reviews focused on defects [10, 59, 60].

a) Porosities and lack-of-fusion defects

Porosities and lack-of-fusion voids have been extensively reported and investigated in the literature as prevalent issues in the SLM process [47, 61-65]. They are generally the result of either excessive or insufficient input energy; therefore, they may be efficiently controlled and minimised by tuning the process parameters. Researchers have categorised pores into three types based on their formation mechanisms [3, 60]:

(1) Gas pores (see Fig. 1.5(a) and (b)): Gas pores are defined as flaws arising from trapped gases within the melt pool. They are usually small in size and have a spherical shape. Gas pores originate from different sources. Firstly, gas can be entrapped inside the powder feedstock during the atomization process [66]. Secondly, the gas present between the powder particles due to low packing density is released in the molten pool. Due to the rapid cooling, gas bubbles can not escape out of the molten pool and are locked in during solidification [67]. Moreover, the increase in gas solubility at elevated temperatures makes the entrapment of residual atmospheric gases in the building chamber or moisture on the powder bed surface easier [60].

(2) Lack-of-fusion defects (LOF) (see Fig. 1.5(c) and (d)): LOF defects are voids with un-melted powder particles. Unlike gas pores, they are generally large and have

irregular shapes, as shown in Fig. 1.5. The main cause of this type of porosity is insufficient laser energy density, affecting the melt pool size. A shallow molten pool results in a lack of penetration of liquid metal and poor bonding into the previously solidified layer. Lack-of-fusion may also occur between adjacent scan tracks due to a lack of intra-layer overlap when the melt pool width is too small [68]. Hatch spacing and layer thickness must be carefully selected so they do not exceed melt pool width and depth, respectively, to ensure complete melting and avoid LOF [69].

(3) Keyhole pores (see Fig. 1.6): In contrast to lack-of-fusion defects, keyhole pores are caused by excessive energy density, inducing a transition from conduction mode to keyhole mode. In this melting mode, the metal boiling temperature is reached and evaporation of metal fluid takes place. Due to the recoil pressure of evaporating elements, a vapor cavity forms within the molten pool, leading to exceptionally deep laser penetration and the re-melting of multiple layers [70]. Once the laser proceeds on its assigned path, the molten pool temperature begins to drop. The decrease in recoil pressure, accompanied by the increase in surface tension, causes an abrupt collapse of the keyhole sidewalls. Due to the fast flow, the trapped gas bubbles cannot come to the surface before solidification, resulting in pores at the bottom of the melt pool [63]. Keyhole pores may also occur at the end of a scan track or at a laser turn point as a result of laser beam deceleration and acceleration [71, 72].

Porosities can be minimized by the appropriate selection of energy density and scanning strategy to produce a full dense material. Hot isostatic pressing (HIP) is a thermo-mechanical post-treatment that is commonly used to close porosities and micro-cracks.

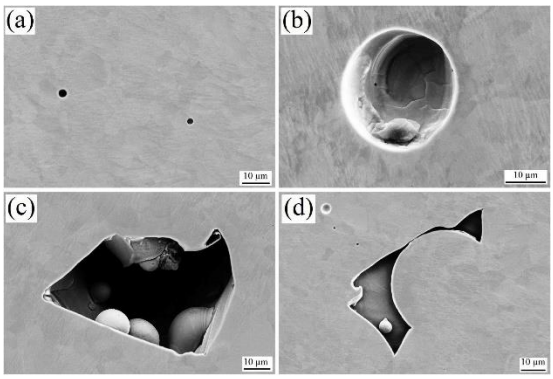

Figure 0.5. SEM micrographs showing different types of porosities in SLM-produced 316L Stainless steel: (a,b) gas pores and (c,d) Lack-of-fusion defects. Reprinted with permission from Ref. [73]

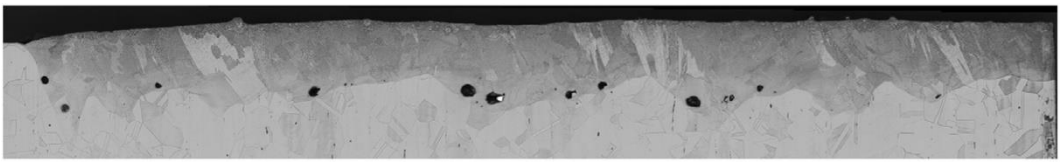

Figure 0.6. Example of keyhole porosity at the bottom of the scan track. Reprinted with permission from Ref. [70]

b) Balling

Balling is another typical defect affecting SLM part quality. It is attributed to Plateau-Rayleigh capillary instability. During the scanning process, the laser beam melts the powder particles to form a cylinder of liquid metal. The stability of the liquid cylinder is related to the ratio of its length L to its diameter D through the following equation [74]:

$$L/D < \pi \quad (2)$$

At high scanning speed (low energy density), the molten pool tends to elongate and the instability condition becomes satisfied. Hence, the liquid cylinder breaks up into smaller spherical beads, tending to minimize its surface energy [56, 75]. Balling occurrence is influenced by both applied laser parameters (e.g. scan speed, laser power, and layer thickness) and powder material properties (melting point, density, thermal conductivity) [74].

SLM parameters control the temperature and, accordingly, the viscosity of the molten pool, which in turn affects the wettability of liquid metal [76]. Low energy input leads to a limited amount of liquid phase possessing high viscosity. Under this condition, the molten material cannot spread and wet the underlying substrate, and instead forms coarsened agglomerates, which tend to transform into ball-shaped structures owing to the surface tension reduction [77, 78]. In addition to these factors, wetting ability can also be worsened due to the presence of an oxide contamination layer on the melt surface and the substrate, inducing balling initiation [59]. Numerous problems are associated with the balling phenomenon, including poor inter-layer bonding, high surface roughness, and reduced density due to pores and lack-of-fusion defects formed between discontinuous melt tracks [59, 68]. Consequently, part geometry and mechanical properties are deteriorated. In more severe cases, coarsened metal balls might obstruct the coating mechanism, leaving the part unfinished [76]. Thus, balling occurrence is an extremely detrimental issue for SLM-fabricated parts that needs to be eliminated. Relevant control methods reported in the literature include increasing input energy density (i.e., increasing laser power, lowering scan speed, and decreasing layer thickness), reducing the oxygen content in the atmosphere, adding a small amount of deoxidant, and employing laser re-melting techniques [76, 77, 79].

c) Residual stress, distortion and cracking

Residual stresses arise from the large thermal fluctuations experienced by the solidified material due to the rapid heating and rapid cooling cycles during the SLM process. These stresses are detrimental since they can lead to part distortion, cracking, and delamination of the fabricated metal part. As a result, the dimensional accuracy and mechanical strength of the parts are affected [80]. These defects are a significant challenge in SLM because they cannot be repaired by post-processing techniques. Thus, a lot of research has been done to measure, model, predict, and mitigate residual stresses in SLM-produced stainless steel [79, 81-86]. A deep knowledge of the thermal stress evolution during the LPBF process is necessary to comprehend and alleviate the aforementioned problems.

Mercelis [82] proposed two main thermal mechanisms to explain the origin of residual stresses: (1) the temperature gradient mechanism (TGM) and (2) the cool-down phase of the molten top layers. The first phenomenon is induced by the large thermal gradient developed in the immediate vicinity of the laser spot. Due to the high temperature, the heated top layer tends to expand, but this thermal expansion is inhibited by the colder underlying material. Thus, elastic compressive strains are formed in the top layer. When the yield strength of the material (which is lowered by the temperature rise) is reached, the upper layers become plastically deformed. During the cooling stage, those upper layers tend to shrink and bend in the opposite direction, but the shrinkage is partially restricted by the plastic deformation developed during the heating stage. Thus, tensile residual stresses are formed [86, 87].

The second mechanism that generates residual stresses is the cool-down phase of the previously melted top layers, which experience re-melting and re-solidification. The thermal contraction leads to material shrinkage, which is again restrained by the underlying layers. Thus, tensile stresses are introduced in the newly deposited layer and compressive stresses below [82].

When the magnitude of residual stresses surpasses the yield strength of the material, distortion occurs, leading to deviation of the part from its actual shape and size during and/or after the fabrication process [88]. This deviation may be large enough to obstruct the movement of the roller and cause the SLM process to be interrupted, resulting in an unfinished or badly finished part [89]. Distortion can also occur upon removal of the built part from the base plate. The resultant dimensional inaccuracy could be detrimental to its functionality, rendering it unusable for critical applications [90]. Residual stress can also promote crack initiation and propagation to relieve internal forces, if its magnitude exceeds the ultimate tensile strength of the solid material [91, 92]. When the stress is located at layer interfaces or at the solid-substrate interface, cracking may propagate and cause the separation of the adjacent layers, leading to delamination defects [3, 91]. Aside from residual stresses, metallurgical and microstructural factors, which are not discussed here, play an important role in cracking and delamination occurrence [3, 68, 93].

Mitigation strategies for residual stresses and related defects in SLM can be categorised into in-situ methods and post-processing methods. Preheating of the substrate or the feedstock powder is the most common in-situ technique to decrease the high cooling rate and thus reduce residual stresses through a less steep thermal gradient [45, 86, 94]. Laser rescanning after every deposited layer has also been used in the SLM process for residual stress reduction [94, 95]. Several studies have shown that scan vector length and scan vector orientation have a significant influence on residual stress distribution and part distortion [86, 96]. As a result, adopting "Island scanning strategy" or a layer-wise alternating scanning strategy is an effective way to achieve a more uniform stress field with low magnitude [84, 97]. Other process parameters, such as laser power, scan speed, and layer thickness, can be optimised to mitigate residual stress [98, 99]. However, this approach presents the risk of introducing other process defects. Hence, microstructural and mechanical properties should be taken into consideration when selecting the optimal parameters to make high-quality parts [98].

In terms of post-processing techniques, stress relief heat treatment is the most common practice applied to SLM-fabricated components to reduce residual stress [95, 100]. It is usually performed before base plate removal in order to avoid distortion in the final part [101]. Other post-processing treatments, such as shot peening and laser shock peening, can be used to introduce desirable compressive stresses and improve fatigue life [102]. These methods, although advantageous, raise manufacturing costs.

1.2.4 Stainless steels in selective laser melting

Stainless steels are iron-based alloys that contain a minimum of about 12% of Chromium, the amount needed to provide good corrosion resistance and heat-resistant properties. Other alloying elements such as nickel, manganese, molybdenum, copper, titanium, silicon, niobium, aluminum, sulfur, and selenium can be added to have a peculiar combination of properties [34]. Thus, stainless steels are nowadays used in an almost endless number of applications thanks to their unrivaled variety of achievable microstructure

features. These applications include automotive and transportation [103] , architecture and construction [104], chemical and power industries [105], food industry [106], marine systems [107], medical implants [6, 108], aircraft components [109, 110], etc..

They are usually classified into subcategories, which are namely ferritic, austenitic, martensitic, duplex, and precipitation hardening [34]. Depending on the thermal history and the composition, each grade is distinguished from others by its microstructural and crystallographic features. During the last two decades, there has been a rapid increase in publications related to the SLM process of stainless steel. To date, different grades of stainless steel have been successfully implemented in L-PBF systems with superior mechanical properties compared to conventionally processed stainless steels. However, issues regarding process control and standardization hinder the adoption of SLM technology. A deeper understanding of process-structure-property relationships and machine-to-machine variability is required in order to ensure quality, consistency, and reproducibility [8]. The present paper provides an overview of commonly printed grades of stainless steel powder.

1.2.4.1 Austenitic stainless steels

Austenitic stainless steels are the most common and largest family of stainless steel. They have a face-centered cubic (FCC) crystal structure achieved by adding austenite-stabilizing elements such as nickel, manganese, and nitrogen to maintain phase stability at all temperatures [107]. This class of steel is highly attractive in the marine, chemical, petrochemical, food, and biomedical industries because of its good ductility, toughness, and corrosion resistance, in addition to its biocompatibility. The additive manufacturing of austenitic stainless steels is widely investigated in the literature. The published papers on austenitic stainless steels processed by SLM are essentially dealing with 316L stainless steel and less with 304. The chemical compositions of these two common grades are given in table 1.1. The addition of 2% molybdenum in 316L provides greater resistance to acids and localized corrosion such as pitting and crevice corrosion compared to 304L. The lower Ni

and Mo content in 304L, which are expensive alloying elements, leads to a reduced price. Therefore, 304L is commonly used instead of 316L if the service environment is less harsh.

Table 0.1.

Nominal Chemical composition of austenitic stainless steel powder commonly used in SLM, Ref. [111].

Grade Name	Composition (wt. %)								
	Fe	C	Cr	Ni	Mo	Mn	Si	P	S
AISI 316L	Bal.	<0.03	16.00-18.00	10.00-14.00	2.00-3.00	<2.00	<1.00	<0.045	<0.03
AISI 304L	Bal.	<0.03	18.00-20.00	8.00-12.00	-	<2.00	<1.00	<0.045	<0.03

a) Microstructure of SLM-produced austenitic stainless steels

Selective laser melted parts are formed through rapid solidification rates, high thermal gradients, and repetitive heating and cooling cycles, resulting in a unique microstructure out of equilibrium [48]. The SLM parameters modulate the thermodynamic mechanisms that govern the formation and evolution of key microstructural features, including the solidification morphology, grain size, crystallographic texture, secondary phases, etc. [40]. Austenitic stainless steels produced by SLM usually show a pure FCC austenite phase [20, 62, 112-119]. Nevertheless, a small fraction of δ-ferrite phase have been reported in a few works [14, 66, 120-123]. In fact, the chemical compositions of the 316L and 304L stainless steel powders with a relatively high Cr_{eq}/Ni_{eq} ratio promote austenitic-ferritic (AF) or ferritic-austenitic (FA) solidification modes [41, 124]. In the case of AF mode, austenite precipitates as a primary phase with subsequent ferrite formation in the intercellular regions according to the sequence $L \rightarrow (L+\gamma) \rightarrow (L+\gamma+\delta) \rightarrow (\gamma+\delta)$ [120, 124]. In the case of the FA mode, solidification starts by nucleation of δ-ferrite, followed by the formation of austenite in interdendritic regions. Through further cooling, δ-ferrite undergoes peritectic transformation to austenite. Due to the high cooling rate of SLM process, the peritectic

reaction could not be completed and partial δ-ferrite is retained in the austenite matrix [14, 125]. The morphology and volume fraction of ferrite are strongly influenced by the cooling rate, which in turn can be controlled by process parameters such as laser power and scanning strategy [120, 124].

Microstructural characterization performed in the literature [14, 119, 123, 126-130] on both 304L and 316L austenitic stainless steels reported a hierarchical microstructure with common features at multi-length scales as illustrated in Fig. 1.7.

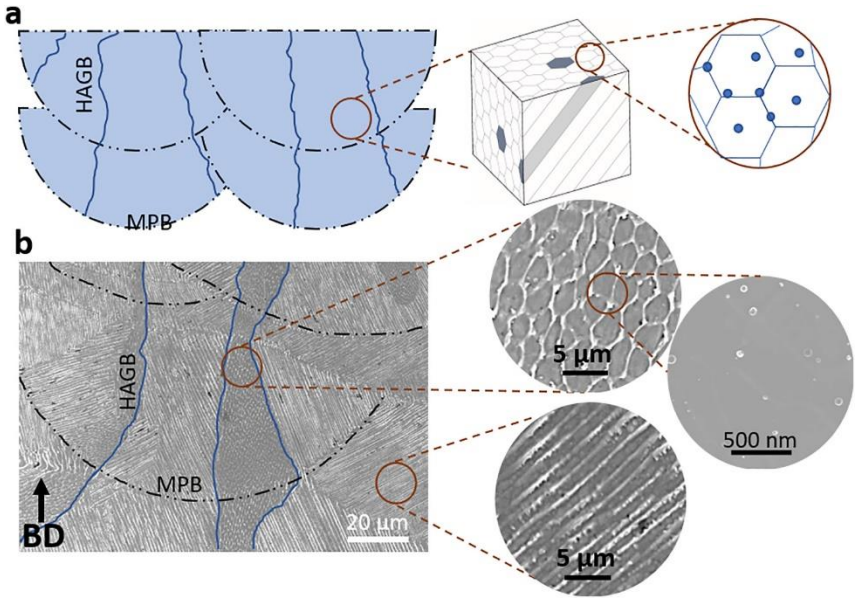

Figure 0.7. Hierarchical microstructure of SLM-fabricated 316L stainless steel showing (a) schematic drawing of the melt pool boundaries (MPB), high angle grain boundaries (HAGBs), cell structure in 3D, and nano-sized oxide inclusions, (b) corresponding SEM micrographs of the microstructural features. Reprinted with permission from [130].

At the micron scale, columnar grains, ranging between 10-100 µm, are observed within the melt pools, growing epitaxially in the direction of the thermal gradient. They are delimited by high-angle grain boundaries. The layer-by-layer nature of the SLM process promotes epitaxial grain growth during solidification as the previously solidified grains provide a ready nucleation site for the melted material. Moreover, the heat transfer along the building direction is higher compared to thermal conductivity through the metal powder or

heat convection with the building environment, leading to directional solidification. As a result, large columnar grains are usually formed along the build direction, normal to the solidifying surface of the melt pool [131, 132].

At the sub-micron scale, an intragranular cellular solidification structure delineated by segregation of heavy alloying elements, such as Mo and Cr, and high dislocation density at the cell walls are seen within the individual large grains. Cells have a size of 1 μm or less and an elongated or polygonal (equiaxed) shape depending on their growth direction. The formation mechanism of the intragranular cellular network is often explained in the literature by compositional fluctuations and constitutional supercooling [119, 126, 133]. According to solidification theory, the microstructure can be controlled by the temperature gradient G and the solidification rate R. The ratio G/R determines the morphology of the solidification structure (planar, cellular, columnar dendritic, and equiaxed dendritic) while the product $G \times R$ (which defines the cooling rate) determines the size of solidification structure [3]. At a relatively high ratio G/R, cellular dendritic structure is favored, which is the case of the SLM process. A finer microstructure can be achieved by a higher cooling rate $G \times R$. Several investigations [117, 134] found that a low energy density (i.e. low laser power and/or high scan speed) leads to a high cooling rate, resulting in a refined primary dendrite spacing (see Figs. 1.8 and 1.9).

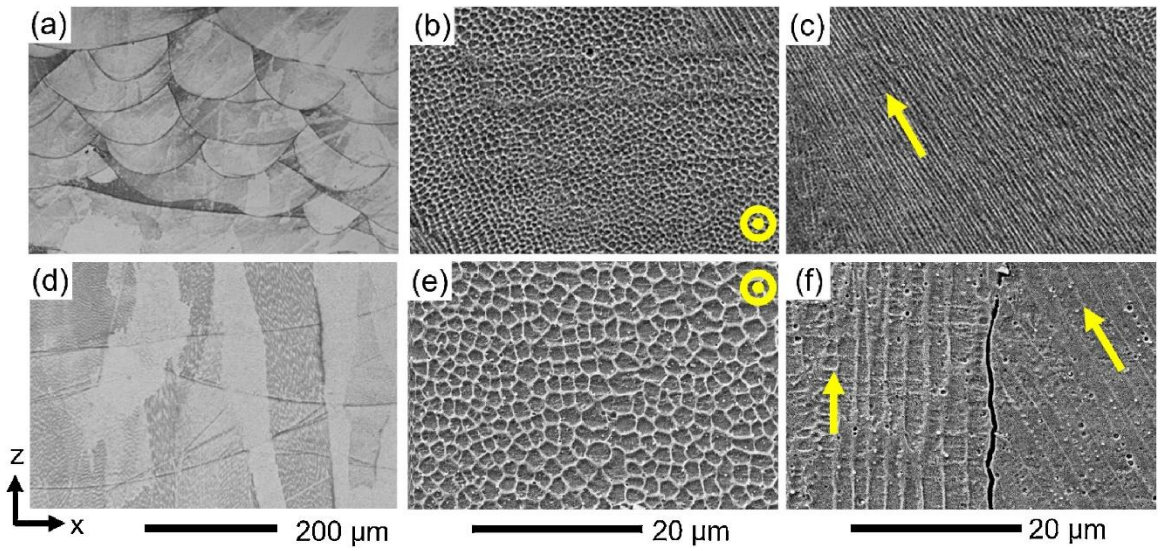

Figure 0.8. Micrographs of 316L SS samples processed with low laser power (a,b,c) and high laser power (d,e,f). (a,d) show melt pools and columnar grains, (b,e) show cells growing parallel and (c,f) perpendicular to the XZ plane. The yellow arrow indicate the cell growing direction. Reprinted with permission from Ref. [135].

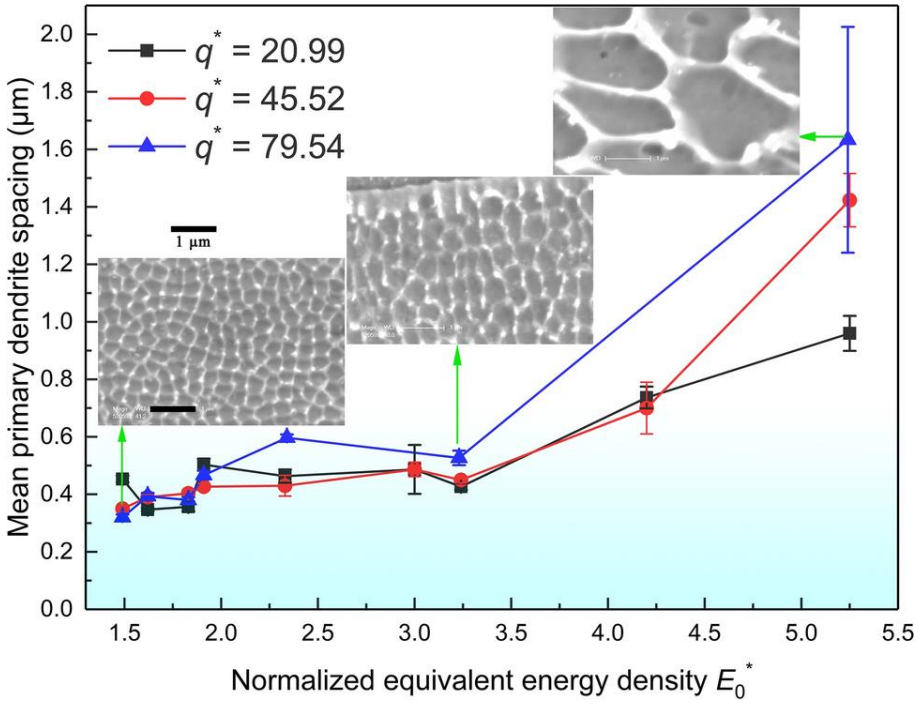

Figure 0.9. Effect of laser energy density on primary dendrite spacing. Reprinted with permission from Ref. [134]

At the nano scale, amorphous oxide inclusions are usually formed along the cell walls and in the matrix. These randomly dispersed nanoparticles, with a size up to several hundred nanometers, are mainly enriched in O, Si, and Mo, as shown in Fig. 1.10. Their formation is ascribed to the reaction between Si present in the precursor powder with the residual oxygen in the building chamber [62].

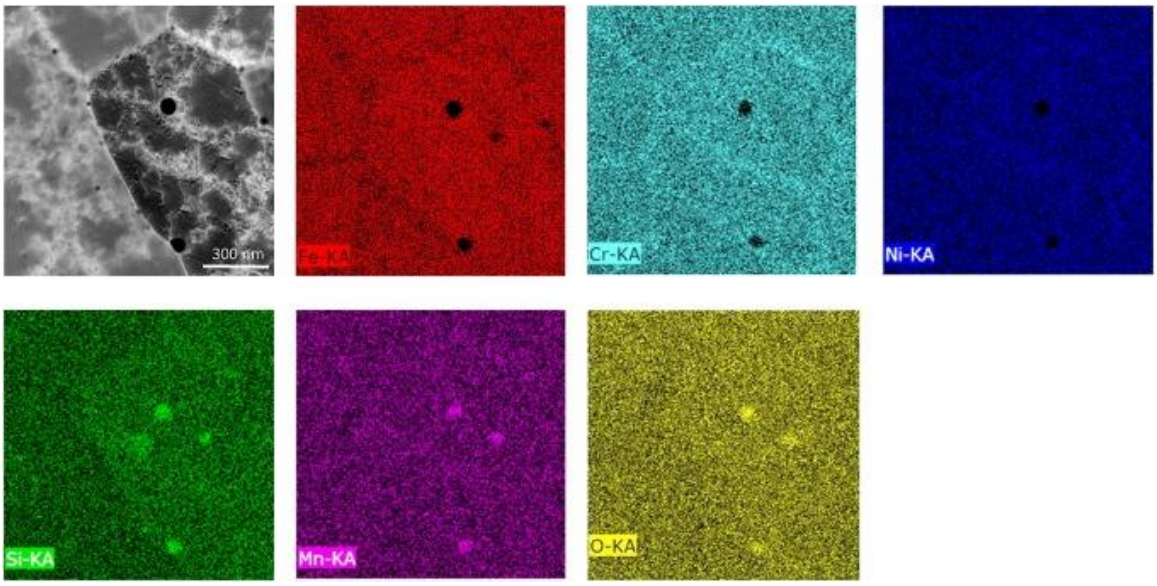

Figure 0.10. HAADF STEM image with corresponding EDS elemental map showing micro-segregation of Cr at cell walls and Si-Mn-O rich nanoparticles in SLM 304L SS. Reprinted with permission from Ref. [14]

In SLM-produced austenitic stainless steels, a strong <001> crystallographic fiber texture aligned along the building direction is typically observed [101, 136]. This direction is known to be the preferred crystallographic direction for cubic materials. Thus, columnar grains with an easy growth direction aligned to the maximum heat flow direction are formed as a result of competitive epitaxial growth [3, 14, 133]. However, the formation of microstructure with random texture has also been reported [113, 137]. In fact, it has been shown that texture basically depends on the local heat flow directions and the geometric features of the melt pool that are determined by processing parameters [138]. The influence of scanning strategy, laser energy density, and laser power on texture has been widely investigated [14, 66, 120, 135, 139]. Efforts are being made to achieve superior mechanical

properties by controlling crystallographic texture [140, 141]. For example, Sun et al. [15] obtained a tailored <011> crystallographic texture instead of the common <001> crystallographic texture by using higher laser power and a bidirectional scanning strategy (see Fig. 1.11). Their approach enabled the activation of nano-twinning deformation mechanisms, resulting in enhanced strength and ductility.

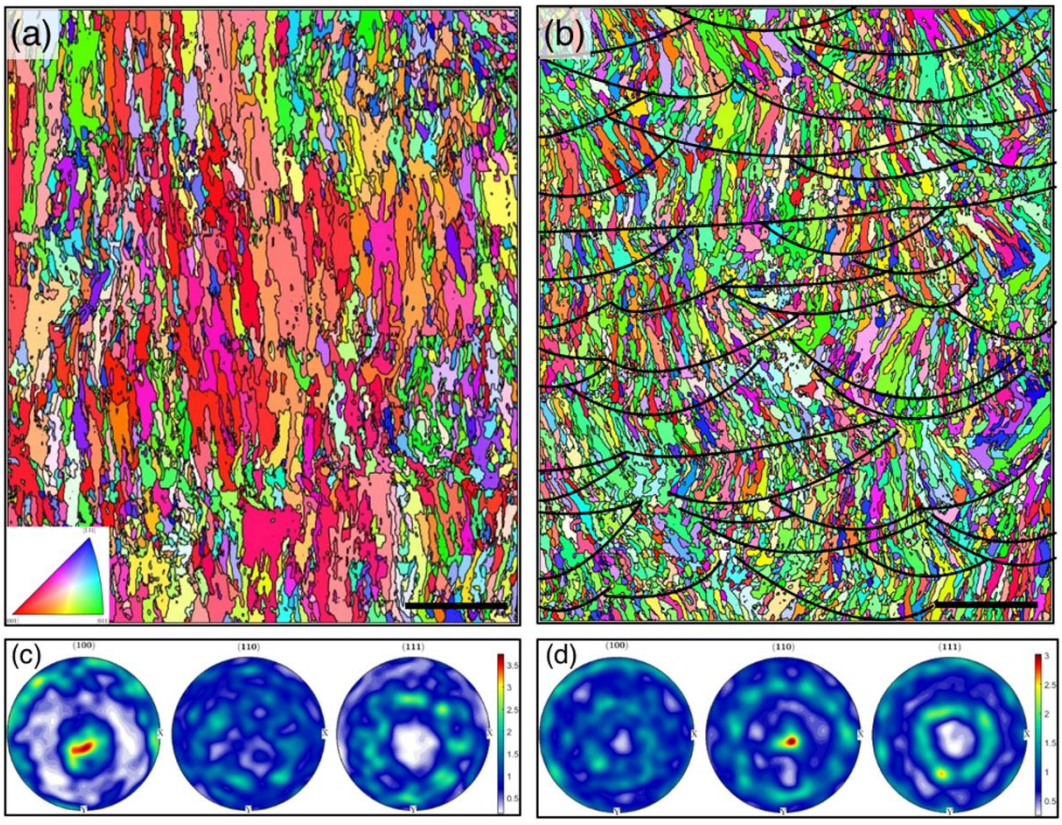

Figure 0.11. EBSD IPF color maps with respect to build direction and their respective pole figures for the SLM-built 316L SS with laser power of (a,c) 380W and (b,d) 950W showing change of crystallographic texture from <001> to <011>. Adapted from Ref. [15].

Investigations into post-process heat treatment of SLM austenitic stainless steels revealed that as-built microstructural features remain stable up to 800 °C [17, 133, 142-144]. At higher temperatures, the melt pool boundaries, cellular sub-structure, and dislocations completely disappear, as can be seen in Fig. 1.12. Hot isostatic pressing (HIP) resulted in complete recrystallization of grains [145]. Phase composition may also be altered due to post-

treatment. Kurzynowski et al. [120] observed the precipitation of σ-phase after stress relieving at 800 °C for 5h activated by the presence of ferrite and residual stresses in as-built 316L. Saeidi et al. [142] reported the occurrence of phase transformation from almost pure austenite to a dual austenite/ferrite structure following annealing at 1100 °C.

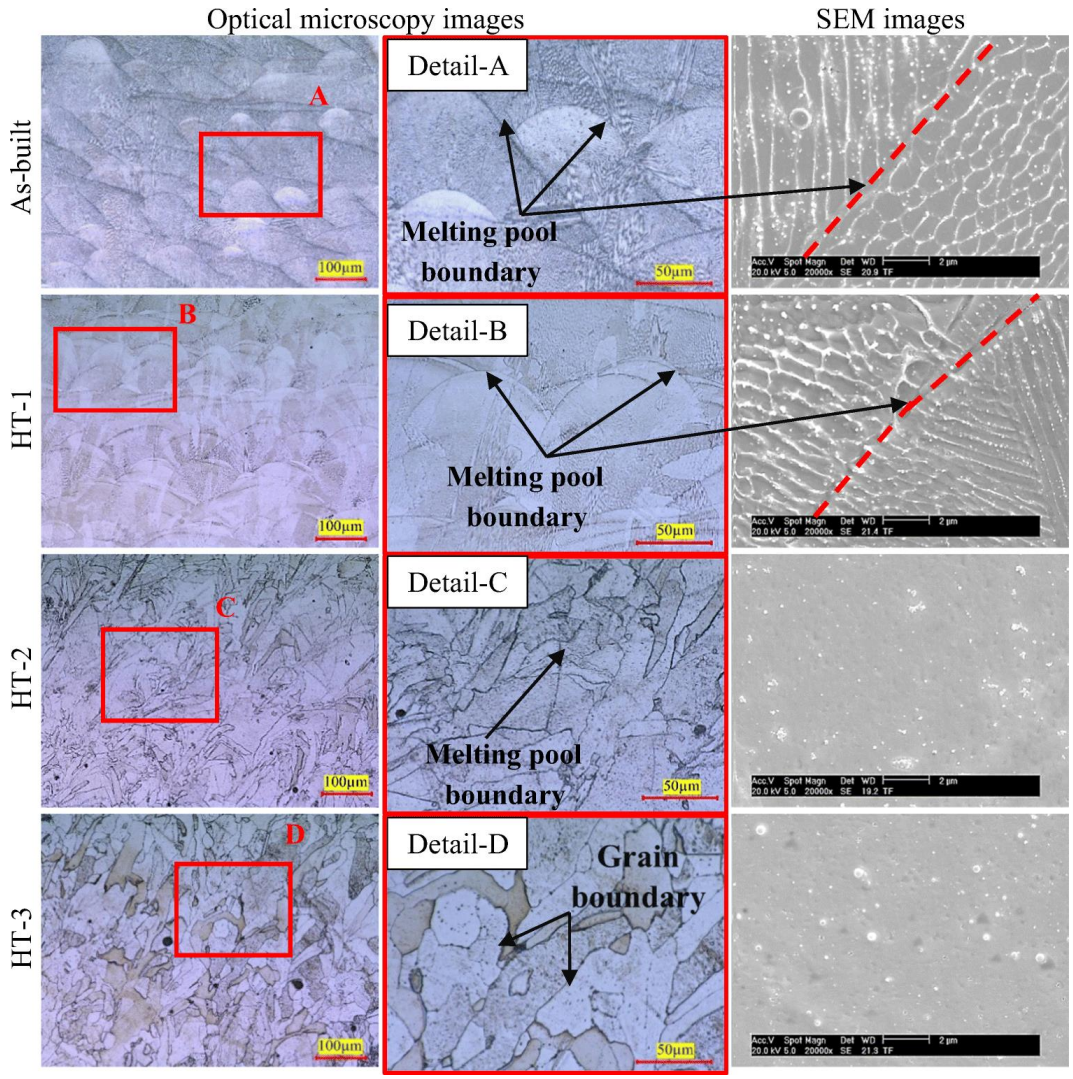

Figure 0.12. The influence of heat treatment on the microstructure of SLM built 316L SS. (HT1 = 600° C/2h, HT2 = 850°C/2h, and HT3 = 1100°C/2h). Reprinted with permission from Ref. [17]

b) Microhardness and Mechanical properties of austenitic stainless steels

In this section, the strength, ductility, and microhardness of SLM-Built austenitic stainless steel components are reviewed with an emphasis on the process-structure-properties relationship. Due to the disparate devices, heat sources, and processing parameters used throughout the literature, volumetric energy density is used to compare studies where possible. Table 1.2 lists the obtained yield strength (YS), ultimate tensile strength (UTS), elongation at failure (El.), and microhardness (H) for 316L and 304L austenitic stainless steels fabricated by SLM in their as-built condition, along with the minimum standard requirements according to ASTM A240.

It can be observed that there is a large variability in the attained properties values from different ranges of laser energy density. The reason for this variation may be attributed to the different scanning strategies and processing parameters leading to different thermal histories [3]. The disparity in results is also due to the different build geometries and the process inherent defects [57]. It has been shown that porosity have a negative impact on the strength of the material. Defects at weak regions act as stress raisers and promote the formation of micro-cracks under loading, leading to a brittle failure mode [146]. The summary in table 1.2 also reveals the effect of building orientation on mechanical properties. Anisotropy of the mechanical properties is usually explained by morphological texture and columnar structure growing along the building direction due to directional solidification [113]. In general, the horizontal build has higher yield and ultimate tensile strengths and lower elongation at failure than the vertical build [113, 141, 147, 148].

Table 0.2.

Mechanical properties of austenitic stainless steel grades fabricated by SLM

SS Grade	Equipment	P [W]	V [mm/s]	E [J/mm^3]	Building direction	ρ [%]	YS [MPa]	UTS [MPa]	El. [%]	H [HV]	Ref.
304L	Concept Laser M3linear	95	70 90	377 293	H	92.8 91.6	182 156	393 389	25.9 22.1	192 196	[112]
304L	Self-developed machine	200	25	-	H I V	100	540 380 450	704 550 570	38 30 58	-	[148]
304L	3D Systems ProX 300	182	1000	110.3	H V	-	455 410	707 665	45 55	-	[123]
304L	Self-developed machine	200	800	125	H V	99.98	500 460	800 750	48 50	250	[113]
304L	3D Systems ProX 300	200	1400	65	-	99.99	485	712	61	-	[149]
304L	ORLAS Creator	105	100 400	700 175	-	99 97.5	540 430	660 530	36 32	233-254	[14]
304L	EOS M290	220	1100	62.5	H V	99.9	457 411	653 612	67 72	-	[122]
316L	Renishaw AM250	200	1000	40	V	≥99.8	487	594	49	228	[119]
316L	SLM 280HL	400 1000	-	-	H	99.7 99.8	500 400	640 460	47 4.2	241 213	[135]
316L	Dimetal-100	300	700-1200	104-178.6	-	≥98	-	530-590	15-21.1	260-281.6	[117]
316L	SLM 250 Realize MCP	200	Up to 1000	-	H I V	≥99.9	663 649.3 557	685 669.3 591	25 35.6 42	235	[147]

316L	Sisma MYSINT100	100-150	700	102-214.3	I V	≥98	510-530 425-490	610-650 550-580	27-41 42-71	230	[62]
316L	M1 CUSING Concept Laser	180	1600	53.57	H V	96	397 387	668 564	37 35	226 221	[150]
316L	SLM 280HL	200	800	69.4	H I V	≥99	516.5 589.9 438.6	634.4 699 512	33.2 32.6 11.8	226.7 227.8 223.6	[151]
316L	Renishaw AM250	200	5000	7.27	-	-	518-561	662-688	45.3-52.7	-	[116]
316L	Concept Laser	90	1000	20	H V	97.7-98.1	512-536 430-448	622-668 509-528	20.4-24.7 12.4-11.6	-	[152]
316L	EP-M250	206 360	900 2465	84.77 54.09	H	98.93 98.6	584 549	773 708	46 28	-	[134]
316L	SLM 125HL	200	800	69.4	-	99.97	563	710	48.3	-	[118]
316L	EOS M290	195	800-1400	58-203.1	V	98.7-99.9	452-510	530-570	33-52	-	[130]
316L	4 different devices	73.5-148.8	300-1000	114.4-245	H V	-	493 446	626 551	43 46	-	[127]

Standard Reference Values

Grade	Condition	YS [MPa]	UTS [MPa]	El. [%]	H [HV]	Ref.
316L 304L	Annealed-hot finished	175	485	40	155	[153]

H = horizontal (i.e. loading axis is perpendicular to build direction), V = vertical (i.e. loading axis is parallel to Build direction), I = loading axis is inclined by 45° with respect to Build direction

Despite the high variability of the reported results, SLM-produced austenitic steels often have superior yield strength and tensile strength in the as-built state, compared to wrought counterparts. The yield strength demonstrated by SLM-built 316L and 304L SS was in the range of 400-660 MPa, which is two to three times higher than that of wrought material. Ultimate tensile strength has shown a relatively smaller increase, being in the range of 460-800 MPa (compared to 485-620 MPa for conventional). Interestingly, this exceptional increase in strength is achieved without loss of ductility. Although some researchers obtained lower elongation to failure, the majority of studies reported elongation to failure in the range of 32-67%. Thus, it is reasonable to claim that SLM-fabricated austenitic stainless steels demonstrate a combination of high strength and good ductility.

The superior strength in SLM-produced austenitic stainless steels is believed to originate from the unique hierarchical microstructure described in the previous section. All microstructural features will interfere with the dislocation movement [130]. The smaller grain size of the cellular structure leads to Hall-Petch strengthening since cell boundaries hinder the dislocation slips during deformation [119, 122, 128, 132]. The high population of piled-up dislocations induced by rapid heating and cooling during the SLM process also contributes significantly to the material strengthening through hindering plastic deformation [116, 122, 141]. Moreover, the silicon-rich nano-inclusions may act as pinning points and halt the dislocation's movement, which results in a hardened austenitic steel [122, 126, 130].

In addition to the enhanced strength compared with that of their conventional counterparts, the SLM-built austenitic stainless steels exhibit comparable ductility due to a low but steady strain hardening rate at high stress levels, which arises from the activation of multiple deformation mechanisms, such as dislocation slips, cellular wall evolution, and deformation twining [123, 141]. Many researchers [14, 15, 116, 123, 128, 132, 141] have demonstrated that SLM processed austenitic stainless steels have evaded the strength-ductility trade-off thanks to twinning-induced plasticity. The interaction of the twin boundary and dislocation increases the dislocation storage capacity, resulting in simultaneously enhanced strength and ductility [14]. Besides the TWIP effect, a strain hardening by

transformation-induced plasticity (TRIP) was also reported in 304L exclusively due to its low Ni content, which is an austenite stabilizer [123, 154].

According to the available literature, the average Vickers hardness values for SLM fabricated 304L and 316L stainless steels range from 200-280 HV, which is significantly higher than that of annealed counterparts (≈ 155 HV). Similarly to strength, the superior hardness is attributed to the unique microstructural features inherent to the SLM process. Tucho et al. [129] and Cherry et al. [155] investigated the correlation between laser energy density, porosity, and hardness. Both concluded that hardness is highly influenced by the level of porosity, which is in turn controlled by laser energy density. When the energy density is in an optimum range, a fully dense material is produced, resulting in high hardness. Outside of the optimum range, defects like balling or lack-of-fusion are likely to form, which lowers hardness.

Several researchers have studied the impact of post-process treatments on the mechanical properties of SLM built 316L ASS [17, 142, 145, 156, 157]. It has been shown that strength and hardness decrease with increasing annealing temperature as a result of grain coarsening. HIP significantly reduced yield strength but improved ductility [145].

c) Fatigue properties of austenitic stainless steels

The fatigue strength of SLM processed austenitic stainless steels is a decisive factor for many applications, such as biomedical implants and aerospace components, which are subjected to cyclic loading. From literature, it is already known that process-induced defects, along with surface roughness and residual stresses, can significantly degrade the high cycle fatigue performance of additively manufactured parts by causing stress concentration and early crack initiation [39, 158]. Generally, 316L and 304L ASS manufactured by SLM exhibit good fatigue performance, which is comparable to that of their conventionally produced counterparts [62, 101, 152, 159-163]. Spierings et al. [160] investigated the influence of surface quality on the fatigue life of 316L. They found that the fatigue limit at R = 0,1 (stress ratio) increased from 200 MPa to 269 MPa when surface roughness decreased

from 10 µm to 0.1 µm by machining and polishing. Riemer et al. [101] studied the high cycle fatigue (HCF) performance and fatigue crack (FCG) of SLM-processed 316L SS in different testing conditions. The fatigue limit of the as-built specimen with a turned surface is comparable to that of conventional material. Stress relieving at 650 °C had no significant influence on the fatigue strength because the microstructure remained stable at this temperature. Both as-built and stress-relived conditions showed anisotropic behavior for crack growth rate. When the crack growth direction is parallel to the building direction, the crack can easily grow along the elongated grain boundaries, leading to a high FCG rate (Fig. 1.13b). For crack growth normal to the building direction, the crack path is more tortuous, which slowed the growth rate (Fig. 1.13a). On the other hand, HIP at 1150° C induced a drastic change in microstructure with partial recrystallization of grains. Thus, more isotropic crack propagation and a higher fatigue limit are observed (Fig. 1.13c). Zhang et al. [161] investigated the correlation between HCF properties and porosity. Results from their work showed that for 316L SS, porosity does not impinge on the HCF properties when processing is done within the optimum range (energy density in the range of 70-130 J/mm^3). This defect-tolerant behavior is believed to be a result of the high ductility of 316L SS.

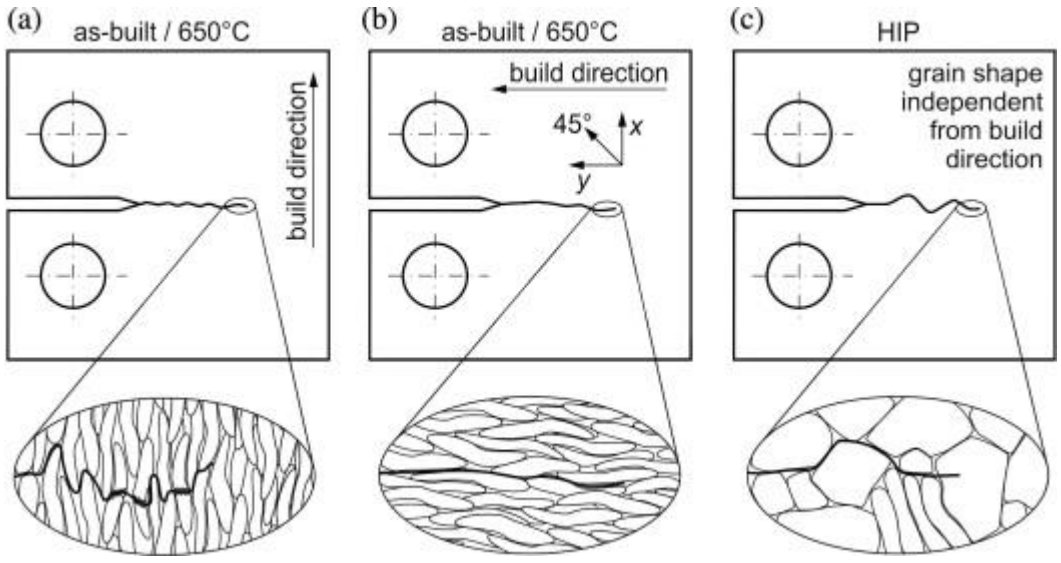

Figure 0.13. Schematic illustration depicting the effect of grain orientation and morphology on crack propagation. Reprinted with permission from Ref. [101]

d) Corrosion resistance

Austenitic stainless steels are widely employed in applications requiring resistance to pitting and crevice corrosion, such as marine engineering and medical implants [164]. The corrosion properties of stainless steels are known to be dependent on their microstructure and chemical composition [40]. Pitting corrosion events initiate near second-phase precipitates and alloy impurities such as manganese sulfide (MnS) inclusions [165]. MnS are a common impurities dispersed in the matrix of traditional austenitic SS that promote stable pit initiation and growth [166]. Regarding additively manufactured material, Sander et al. [167] found that SLM printed 316L is more resistant to stable pit initiation than wrought material, with a higher pitting potential and a lower metastable pit frequency. It is hypothesized that rapid solidification of the SLM process reduces the number and size of MnS inclusions. Accordingly, pitting susceptibility was lowered. This hypothesis was also confirmed by Chao et al. [165], which claimed that oxides/oxynitrides particles formed during the SLM process have a homogenous Cr composition and no MnS inclusions are present. However, the process's inherent porosity resulted in inferior repassivation. This is in agreement with other studies [168, 169]. Schaller et al. pointed out a significant enhancement in pitting potential of polished SLM 304L, far exceeding that of polished wrought 304L. Kong et al. [108] reported that SLM 316L, formed at high laser power ,showed a thicker passive film, higher pitting potential, and lower corrosion rate than the quenched 316L in simulated body fluid, which makes it a good candidate for biomedical implants. Laleh et al. [170] investigated the intergranular corrosion (ICG) resistance of SLM-produced 316L SS. The results reported in their work show a substantially higher IGC resistance of SLM 316L compared to its commercial counterpart. This behavior was related to the absence of localized Cr-depletion and the high number of fine grains with twin boundaries and low-angle grain boundaries.

The above-mentioned promising properties prove the efficiency of the SLM process in producing austenitic stainless steels with enhanced mechanical, fatigue, and corrosion properties, making them suitable for critical applications.

1.2.4.2 Martensitic and precipitation hardening stainless steels:

The martensitic family of stainless steels was developed mainly to satisfy the property requirements for high hardness, high strength, good wear resistance, and primary corrosion resistance [171]. They have an austenitic structure at high temperatures, but when quenched during heat treatment, a diffusionless transformation occurs spontaneously to from a martensite structure [107]. Unlike ferritic and austenitic stainless steels, they are very amenable to heat treatment as they can be hardened by quenching and then tempered to achieve improved ductility and toughness [34]. These properties make them suitable for a variety of applications like medical tools, valves, pumps, bearings, cutlery, razor blades, injection molds, etc. [172]. However, due to their relatively lower chromium content (normally between 11% and 18%), martensitic stainless steels are the most marginally corrosion resistant of all the stainless steel alloys; their field of application, in fact, is limited to only slightly aggressive environments [107].

The precipitation-hardening (PH) stainless steels are chromium-nickel grades that provide an optimum combination of the properties of martensitic and austenitic grades. The advantage of the PH alloys over the strictly martensitic stainless steels is that they attain great strength with higher toughness and higher corrosion resistance [107]. These improved properties are attributed to their higher chromium, nickel, and molybdenum contents, along with their restricted carbon level. PH stainless steels can be austenitic, semi-austenitic, or martensitic. However, martensitic PH steels are the most common in both traditional and additive manufacturing. They are strengthened by the precipitation of a coherent second phase during aging heat treatment. Copper (Cu) and niobium (Ni) are the main hardening elements in martensitic PH stainless steels [173].

Among these alloys, 17-4 PH and 15-5 PH are the most commonly used martensitic PH stainless steels in metal additive manufacturing due to their good weldability and their cost effectiveness [174]. These specific alloys are widely employed in the aerospace, marine, nuclear, chemical, and petrochemical fields [21]. Recently, a few studies have been

conducted on the fabrication of 420 martensitic stainless by the SLM process as a promising material in tooling applications such as injection molds [13, 175]. The chemical composition of the reviewed alloys is given in table 1.3. C-X stainless steel is another precipitation hardening stainless steel, recently developed and commercialized by EOS Gmbh [176]. However, due to the lack of literature dealing with it, CX steel will not be further discussed.

Table 0.3.

Chemical composition of martensitic stainless steel powders commonly used in SLM, Ref. [111]

Grade Name	Chemical Composition (wt.%)									
	Fe	Cr	Mn	Ni	C	Si	P	S	Cu	Nb
17-4 PH	Bal.	15-17.5	≤1.0	3.0-5.0	≤0.07	≤1.0	≤0.04	≤0.03	3.0-5.0	0.15-0.45
15-5 PH	Bal.	14-15.5	≤1.0	3.5-5.5	≤0.07	≤1.0	≤0.04	≤0.03	2.5-4.5	0.15-0.45
AISI 420	Bal.	12-14	<1.0	-	0.15-0.40	<1.0	<0.04	<0.03	-	-

In this section, the microstructure and performance of martensitic stainless steels processed by SLM will be discussed with a focus on precipitation hardening grades, particularly 17-4 PH and 15-5 PH SS, as they are the most researched in the literature. SLM of 420 martensitic steel will also be briefly discussed.

a) Microstructure of SLM-fabricated PH stainless steels

The microstructure of SLM-fabricated PH stainless steels consists of overlapping melt pools with epitaxial columnar grains and an inner fine cellular-dendritic structure oriented parallel to the direction of heat flow and towards the center of the melt pool [177-179]. In addition to the large columnar grains, fine equiaxed grains tend to form at the melt pool boundaries, as shown in Fig. 1.14a and b [29, 30, 180]. This microstructural refinement is supposed to be the effect of several thermal cycles and rapid cooling on the recrystallization and/or local transformation of grains in the heat-affected zone [29, 30].

Generally, no Cu-precipitates are observed in the as-built microstructure of PH stainless steels, whereas Mn-Si-rich oxide inclusions have been widely reported [21, 181]. Several investigations into the as-built microstructure of PH stainless steels revealed a strong fiber <001> crystallographic texture along the building direction (see Fig. 1.14(a,b)) [27, 29, 182]. However, texture-free material is also reported, especially when bidirectional or rotating scanning strategies are used [180, 181, 183].

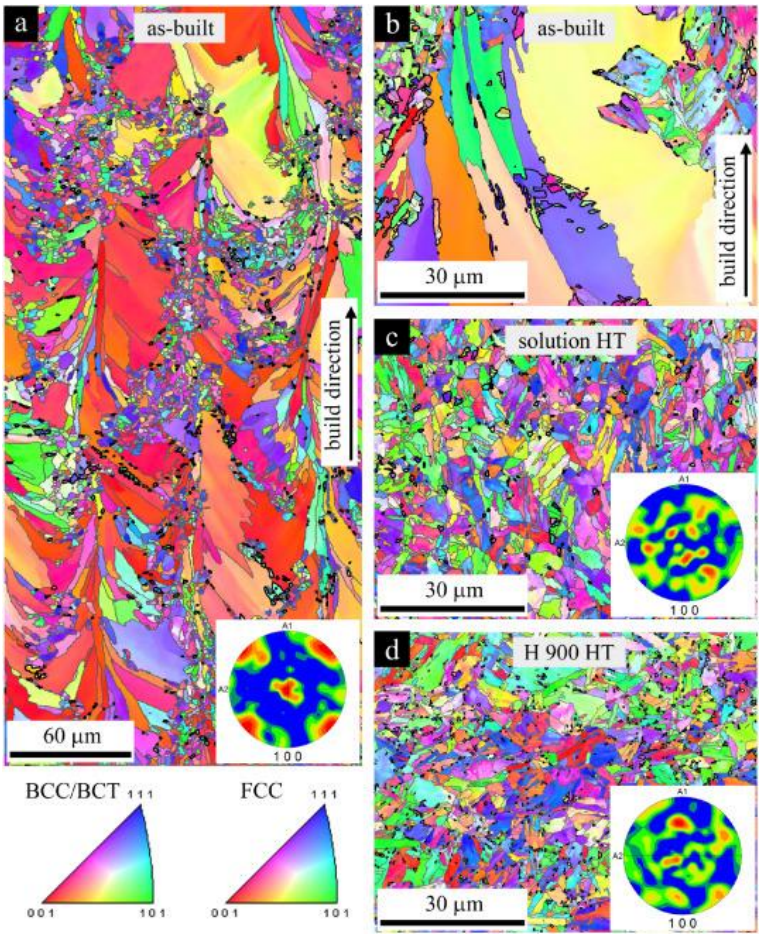

Figure 0.14. EBSD orientation maps obtained from SLM processed 17-4 PH SS in different conditions: (a,b) as-built sample, (c) solution heat-treated sample, (d) H900 heat-treated sample. FCC/BCC phase boundaries are highlighted with bold black lines. Reprented with permission from Ref. [29]

Unlike wrought PH stainless steels, which are fully martensitic, the SLM-fabricated PH stainless steels are said to comprise martensite, retained austenite, and even δ-ferrite. The

reviewed literature shows a great divergence among the results regarding phase composition and phase fractions of SLM-processed PH stainless steels. For instance, Facchini et al. [26] produced a mostly austenitic microstructure (72% austenite and 28% martensite) by selective laser melting of 17-4 PH stainless steel. Oppositely, Yadollahi et al. [18] and Nong et al. [53] reported a dominantly BCC martensitic structure with less than 7% of retained austenite in 17-4 PH and 15-5 PH SS, respectively.

It is known that due to the very low carbon concentration in PH alloys (<0.07%), the martensite exhibits a nearly BCC structure just like ferrite. Thus, the two phases cannot be distinguished by X-ray diffraction (XRD) and Electron Backscatter Diffraction (EBSD) [173]. Some recent studies [27, 29, 184] claimed that the predominant BCC phase of columnar grains in the as-built 17-4 PH stainless steel is ferrite rather than martensite because no characteristics of martensitic microstructure, such as martensite laths or large misorientations, are observed in these grains. In these studies, small martensite blocks are found to be formed at the melt pool boundaries in the fine-grained zone along with FCC equiaxed austenite grains [29, 30].

Several explanations for the high variability in the reported results have been proposed. Recent studies have revealed that the chemical composition of the precursor powder plays a crucial role in the solidification mode and the resulting microstructure. Given their high Cr_{eq}/Ni_{eq} ratio, martensitic PH stainless steels typically solidify as primary δ-ferrite from the liquid state. During solidification, the δ-ferrite phase transforms to austenite upon cooling below the solidus temperature due to solid-state diffusion. Subsequently, when the martensitic start temperature (Ms) is reached, austenite to martensite transformation occurs until room temperature [27]. However, due to the high cooling rates in the SLM process, the $\delta \rightarrow \gamma$ transformation cannot be completed or might even be by-passed and, therefore, the ferrite phase remains dominant at room temperature [27]. Vunnam et al. [182] demonstrated that ferrite to austenite transformation kinetics depend on the initial powder chemical composition, resulting in variability in the microstructure and phase composition in the as-built condition. It has been shown that the residual δ-ferrite volume fraction decreases with

decreasing the ratio Cr_{eq}/Ni_{eq} of the feedstock powder of PH stainless steels [182, 184]. On the other hand, the fraction of retained austenite compared to martensite has been of particular interest in the SLM of PH stainless steels as it strongly affects the mechanical properties. The retention of this metastable phase is commonly attributed to the large strain at grain boundaries, the high dislocation density, the fine grain size and interdendritic spacing, the concentrations of the alloying elements, and the supersaturation of the austenitic phase with stabilizing elements [177, 179]. Any of these factors would lower the Ms temperature to room temperature or below, which leads to the incomplete transformation of austenite to martensite [178]. In this context, several studies investigated the effects of atomizing medium and build chamber atmosphere on the final microstructure of PH stainless steels processed by SLM [179, 185, 186]. It has been shown that using nitrogen gas for powder atomization and/or as a shielding gas in the build chamber results in higher fractions of retained austenite. The formation of retained austenite appears to be likely due to the entrapment of nitrogen, which has an austenite stabilizing effect [179]. Additionally, microsegregation resulting from rapid cooling could also induce a localized concentration of austenite stabilizing elements such as Ni in the intercellular areas [173]. Variability in the retained austenite fractions in SLM processed PH stainless steels has been also related to other processing parameters such as scanning strategy [36, 53], and building direction [18, 180]. These studies revealed that the retained austenite concentration in SLM fabricated parts was affected by the thermal history. Nong et al. [53] studied the effect of different scanning strategies on the microstructure of SLM-fabricated 15-5 PH stainless steel. They found that complex thermal cycling and finer grain size in the island scanned led to larger amounts of retained austenite. In a recent study, Lv et al. [21] found that the austenite volume fraction in SLM 15-5 PH decreased with built height. These findings were explained by the fact that the bottom specimen (i.e., bottom layers) experienced an in-situ heat treatment due to thermal cycling promoted by the fusion of subsequent layers of material, which resulted in the reversion of martensite to austenite.

Several studies focused on the effect of heat treatment on SLM-processed PH stainless steels. Different standard and non-standard heat treatments were investigated. For wrought 17-4 PH and 15-5 PH, a solution heat treatment is typically applied in the austenitic domain (~1050 °C), followed by quenching, to obtain a fully martensitic structure. This solutionized condition is often referred to as 'condition A' (CA). A subsequent aging treatment in the range 480 °C - 620 °C is conducted, which results in precipitation hardening by copper precipitates. Precipitation begins with small and coherent spherical Cu-clusters with a BCC structure, which transform into elliptical incoherent FCC structure, called ε-Cu upon overaging [187]. Many studies reported that solution heat treatment relived the residual stress and homogenized the microstructure of SLM-fabricated PH stainless steels [29, 183, 188]. Sun et al. [29] found that solution heat treatment removed the <001> texture of the as-built microstructure and reduced the volume fraction of retained austenite, leading to a more conventional fully martensitic structure (Fig. 1.14). Their comparison between SLM and wrought material in condition A showed a similar microstructure with a finer grain size in the SLM heat-treated sample, which was attributed to the higher volume fraction of oxide inclusions and carbides that pinned grain boundaries. Nong et al. [188] reported that both SLM and wrought 15-5PH demonstrated a similar precipitation behavior for copper in size and volume density upon H900 standard heat treatment, as shown in Fig. 1.15. The amount of retained austenite is found to increase slightly during aging heat treatment due to the reversion of martensite. However, direct aging without prior solutionizing induced a higher fraction of reverted austenite due to the segregated austenite stabilizing elements in the as-built microstructure [181, 184].

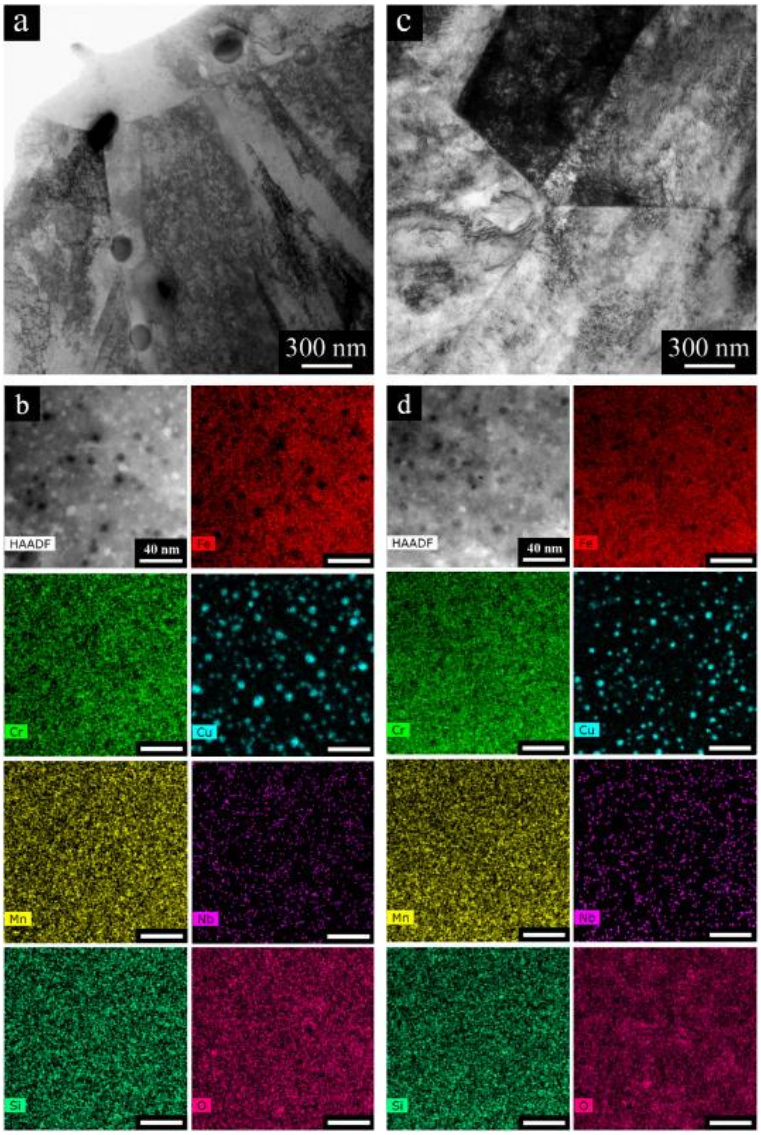

Figure 0.15. STEM data of the H900 aged SLM sample (a,b) and wrought sample (c,d). (a) and (c) lower magnification HAADF images; (b) and (d) higher magnification EDS maps showing similar precipitation behavior in both specimens. Reprinted with permission from Ref. [29]

b) Mechanical properties of as-built and heat treated PH stainless steels

The hardness and tensile properties of 15-5 PH and 17-4 PH martensitic stainless steels processed by SLM are summarized in Table 1.4. A large dispersion of the mechanical property values is observed due to the high variability in phase composition and phase

fractions discussed previously. In the as-built condition, PH stainless steels show lower strength and hardness compared to their peak-aged counterparts and superior elongation at failure. This behavior is related to the retained austenite and the absence of Cu-precipitates. LeBrun et al. [28] investigated the effect of retained austenite on the mechanical properties of SLMed 17-4 PH stainless steel. They found that tensile strength and hardness decrease with the increase in the volume fraction of the retained austenite, while ductility is enhanced due to the stress-induced transformation of metastable austenite to martensite [28]. An appropriate heat treatment is needed to enhance the strength of SLM-processed PH stainless steels by reducing the retained austenite and promoting precipitation of copper [18]. Following standard solutionizing and subsequent aging heat treatment at 480 °C for 1h (referred to as H900), SLM processed PH SSs exhibited higher yield strength, higher ultimate tensile strength, and higher hardness than those of aged conventional materials [28, 181, 188], due to the strengthening effect of coherent Cu precipitates and nano-oxide inclusions. However, elongation at failure after the same heat treatment is usually lower than that of wrought-aged counterparts due to early fracture from embedded porosity [28]. Li et al. [30] successfully obtained mechanical properties of SLM-manufactured 17-4 PH comparable to traditionally wrought material by tuning the homogenization heat treatment. A Solution heat treatment at 1150 °C for 1h followed by aging at 482 °C for 1h resulted in the best trade-off between strength and ductility, with an elongation of 10.5% and UTS of 1399 MPa. Several researchers investigated direct aging of SLM-processed PH SSs without prior solution heat treatment [19, 28, 180, 181]. It has been observed that direct-aged samples show a slight increase in strength and hardness and a pronounced work hardening capacity due to the high fraction of the retained austenite and limited precipitation hardening [181]. Overaging (H1150) increases ductility and reduces strength and hardness owing to the combined effect of coarsened Cu-precipitates and an increased amount of retained austenite [189].

Table 0.4.

Mechanical properties of martensitic PH stainless steels fabricated by SLM

Grade	Equipment	Condition	BD	Austenite volume fraction [%]	YS [MPa]	UTS [MPa]	El. [%]	H [HV]	Ref.
17-4 PH	EOS M270	600°C/2h	-	72	600	1300	28	380	[26]
17-4 PH	EOS M270	788°C/1h	H I	-	610 737	1072 914	7.2 8.6	-	[159]
17-4 PH	EOS M280	AB H900 H1025 H1150 CA CA-H900 CA-H1025 CA-H1150	H	36 40.5 10.4 5.6 0 3.3 4.7 20.7	661 945 870 1005 939 1352 1121 859	1255 1417 1358 1319 1188 1444 1172 1017	16.2 15.5 13.3 11.1 9.0 4.6 9.6 16.6	333 375 399 381 330 417 350 317	[28]
17-4 PH	EOS M270	AB 650°C/2h 788°C/2h 788°C/2h + H900	-	50 - - -	570 619 857 1126	944 915 1487 1457	50 12 7 12		[179]
17-4 PH	EOS M280	AB 1150°C/0.5h + H900 1150°C/1h + H900 1150°C/4h + H900 1150°C/8h + H900	H	-	784 1130 1280 1309 1165	922 1231 1399 1431 1239	16.7 6 10.5 7.2 9	328 426 466 470 438	[30]

17-4 PH	Self-developed machine	AB 788/2h 788/2h + H900 H900	H	6.2 1.5 5 17.9	803 966 1276 1173	1228 1268 1381 1478	12.7 8.8 13.6 9.8	365.4 420.1 488.6 453.2	[181]
17-4 PH	ProX 100	AB CA-H900	V H V H	3 7 - -	580 650 1020 1250	940 1060 1150 1410	5.8 14.5 2.8 11	-	[18]
15-5 PH	EOS M290	AB CA CA-H900 H900	V H V H V H V H	10 9.6 - - 18.6 15.4	-	-	-	377 381 328 336 430 444 462 455	[180]
15-5 PH	EOS M270	H900	V H	-	1100 1297	1467 1450	14.92 12.53	-	[190]
15-5 PH	EOS M270	AB CA-H900 CA-H1150	H	13	1050 1300 950	-	8.5 3.3 6.8	-	[189]
15-5 PH	SLM Solutions	AB CA-H900	-	10.8 1.92	625 1317	1143 1496	21.5 14.4	362.6 513.5	[188]
15-5 PH	HBD-280	AB	H	16.31	944	1230	20	380.6	[21]

Standard Reference Values

Grade	**Condition**	**YS [MPa]**	**UTS [MPa]**	**El. [%]**	**H [HRC]**	**Ref.**
17-4 PH	CA-H900	1170	1310	10	40	[191]
15-5 PH	CA-H900	1170	1310	10	40	[191]

AB: as-built state, CA: condition A state (≈1050° C for 0.5h followed by air or water-quenching); CA-H900 (condition A + aging at 482° C for 1h); H900 (aging at 482°C for 1h); H1025 (aging at 550°C for 4h); H1150 (aging at 620°C for 4h)

c) Fatigue properties of martensitic PH SSs processed by SLM

A few studies investigated the fatigue performance of SLM-fabricated 17-4 PH and 15-5 PH. The results indicated that the presence of process-induced defects such as lack of fusion, pores, and surface roughness is detrimental to fatigue life, resulting in lower fatigue strength compared to wrought material. Yadollahi et al. [18] and Sarkar et al. [192] investigated the effects of building orientation and different heat treatments on 17-4 PH and 15-5 PH, respectively. Building orientation was found to have a significant influence on fatigue properties. The lower fatigue strength of the vertically built specimens was mainly attributed to the higher stress concentration of defects being perpendicular to the loading axis [192]. Solution annealing and subsequent peak aging were beneficial for low cycle fatigue (LCF) but detrimental for high cycle fatigue (HCF) of PH SSs. This was ascribed to the fact that aged specimens become brittle and more sensitive to defects in HCF, where the crack initiation governs the fatigue life [18]. Nezhadfar et al. [193] investigated the effect of the shield gas on fatigue crack initiation and growth behavior of SLM 17−4 PH SS and demonstrated enhanced crack growth resistance and axial fatigue properties in the high cycle regime using nitrogen as a shielding gas. They revealed that the reason for this improvement is the finer microstructure, smaller defect size, and higher retained austenite fraction obtained under the N_2 atmosphere compared to Argon.

d) Corrosion resistance of SLM-processed martensitic PH SSs

According to the existent literature, SLM-fabricated 15-5 PH and 17-4 PH showed greater resistance to corrosion than wrought material [194-197]. Irrinki et al. [196] found that full-dense samples made from both gas-atomized and water-atomized 17-4 PH powders exhibited higher polarization resistance than the wrought sample. A recent study on the electrochemical behavior of SLM-processed 17-4 PH revealed a higher resistance to localized corrosion and pitting in 0.1 M NaCl solution and a more stable passive film compared to wrought material [195]. This improvement in the corrosion performance was related to the fine microstructure with homogenously distributed NbC precipitates and the

retained austenite enriched in nitrogen, which is known to have a beneficial influence on the corrosion resistance [194, 195]. Wang et al. [197] proved that retained austenite at the melt pool boundaries of SLM-built 15-5 PH has higher surface potential than martensite. Thus, samples that were directly aged (i.e., with a higher fraction of retained austenite) showed higher pitting potential and improved passive behavior compared to samples that were solutionnized before aging. Controversially, Sarkar et al. [19] investigated the effect different heat treatments on pitting corrosion of SLM 15-5 PH and found that samples aged without solution annealing corrode more the samples aged after annealing. This was attributed to the higher amount of chromium carbides in directly aged samples. Therefore, the corrosion performance of PH stainless steels needs to be more deeply elucidated in the future, since corrosion resistance is the primary characteristic for the use of stainless steels in various applications.

e) Selective laser melting of 420 martensitic stainless steel

420 stainless steel is a widely used material in tooling applications such as injection molds owing to its high strength, hardness and corrosion resistance. In the last decade, a growing interest has been addressed to SLM processed 420 stainless steel to take advantage of its geometrical flexibility. Zhao et al. [13] investigated the effect of process parameters on phase composition, density, and hardness of SLM 420 and claimed that it could meet the requirements of injection mold application with a relative density of 99 % and a hardness of 50.7 HRC. Krakhmalev et al. [198] demonstrated that thermal cycling caused in-situ partitioning and austenite reversion, resulting in a thermally decomposed martensite and high amount of austenite. A few studies investigated the microstructure and mechanical properties of SLM-fabricated 420 [37, 175, 199]. Despite the phase composition being a mixture of austenite and martensite, promising tensile strength and hardness are obtained, surpassing those of conventional material. The reported UTS is in the range of 1000-1697 MPa and elongation is in the range of 2.5 - 9.7% in the as-built condition. Low temperature tempering was found to improve yield strength, tensile strength, and elongation while maintaining good hardness (> 50 HRC) [175]. The fine microstructure with sub-micron martensite needles, the

austenite formation, and the transformation-induced plasticity (TRIP) were said to be the reason for these results [199].

1.2.4.3 Duplex stainless steels

Duplex stainless steels (DSS) are a subgroup of the stainless steel family. These are referred to as duplex grades due to the fact that their metallurgical structure is composed of two phases, austenite and ferrite, in about equal proportions. The high chromium concentration provides high corrosion resistance [200], austenite phase contributes to toughness, whereas the presence of ferrite enhances strength [201]. Bi-phase steels have greater ductility than ferritic stainless steels and greater strength and welding capability than austenitic stainless steels. DSS exhibits superior corrosion resistance over both mono-phase stainless steels, owing mostly to the presence of Cr and Mo [201-203].

Duplex stainless steel has a reduced molybdenum and nickel content, which makes it more affordable [107]. Duplex stainless steel can be utilized in a wide range of applications, including chemical processing, oil and gas pipelines for production and transmission, offshore oil and gas drilling and exploration [204]. In general, the application is in competition with higher alloy austenitic grades in harsh environmental conditions with significant mechanical loads.

Publications regarding SLM of DSS grades are quite limited. SAF 2205 and SAF 2507 are the most commonly studies DSS; their chemical compositions are given in Table 1.5. Fatigue properties are not reported since no data are available in the literature in this field.

Table 0.5.

Chemical composition of duplex stainless steels commonly used in SLM, Ref. [111].

Grade Name	Chemical Composition (wt.%)										
	Fe	Cr	Ni	Mo	Mn	Si	C	S	P	N	Cu
2205 (S32205)	Bal.	22	5	3.2	≤2.0	≤1.0	≤0.03	≤0.015	≤0.03	0.18	-
2507 (S3270)	Bal.	25	7	4	≤1.2	≤0.8	≤0.03	≤0.015	≤0.025	0.3	0.5

a) As-built microstructure of SLM-processed duplex stainless steel

According to the SLM process parameters, the morphological and crystallographic texture as well as the average grain size are greatly impacted by the laser power, scanning speed, and volumetric energy density [205]. Saeidi et al. [201] reported a macro-textured mosaic structure with square-like grains in SLM-processed SAF2507. UNS S31803 (SAF 2205) DSS, however, exhibits a columnar grain morphology oriented toward the building direction, which corresponds to the maximum heat flux toward its base plate [204, 206]. These long grains, which are spread across several layers, show that epitaxial grain growth is taking place. However, the epitaxial microstructure is often slowed down at the solidification front by a new grain with random crystallographic orientations, which leads to a more isotropic microstructure [204]. For the as-built state, the temperature gradient and solidification velocity resulted in a completely ferritic phase [201, 204, 206]. As in welding, the rapid cooling rate of 10^4 K/s to 10^6 K/s in SLM results in a complete primary solidification of delta ferrite. Furthermore, austenite and subsequent precipitations are almost completely suppressed in the as-built state [207]. Mirz et al. [208] investigated the effect of building chamber atmosphere on the phase composition of DSS, no substantial differences were observed in the as-built microstructure. Both argon and nitrogen atmosphere resulted in a fully ferritic structure. A high dislocation density is typically observed, like in other metals processed by SLM. It could be justified by quick solidification and self-quenching [201, 204, 209]. In addition to the dislocation loops, chromium nitrides and isothermal nitrides have been seen in the grain interior. The choromium nitrides are believed to develop straight from

the melt pool, also known as quenched-in-nitrides, because of nitrogen's higher solubility in austenite than in ferrite, at high cooling rates. Nitrogen has insufficient time to diffuse or contribute to any austenite stabilization; as a result, some nitrogen forms the nitride phase. The isothermal nitride is a result of intrinsic heat treatment due to the thermal cycling occurring during the SLM process. In addition, fine secondary austenite grains form at grain boundaries as a result of this annealing effect. Secondary austenite and the sigma phase develop from delta ferrite in the following sequence: $\delta \rightarrow \gamma_2 + \sigma$ [201, 204].

When it comes to comparing conventional DSS with SLM processed ones, in conventional DSS, austenite nucleation occurs by static or dynamic recrystallization of the ferritic matrix [210, 211]. An annealing heat treatment can be used to alter the phase composition and redistribute alloying elements between the ferrite and austenite phases [212]. However, in the as-built condition of the SLM-manufactured DSS, austenite production is virtually completely suppressed because of process-related high cooling rates [201, 204].

b) Microstructure of SLM-processed duplex stainless steel after heat treatment

Annealing is a frequent post-treatment for duplex stainless steel. Additionally, studies indicate that the as-built DSS has a pure ferritic phase and that the ferrite/austenite phase ratio can reach a value extremely near to one upon annealing [213-215]. Several heat treatments at temperatures ranging from 900 °C to 1200 °C for 5 minutes each were used to achieve the required austenitic-ferritic microstructure. The high dislocation density of the as-built microstructure promoted a complete recrystallization following heat treatment, based on the formation and motion of high angle grain boundaries. Recrystallization is also determined by the considerable shift in crystallographic and morphologic orientation of the microstructure [204]. In SLMed specimens, similar to normal duplex stainless steel, secondary austenite nucleation occurs during annealing and the formation is temperature dependent. When annealing is performed at a lower temperature (about 900 °C), fine intergranular secondary austenite regions form in the ferritic matrix due to ferrite stabilising

elements such as Cr and Mo being bonded by intermetallic phases such as carbides or nitrides [202, 216]. Secondary austenite occurs largely near ferritic grain boundaries at higher annealing temperatures (about 1200 °C). At this temperature, a coarse-grained delta ferritic microstructure forms; then, secondary austenite nucleates only at recrystallized delta ferritic grain boundaries. Annealing at 1000 °C resulted in the greatest volume fraction of austenite of 34%. This volume decreases when the annealing temperature is increased or decreased (see Fig. 1.16) [202, 204]. Papula et al. [206] found that maximal austenite fraction (46,4 vol%) occurs at high annealing temperatures in the range of 1000 °C-1050 °C for longer annealing time (60min) for the 2205 DSS grade. Annealing reactivates the metastable ferrite to austenite transition that was inhibited by rapid cooling. It has been found that increased annealing temperature results in the transition of more metastable ferrite into austenite, whereas thermodynamic equilibrium promotes the transformation of austenite into ferrite [206]. Annealing of SLM-fabricated UNS S32707 at a temperature range of 1050 °C to 1200 °C for one hour indicates that a good balance between the two phases could be reached at 1100 °C. As the temperature further increases, the ferrite phase percentage increases from 59.5 % to 63.4 % for 1100 and 1200 ° C, respectively [217].

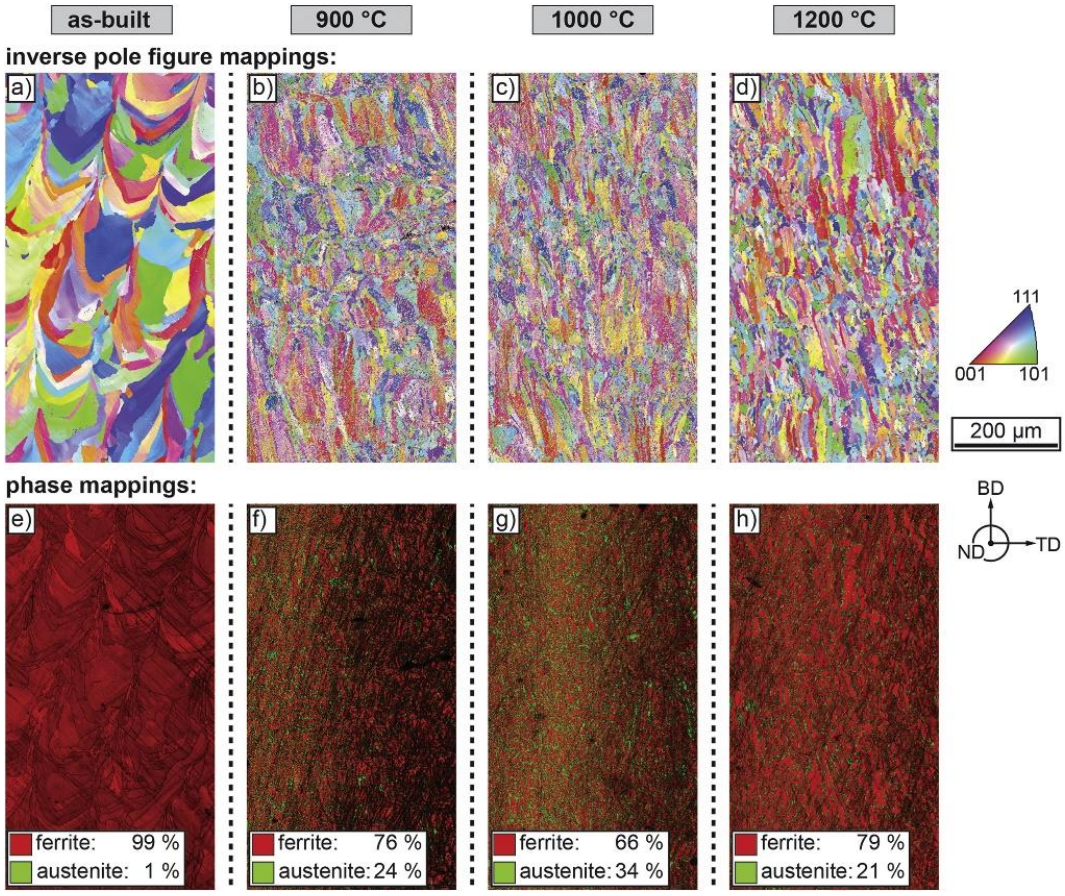

Figure 0.16. EBSD maps: (a)-(d) inverse pole figure maps, (e)-(h) corresponding phase maps of the as-built and solution annealed samples, showing evolution of austenite phase with heat treatment temperature. Reprinted with permission from Ref. [204]

c) Tensile behavior of duplex stainless steel

Tensile tests show that heat treatment has a significant impact on the final mechanical response. When compared to heat-treated specimens, the nearly complete ferritic as-built specimens have a higher ultimate tensile strength and a lower elongation at fracture [206], as can be seen in Fig. 1.17. This behavior could be explained by nitride precipitation as well as nano-sized dislocations in as-built specimens that hinder dislocation movement, resulting in higher strength. Different crystalline grain orientations, as well as boundary impurities and precipitates, prevent slip/slide effects [201]. The best combination of strength and elongation was obtained after annealing at 1000 °C [204]. When compared to the conventionally

produced material with a similar chemical composition, the SLM-processed and heat-treated 2205 DSS had significantly higher microhardness (255–280 HV1), yield strength (520–560 MPa), and tensile strength (810–870 MPa), while uniform elongation was in a similar range (23–25 percent) [206]. SLM-processed UNS S32707 DSS grade showed the best comprehensive mechanical properties after annealing at 1150°. The measured tensile strength, yield strength, elongation, section shrinkage, microhardness, and impact absorption energy, in this condition, were 901 MPa, 658 MPa, 36.4 percent, 48.4 percent, 291.5 HV, and 132 J, respectively [217]. According to [208], hot isostatic pressing has a significant influence on tensile behavior, as it reduces the porosity of SLM specimens. The ultimate tensile strength increased to 724.9 MPa by HIP post-treatment followed by solution annealing at 1080 °C for 60 min, while the value for the only annealed sample is 692.2 MPa.

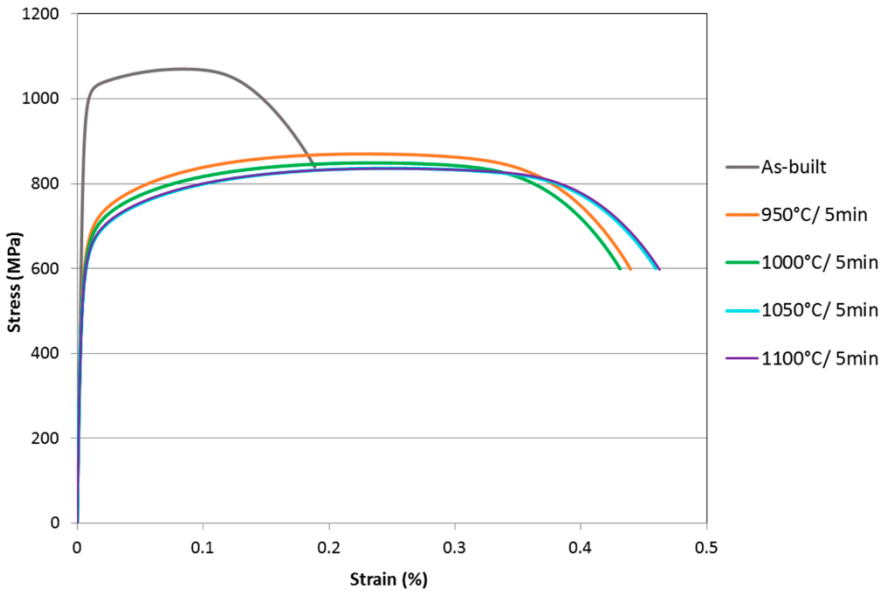

Figure 0.17. Stress stain curve for 2205 DSS processed by SLM in the as-built and annealed conditions, Ref. [206].

d) Corrosion behavior

The results of a study on the effect of building direction and annealing on SLM-processed 2205 duplex stainless steel indicate that the build orientation and annealing were

not as important as the chemical composition in predicting passivity and pitting resistance [213]. In contrast, Papula et al. [206] observed that annealing heat treatment increased the pitting corrosion resistance of the as-built SLM-processed material. The study of annealing temperatures (1050 °C-1200 °C) on UNS S32707 grade reveals that pitting resistance for as-built material would be improved in the annealing solution, with the maximum pitting resistance occurring at 1100 °C [217].

1.2.4.4 Ferritic stainless steels

Ferritic stainless steel refers to the class of stainless alloys with chromium concentration between 10.5 % and 30 % and less than 0.20 % carbon. These allays are not heat treatable and the only method to harden them is cold rolling [34]. Thanks to their superior chloride stress-corrosion resistance, smaller linear expansion, higher thermal conductivity, and lower cost compared to austenitic stainless steel, ferritic stainless steels are frequently used in the construction [218] and in safety-related applications such as reactor pressure vessels, steam generators, valves, and pipes [219].

Oxide dispersion strengthened (ODS) steels are ferritic stainless steels that contain a fine dispersion of Y, Ti, Nb oxides in the ferritic matrix, improving their high-temperature strength and creep strength [220]. They are used for high temperature applications such as turbine blades and heat exchanger tubing [221]. ODS steels are usually processed using powder metallurgy methods. Stainless steel powder is mechanically alloyed with oxide powder. The powder mixture is then consolidated by HIP or hot extrusion [219]. Since their conventional processing is difficult, production of ODS using SLM process is attracting the interest of researchers. However, the use of ferritic stainless steels in SLM process is still in its early stage, with little available studies in the topic. PM2000 alloy and FeCrAl are the some of the common ODS alloys used in AM [222].

a) Microstructure of ferritic stainless steels

Microstructural evolution of ferritic stainless steels at various process parameters during the SLM process has received little attention. A study by Jiang et al. [218] investigates the microstructure, microhardness, and corrosion behavior of ferritic stainless steel by varying laser power, scan speed and hatching distance. The as-built microstructure was mainly composed of α-Fe and a small amount of $Cr_{23}C_6$. A cellular morphological structure was visible in the microstructure of the SLM specimens with a random crystallographic texture. Scanning speed had a significant effect on microstructure; its increase resulted in finer grain size, a smaller amount of $Cr_{23}C_6$, a larger proportion of LAGBs, and a higher dislocation density. Karlsson et al. [221] compared SLM-produced 441 ferritic stainless steel with its cast and hot-rolled counterpart. A significant difference was observed with an anisotropic and finer microstructure containing Ti and O-rich precipitates. In contrast, cast and hot rolled samples showed coarser grains with TiN and Nb(C,N) precipitates. Similar precipitation behavior was observed in SLM fabricated Fe-14Cr ODS SS, where only Y-Ti-O were observed without the presence of carbides, titanium or aluminum oxides, which are typically present in conventional ODS SSs [219]. However, the SLM built microstructure in this study was coarser than that of conventional ODS.

b) Mechanical properties of SLM-processed ferritic stainless steels

Very limited data is available in the literature about the mechanical properties of ferritic stainless steels. Boegelein et al. [223] investigated the tensile properties of thin-walled builds made of SLM-processed ODS-PM2000. They showed that post-build annealing at 1200 °C for 1 hour improved the yield strength, which became comparable to that of conventional material.

Another study comparing SLM ferritic stainless steel SS441 to hot-rolled alloy demonstrates improved mechanical properties of SLM-printed material, with more than 30 times higher impact energy. The enhanced mechanical properties of the SLMed sample were

attributed to a smaller grain size, which resulted in a greater Hall-Petch strength. The results proved definitively that SLM is a viable manufacturing process for ferritic stainless steels with increased strength [221]

1.2.5 Summary and outlook

Stainless steels are in high demand in almost all industrial sectors due to their widespread supply chain, their non-reactive nature, and their relatively low cost. Therefore, their use in additive manufacturing is receiving significant attention. Selective laser melting is one of the most popular and fastest growing additive manufacturing technologies. This review underlines the potential of the SLM process to produce fully-dense near-net-shape parts with promising properties using different grades of stainless steel. These achievements, along with SLM's abilities to produce customized components, complex geometries, and lightweight structures, contribute to the wide adoption of the SLM process in stainless steel production. The published research on SLM of stainless steels reflects the opportunities and challenges of this processing route. Diverse stainless steel grades belonging to different classes (i.e. austenitic, martensitic, precipitation hardening, and duplex) have been addressed in the literature, with the majority of papers focused on 316L austenitic stainless steel. The following is a summary of the most important findings from the extant literature on SLM of stainless steels:

- Using optimized process parameters, defect-free parts made from stainless steel can be processed routinely. A less than 0.1% of porosity can exist with no detrimental effect on monotonic and cyclic mechanical behavior.

- The fast cooling rate and directional temperature gradient of the SLM process result in a hierarchical microstructure with a considerable volume fraction of nano-inclusions and a strong crystallographic <100> texture along the building direction.

- For martensitic, precipitation hardening, and duplex stainless steels, significant changes are observed in the phase composition of the SLM-built microstructure

compared to the conventional materials. This is mainly attributed to the high cooling rate, which may alter the primary solidification mode and make solid-state phase transformations unachievable or incomplete. A heat treatment is usually required to achieve the intended microstructure.

- SLM-produced stainless steels typically exhibit comparable or even higher hardness and tensile strength than those of conventionally processed counterparts due to the fine grain size, hierarchical microstructure features and ODS effect of nano-inclusions. Although ductility seems to be negatively affected by process-induced porosity, good combinations of strength and ductility have been achieved either by in-situ tailored microstructure or by post-heat treatment.

- Being brittle, thus, more sensitive to defects under cycling loading, martensitic PH SSs showed poor fatigue properties. Whereas SLM austenitic stainless steel had more defect-tolerant behavior, resulting in satisfactory fatigue resistance thanks to their ductility. In both cases, surface machining seems to be necessary to matchthe fatigue properties of conventional material.

- The corrosion resistance of SLM-fabricated stainless steels is generally better than that of conventionally produced material. However, the mechanisms behind these enhanced properties are not well addressed in the literature and need to be clarified in the future.

Despite the significant effort that has been undertaken in the field of SLM of stainless steel so far, there are a number of challenges that still need to be addressed. In-process routes to minimise defect formation, reduce residual stresses and control anisotropy are essential for the progression of SLM as a single-step process with reduced production time and cost. Moreover, when post-heat treatment is inevitable, such as for precipitation hardenable stainless steels, optimised heat treatment processes are required since standard ones are not designed for SLM-processed stainless steels. Furthermore, the high divergence of SLM-produced stainless steel properties reflects a lack of control over the attained microstructure.

Thus, a deeper understanding of the process-structure-property relationships is required to achieve repeatability and reliability in the SLM process of stainless steels. These steps will pave the way towards the standardization and qualification of SLM-fabricated components and hence their widespread adoption in different applications. Finally, despite their popularity in additive manufacturing, there is a very narrow group of stainless steels that are commonly printed today compared to the vastness of stainless steel currently processed by traditional manufacturing techniques. A new range of stainless steel grades should be explored and developed to take advantage of the SLM process particularities such as the high cooling rate, the intrinsic heat treatment, and the opportunity to tailor microstructure. These challenges define the path for further research and exploitation.

CHAPITRE 2
EFFET DES PARAMÈTRES DE PROCÉDÉ DE FUSION SÉLECTIVE AU LASER SUR LA DENSITÉ, LA RUGOSITÉ DE SURFACE, ET LES PROPRIÉTÉS MÉCANIQUES DE L'ACIER INOXYDABLE 316L

A. Mansoura[1], N. Barka[1], S.S. Kangranroudi[2]

[1] Université du Québec à Rimouski, Québec, Canada

[2] Université du Québec à Trois-Rivières, Québec, Canada

2.1 RESUME EN FRANÇAIS DU DEUXIEME ARTICLE

La fusion sélective au laser (SLM) est une technique de fabrication additive métallique prometteuse pour la production de composants de hautes performances. Cette technique couche par couche implique l'interaction de divers paramètres de processus. Les modèles prédictifs des performances de l'acier inoxydable 316L fabriqué par SLM en fonction des paramètres les plus influents manquent encore de recherches approfondies. Dans la présente étude, une méthodologie systématique basée sur la méthode de Taguchi et l'analyse de la variance (ANOVA) a été utilisée pour l'optimisation paramétrique du procédé SLM de l'acier inoxydable 316L. Une matrice orthogonale L_9 a été utilisée pour définir un plan expérimental, en tenant compte de la puissance laser, de l'espacement des hachures et de la vitesse de balayage comme paramètres d'entrée, avec trois niveaux pour chacun. Des mesures de microstructure et de porosité ont été réalisées par microscopie optique. Des grains colonnaires s'étendant sur plusieurs couches ont été observés avec une structure cellulaire interne. Les variables de réponse suivantes : densité relative, rugosité de surface, dureté et propriétés mécaniques de traction ont été mesurées. Des niveaux de densification

globalement élevés (jusqu'à 99,97 %) et d'excellentes propriétés mécaniques dépassant celles de l'acier inoxydable 316L produit de manière conventionnelle ont été atteints. L'échantillon construit à P = 170 W, h = 0,08 mm et v = 1000 mm/s (c'est-à-dire une densité d'énergie de 53 J/mm^3) présentait les propriétés de traction les plus élevées avec une limite d'élasticité de 421 MPa, une dureté de 245 HV et un allongement à la rupture de 42 %. L'analyse de la variance des données expérimentales nous a permis de déterminer l'ordre de signification des facteurs les plus influents et de leurs interactions sur chaque variable de réponse. Pour la plage de variation étudiée dans ce travail, l'espacement des hachures s'est avéré être le paramètre le plus influent sur la densité relative et les propriétés mécaniques qui en résultent. L'augmentation de la puissance laser et de l'espacement des hachures a nui à la qualité de la pièce finale en raison du niveau élevé de porosité. Des modèles de régression et des tracés de contour RSM ont également été présentés. Les résultats de cette recherche peuvent être utilisés pour prédire et optimiser avec précision les performances de l'acier inoxydable 316L traité par SLM.

Cet article, intitulé « *Effect of Process Parameters on Density, Surface Roughness, and Mechanical Properties of 316L Stainless Steel Fabricated by Selective Laser Melting* », a été soumis au *Journal of Manufacturing Processes*. En tant que première auteure, ma contribution consiste à la recherche de l'état de l'art, la réalisation des tests expérimentaux, l'analyse statistique, l'interprétation des résultats, et la rédaction du manuscrit. Le professeur Noureddine Barka, deuxième auteur, a fourni l'idée originale, développé la méthodologie et a révisé l'article. Sasan Sattarpanah Kangranroudi, troisième auteur, a également contribué au développement de la méthodologie et à la révision de l'article.

2.2 EFFECT OF PROCESS PARAMETERS ON DENSITY, SURFACE ROUGHNESS AND MECHANICAL PROPERTIES OF 316L STAINLESS STEEL FABRICATED BY SELECTIVE LASER MELTING

2.2.1 Abstract

Selective laser melting (SLM) is a promising metal additive manufacturing technique for the production of high-performance components. The layer-by-layer technique involves the interaction of various process parameters. Predictive models for the performance of SLM processed 316L SS with respect to the most influential factors still lack deep research. In the current study, a systematic methodology based on Taguchi design and Analysis of Variance (ANOVA) has been employed for parametric optimization of the SLM processing of 316L stainless steel. An L9 orthogonal array was used to set an experimental plan, considering laser power, hatch spacing, and scan speed as input parameters, with three levels for each. Microstructure and porosity measurements were carried out using optical microscopy. Columnar grains extending over several layers were observed with an inner cellular structure. The following response variables: relative density, surface roughness, hardness, and tensile properties were measured. Overall high densification levels (up to 99.97%) and excellent mechanical properties exceeding those of conventionally processed 316L SS have been achieved. The sample built at P=170W, h=0.08mm, and v=1000 mm/s (i.e., an energy density of 53 J/mm^3) exhibited the highest tensile properties with a yield strength of 421 MPa, a hardness of 245 HV and an elongation at failure of 42%. Analysis of variance of experimental data allowed us to determine the order of significance of the most influential factors and their interactions on each response variable. For the variation range investigated in this study, hatch spacing has been found to be the most significant parameters on relative density and resultant mechanical properties. Increasing laser power and hatch spacing was detrimental to final part quality due to the high level of porosity. Regression models and RSM contour plots were also presented. The results of this research can be used as design tools to accurately predict and optimize the performance of 316L SS processed by SLM.

Keywords: Selective laser melting, 316L stainless steel, ANOVA, Taguchi, mechanical properties

2.2.2 Introduction

Metal additive manufacturing is advancing rapidly to meet current industry requirements. Initially proposed for rapid prototyping, AM technologies are nowadays used for the production of functional and structural components with complex geometries, integrated functionalities, and tailored structure [8, 38]. The growing interest of researchers and industries for this revolutionary technology led to the emergence of several AM systems such as direct energy deposition (DED), electron beam melting (EBM), selective laser melting (SLM), binder jetting (BIJ), etc. [224]. Of these, selective laser melting is one of the most powerful and most versatile AM systems due to its ability to process a wide range of materials and produce fully dense parts with high dimensional accuracy and high-resolution features [8, 225].

SLM is a powder-bed fusion process that uses a laser beam to selectively melt and fuse metal powder layer-by-layer, as dictated by the CAD data. This unique feature of building parts directly from 3D CAD model promotes flexibility in design, functional integration, part customization, elimination of fixturing and tooling costs, short lead-time, material saving, weight reduction, and elimination of multiple process steps, compared to conventional processing techniques [2, 3]. These advantages make it a leading candidate for manufacturing of mission-critical components for aerospace, medical, energy and automotive applications [9, 49].

To date, a variety of engineering materials including titanium alloys, ferrous alloys, aluminium alloys, nickel alloys, composites, etc., have been successfully processed via SLM, yielding a relative density of 99% or higher [9]. However, many challenges have to be solved before it can become widely adopted in the industrial sector. In fact, SLM process undergoes

complicated physical phenomenon, which may affect the process stability and lead to defect formation such as balling, keyholing, and surface roughness [11]. Moreover, the rapid cooling, high thermal gradient and complex thermal history experienced by the solidified material results in an anisotropic non-equilibrium microstructure [226]. Both defects and microstructural features control the mechanical properties of the final part [101, 227]. Hence, a clear understanding of process-structure-property relationship is essential to build defect-free part and achieve desired properties.

316L austenitic stainless steel is highly attractive in various areas such as marine, chemical, petrochemical, biomedical, and aerospace industries due to its excellent corrosion resistance, high toughness, good cost-effect and biocompatibility [5, 227]. Moreover, 316L SS has a good processability and is widely available in the powder form. Therefore, SLM processing of 316L SS is being extensively investigated to fulfil the demand for the fabrication of complex parts with refined microstructure and enhanced mechanical properties for high-value applications.

Numerous studies have been devoted to understanding the effect of process parameters as key variables in SLM to control the material properties. Cherry et al. [155] investigated the influence of energy density in the range of 41-209 J/mm^3 on porosity, hardness, and surface roughness of SLM-fabricated 316L SS. A high porosity level was observed when energy density was either too high or too low. An optimal density of 99.6% was achieved at an energy density of 105 J/mm^3. Hardness is shown to increase with decreased porosity. Tucho et al. [129] observed a similar trend of a decrease in porosity leading to higher hardness. Energy density was found to be the most influential parameter in controlling porosity and hardness of SLM-fabricated 316L SS. The authors also indicated that larger hatch spacing promotes increased porosity. Liverani et al. [62] focused on the individual effects of laser power, hatch spacing, and building direction on the resulting microstructure and mechanical properties. They found that laser power had the strongest effect on part density, whereas mechanical properties were mainly influenced by building direction. Greco et al. [228] studied the correlation between process parameters and part quality at constant

energy density. Their findings showed that increased laser power had a positive effect on relative density and hardness and a negative effect on surface roughness. The authors claimed that energy density alone is not a good indicator of the resulting characteristics.

Though there are many investigations into SLMed 316L, most of them focus on the influence of energy density on part quality. However, SLM is a complex multi-factor process, which is influenced by several parameters. Simple correlations drawn from experimental results without systematic analysis would not be effective for process optimization. Moreover, analyzing and optimizing all factors by conducting conventional experiments can be exhaustive due to the large number of required experiments [22].

Alternatively, the use of design of experiment techniques (DOE) such as the Taguchi method and statistical analysis such as analysis of variance (ANOVA) and Response surface Method (RSM) are known to be powerful techniques to determine the relationship between process parameters and performance characteristics [23].

Limited research papers used this approach to investigate the influence of process parameters on the performance of SLM-fabricated 316L stainless steel. Miranda et al. [24] used ANOVA and linear regression to determine the main significant factors and their interactions in the SLM process of 316L SS. Their study was limited to density, hardness, and shear strength. Jiang et al. [25] evaluated the influence of laser power, hatch spacing, and scan speed and their order of significance on surface roughness, hardness, and density of 316L SS fabricated via SLM, but did not develop predictive models.

Therefore, this work aims to statistically analyze and predict the effects of laser power, hatch spacing, and scanning speed and their interactions on relative density, surface roughness, hardness, and tensile properties (i.e., strength and ductility).

Systematic methodology using Taguchi design, ANOVA, and linear regression was applied to determine the significant factors and develop empirical predictive models for response variables. RSM contour plots were used to localize optimum processing parameters for 316L SS.

2.2.3 Materials and methods

2.2.3.1 Design of experiment

Design of experiments (DOE) is an effective strategy for determining the correlation between the input parameters influencing a process and the examined outputs of that process [22]. The Taguchi technique uses a special design of orthogonal arrays to examine the entire parameter space with a limited number of tests [229]. Selection of the design parameters is the first step for Taguchi design. It is well known that the SLM process is defined by a very large number of parameters [11]. However previous studies showed that laser power P (W), scan speed v (mm/s), hatch spacing h (mm), and layer thickness t (µm) are among the most influential parameters [25, 57, 129]. Alternatively, volumetric energy density E (in J/mm^3) has been widely used to assess the combined effect of the aforementioned parameters [118]. It is given by the following equation:

$$E = \frac{P}{v\,h\,t}$$

In this study, P, v, and h were selected as factors, while t was maintained constant. Three levels are denoted for each factor as presented in Table 2.1. The L_9 orthogonal array is thus a suitable experimental design for this study. The levels were defined by making a relatively small variation around the optimum set of parameters recommended by the machine manufacturer (P = 195 W, v = 1000 mm/s, h = 0.1 mm). Thus, the sensitivity of the SLM process to the variation of these parameters can be investigated while maintaining stable melting and avoiding critical issues such as balling or keyhole mode.

Table 0.1.

Factors and levels used for Taguchi design

Parameters	**Symbols**		**Levels**	
Laser power (W)	P	170	195	220
Scanning Speed (mm/s)	V	1000	1050	1100
Hatch spacing (mm)	h	0.08	0.10	0.12

2.2.3.2 Material and SLM processing

Gas atomized EOS 316L stainless steel powder, with chemical composition given in Table 2.2, was used as a feedstock material in SLM experiments. The powder particles have a spherical shape, and their size distribution ranges from 20 to 65 µm.

The fabrication of samples was carried out on an EOS M 290 system equipped with a Yb-fiber laser with a beam diameter of 0.1 mm. The printing was done under an argon atmosphere to prevent oxidation. For each parametric condition, three sub-sized rectangular tensile specimens were prepared according to ASTM-E8, i.e. 27 samples are tested in total to reduce errors and increase the precision in analysis and optimization. The layer thickness was kept constant at 40µm. A stripe scanning strategy was adopted with a scan rotation angle of 67°.

Table 0.2.

Chemical composition of EOS 316L stainless steel powder

Element	**Fe**	**Cr**	**C**	**Ni**	**Mo**	**Mn**	**Si**	**P**	**S**	**N**
Content (wt.%)	Bal.	17.0-19.0	≤0.03	13.0-15.0	2.25-3.0	≤1.0	≤1.0	≤0.045	≤0.035	≤0.1

2.2.3.3 Samples characterization

Surface Roughness (Ra) measurements were taken using Mitutoyo Formtracer SV-C3100 machine on the side surface of tensile samples after being sandblasted. The average values of three roughness measurements for each experimental condition are used for statistical analysis. Nine metallographic samples were cut parallel to the building direction (i.e., in the transverse plane), mounted in epoxy and polished to a 0.05µm finish.

Before etching, five images were recorded using Optical Microscopy (OM) at different locations on each specimen. ImageJ, a license-free software, was used to analyse images and determine the percentage of porosity. Relative density (RD) is thus calculated.

To reveal the microstructure, samples were then etched using Glyceregia reagent (15 mL HCl + 10 mL Glycerol + 5 mL HNO_3) for few minutes. Microstructural analysis was carried out using a Clemex Vision-Lite Microscope.

2.2.3.4 Mechanical testing

Vickers hardness testing was performed using a Clemex machine. For each sample, the mean hardness value (Hv) is determined by averaging 20 indentation measurements spaced at 200 µm and performed along the surface's diagonal. The applied load was 0.5 kgf and the dwell time was 10 seconds.

Room temperature tensile tests were carried out on rectangular cross-section specimens (6 mm x 3 mm) with a 25 mm gauge length using MTS-810 tensile testing machine according to ASTM E8 standard. The specimens were tested until rupture using a constant crosshead speed of 0.035 mm/s. The elongation of the tensile specimens during testing was measured by an extensometer.

2.2.3.5 Statistical analysis

After experimental data has been collected, a systematic approach using powerful statistical tools had been conducted to analyze the effect of process parameters on density, surface roughness, microhardness, and tensile properties of 316L stainless steel. Analysis of Variance (ANOVA) is used to investigate which process parameters have a significant effect on the quality characteristics [229]. The initial model included independent variables (P, v, h), quadratic variables (P^2, v^2, h^2) and two-way interactions $(P \times v, P \times h, v \times h)$. Statistically significant factors are determined using the F-test and/or p-value. Comparing p-value with the fixed significance level (α) determines whether the null hypothesis can be rejected or not. The null hypothesis, in this case, states that the effect of the considered factor is not significant on the output response $(RD, Ra, HV, YS, UTS, El.)$ of 316L stainless steel produced by SLM. The null hypothesis is rejected when the computed p-value is less than the designated significance level. In this study, the significance level was set at α = 0.05. The factor's influence can also be quantified by its percentage contribution. ANOVA was performed using Minitab 19 statistical analysis software according to the general stepwise method so that only significant factors are kept in the final model for each output response. Response surface methodology (RSM) is a statistical method used for modeling and analyzing the correlation between the input parameters and output responses [24]. In this method, the main objective is to optimise the response surface, which is a function of the process parameters. The mathematical models for the output responses as a function of selected variables were developed by applying multiple regression analysis to the experimental data. The general quadratic equation model is stated by [230]:

$$y = \beta_0 + \sum_{i=1}^{3} \beta_i x_i + \sum_{i=1}^{3} \beta_{ii} x_{ii}^2 + \sum_{i=1}^{2} \sum_{j>1}^{3} \beta_{ij} x_i x_j + \epsilon \qquad (1)$$

Where y represents the response variable, x_i represent the input parameters, the β's are regression coefficients, and ϵ is the residual error term.

2.2.4 Results and discussion

The Taguchi plan and average values of the measured response variables (i.e., relative density (RD), surface roughness (Ra), yield strength (YS), ultimate tensile strength (UTS), elongation at failure (El.), and microhadness (H)) are given in Table 2.3. The mechanical properties are the average results of three tests with the same process parameters. The corresponding energy density for each parameter combination is also provided for comparison. Sample S.8 showed the highest relative density, whereas sample S.1 exhibited the highest yield strength, hardness, and elongation at failure. Sample S.4 (built with optimum combination recommended by manufacturer) had also comparable properties to S.1, with better surface roughness and higher ultimate strength. These followings will discuss the results of microstructure, statistical analysis and the main effects of process parameters on response variables, and the optimal levels of factors according to ANOVA and RSM.

Table 0.3.

Taguchi plan and experimental results

Sample No.	Factors			E [J/mm^3]	Response					
	P [W]	V[mm/s]	h[mm]		RD [%]	Ra [µm]	YS [MPa]	UTS [MPa]	El. [%]	H [HV]
1	170	1000	0.08	53.13	99.84	4.51	421.3	657	42.6	245.0
2	170	1050	0.10	40.48	98.96	5.64	409.7	643.0	35.4	225.2
3	170	1100	0.12	32.20	94.84	6.47	351.7	522.3	17.4	189.6
4	195	1000	0.10	48.75	99.85	4.07	412.3	660.3	40.7	233.2
5	195	1050	0.12	38.69	98.87	6.05	396.3	632.7	33.9	207.2
6	195	1100	0.08	55.40	99.89	5.32	410.0	657.7	39.9	230.7
7	220	1000	0.12	45.83	99.68	4.89	404.3	645.0	41.4	222.1
8	220	1050	0.8	65.48	99.97	4.30	398.0	643.3	38.3	211.5
9	220	1100	0.10	50.00	99.90	5.32	402.3	646.7	38.8	219.4

2.2.4.1 Microstructure and defects

Optical microscopy images of three SLM 316L stainless steel specimens fabricated with different combinations of parameters according to the Taguchi array are shown in Fig. 2.1. The selected samples have the highest relative densities among the nine Taguchi combinations. The micrographs show the typical microstructural features of SLM processed 316L SS observed in previous studies [116, 126, 128]. The samples consist of a layered structure with well-overlapped melt pools generated by laser beam scans. The rotating scanning strategy resulted in different scan track shapes in the cross-section parallel to the building direction. The melt pool width is in the range of 100-150 µm and the melt pool depth is in the range of 70-90 µm. All samples are dominated by columnar grains with high aspect ratio growing parallel to the maximum heat flow direction, which is normal to the solidifying surface of the melt pool (mainly parallel to the building direction) [117]. However, some equiaxed grains are also observed. This is due to the rotating scanning strategy resulting in a local change of maximum heat flow direction. Growth of columnar grains occurs epitaxially through several consecutive layers. This behavior is attributed to the layer-by-layer nature of the SLM process, resulting in partial re-melting of the previously solidified grains, which offer a ready nucleation site for the melted material [3, 131]. Columnar grains exhibit a length ranging from 50 µm to more than 300 µm. The high magnification micrographs in Fig. 2.2 reveal the intragranular cellular substructure commonly reported in the literature [119, 120, 135, 141]. Cells have a size of 1 µm or less and an elongated or polygonal (equiaxed) shape depending on their growth direction. Saeidi et al. [126] and Wang et al. [128] investigated the cellular substructure by STEM and TEM and found that cell walls are enriched with Mo and Cr and decorated with a high dislocation density. They explained the formation of this substructure by compositional fluctuation and microsegregation of alloying elements. No relevant differences in microstructural features have been observed between different samples using optical microscopy. More advanced techniques could be used in future work to investigate the effect of processing parameters on microstructure. However, it has already been shown that melt pool size, grain size, and cell size are correlated to laser energy density

and laser power [134]. Low energy density results in a high cooling rate, leading to a refined microstructure [135].

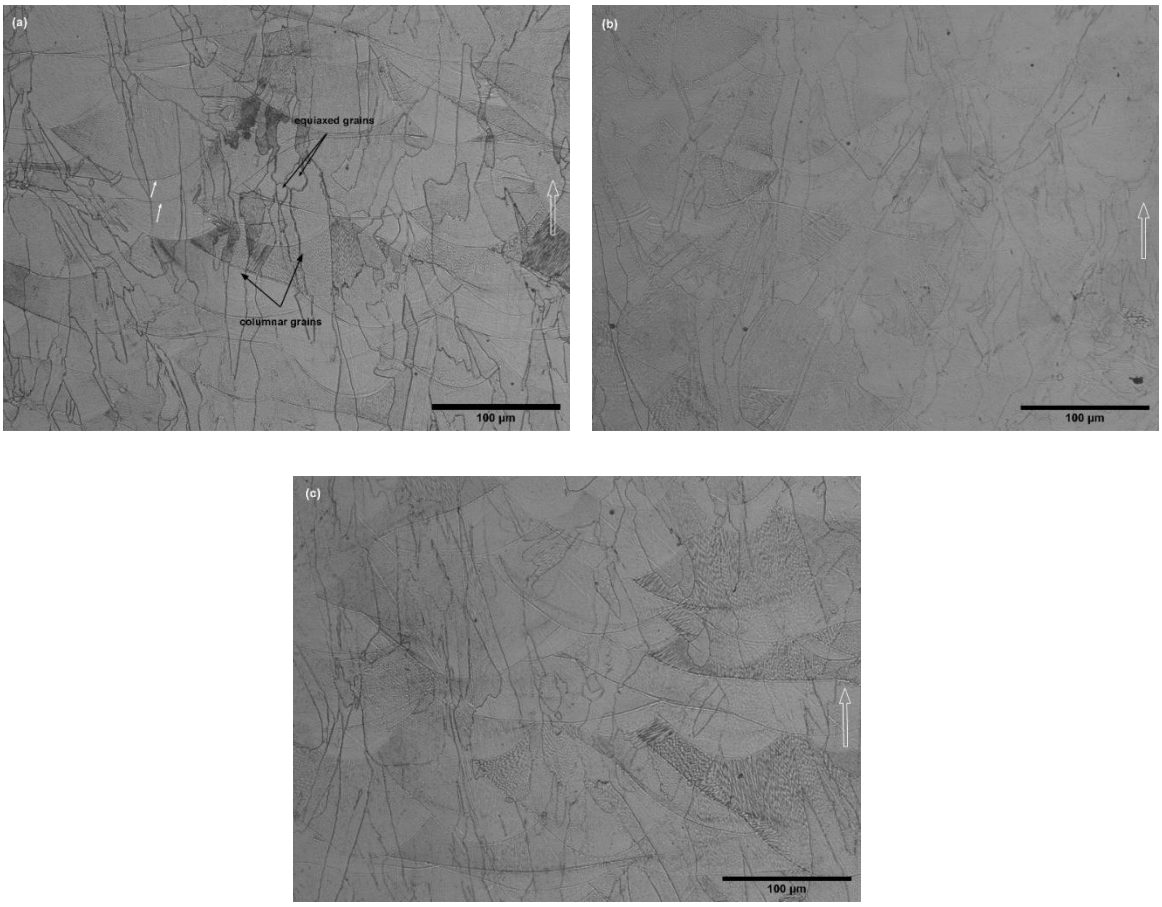

Figure 0.18.Low magnification optical micrographs of 316L SS fabricate by SLM with different process parameters (a) S.1 (P=170 W, v=1000 mm/s, h=0.08 mm), (b) S.4 (P=195 W, v=1000 mm/s, h=0.1 mm), (c) S.8 (P=220 W, v=1050 mm/s, h=0.08 mm). The white arrows indicate melt pool boundaries and epitaxial growth. Building direction is shown with open arrows.

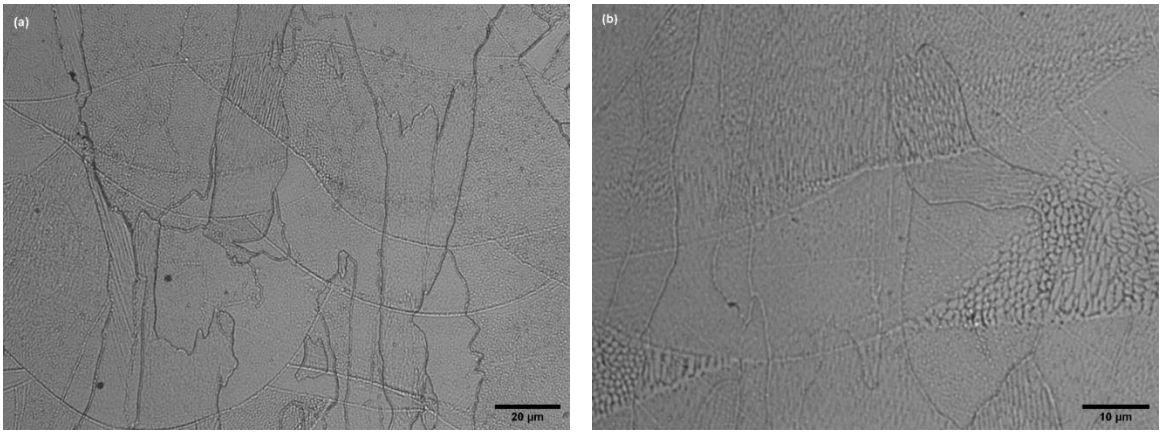

Figure 0.19. High magnification OM of S.1 showing cellular sub-structure; (a) 50x (b) 100x

Solidification defects were also observed using OM before etching. Fig. 2.3 demonstrate the different types of porosity resulting from different processing parameters. It can be seen that the different process parameters combinations resulted in different size and shapes of porosity. For example, the low laser power and high hatch space in S.3 led to a large amount of lack-of-fusions voids with unmelted powder (see Fig. 2.3(b)). In fact, the corresponding energy density for this combination of parameters being the lowest ($E=32.2J/mm^3$) is insufficient to melt all the powder and create well-overlapping melt pools. The poor bonding defect in Fig. 2.3(a) is also due to low energy density leading to a lack of penetration of liquid metal into the previously solidified layer [67]. Both defects have irregular shapes. At high energy density, spherical gas porosities have been observed (Fig. 2.3(c)). Gas bubbles may originate from the atomization process or from building atmosphere. Due to the rapid cooling, gas bubbles can not escape out of the molten pool and are locked in during solidification [67].

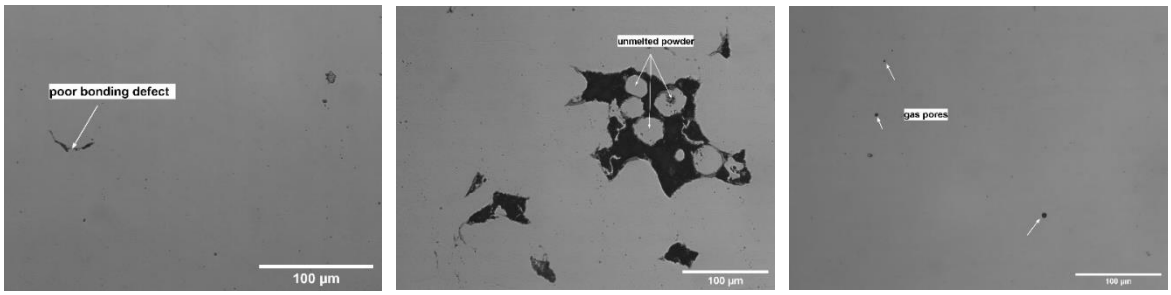

(a) (b) (c)

Figure 0.20. Different types of defects in SLM samples: (a) poor bonding in S.7 (P= 220 W, v=1000 mm/s, h=0.12 mm); (b) lack-of-fusion voids with unmelted powder in S.3 (P=170 W, v=1100 mm/s, h=0.12 mm); gas pores in S.8 (P= 220 W, v=1050 mm/s, h= 0.08 mm)

2.2.4.2 Relative density

Relative density was measured at five different location for each metallographic specimen with defined parameter combination. Mean results in table 2.3 show that the majority of 316L SS samples achieved a near full density, with the highest relative density of 99.97%. Only two samples (S.3 and S.5) were below 99% relative density. It can be easily noticed that relative density is correlated to laser energy density, where the lowest energy density of 32.2 J/mm^3 (S.3) resulted in the lowest relative density (94.84%) and the highest energy density of 65.48 J/mm^3 (S.8) resulted in the highest relative density. The average relative density and the corresponding standard deviation of each sample are plotted against the laser energy density as shown in Fig. 2.4. These findings are consistent with the literature [62, 129]. A further increase in energy density would probably decrease the relative density again due to the keyhole effect [118].

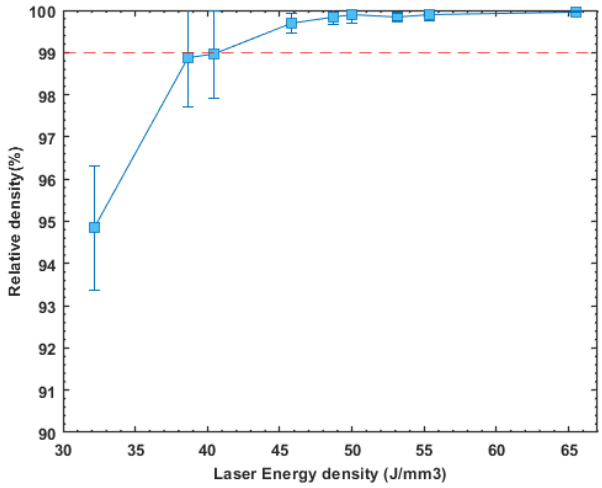

Figure 0.21. Effect of laser energy density on relative density of 316L SS

Analysis of variance (ANOVA) is carried out to quantify the effect of each process parameter individually on the relative density. ANOVA results, given in table 2.4, show that the three investigated factors P, v, and h, and the interactions $P \times v$ and $v \times h$ have a significant effect on the relative density, having p-values less than 0.05 (significance level). Considering the contribution percentage, it can be concluded that the significance order of parameters on relative density is: $h > P > v > v \times h > P \times v$. In order to have a better visual perspective of the impact of each process parameter on the density of SLM-fabricated parts, the main effect plots are shown in Fig. 2.5. These plots present separately the effectiveness of each parameter at varying levels on the average relative density of SLM-processed 316L. It can be observed that relative density increases with an increase in laser power. This effect is more pronounced between 170 W and 195 W. At low laser power, the laser energy density was insufficient to melt the powder and achieve overlapping. Both scanning speed and hatch spacing showed a negative effect on relative density. This is again related to the decrease in energy density, leading to poor interlayer bonding. The steepest drop in relative density is perceived when hatch spacing is increased from 0.1 to 0.12 mm. This is mainly due to voids and lack-of-fusion porosities between adjacent layers.

Table 0.4.

ANOVA results for relative density

Factor	Degree of freedom	Sum of squares	Contribution	Mean squares	F-value	p-value
h	1	6,6369	30,60%	3,46852	72,85	0,003
P	1	5,8174	26,82%	3,68038	77,30	0,003
V	1	3,7449	17,27%	0,86588	18,19	0,024
P*V	1	1,7073	7,87%	3,84336	80,72	0,003
V*h	1	3,6374	16,77%	3,63742	76,40	0,003
Error	3	0,1428	0,66%	0,04761		
Total	8	21,6868	100,00%			

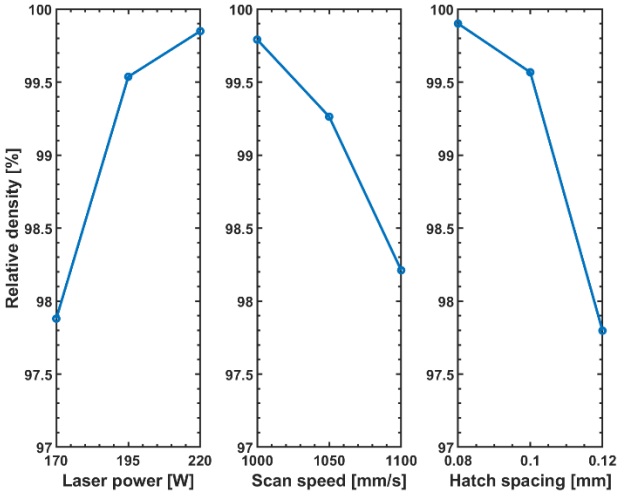

Figure 0.22. Main effect plot of process parameters on relative density

The empirical predictive model for relative density in terms of key processing parameters and their interactions for SLM-fabricated 316L stainless steel is given by:

$$RD = 198.4 + 1363\,h - 1.123\,P - 0.0952\,v + 0.001082\,P \times v - 1.316\,v \times h \qquad (2)$$

For $170 < P < 220\,W, 1000 < v < 1100\,mm/s,\ and\ 0.08 < h < 0.12\,mm.$

The model summary for the fit regression model is given in table 2.5. “S” represents the standard deviation of the distance between the experimental values and the fitted values.

Thus, the small value of S indicates a good fit. The R^2 value means that the regression model explains 99.34% of the variation in relative density. The predicted R^2 determine how accurately the model predicts the relative density for new observations. The agreement between R^2, adjusted R^2, and predicted R^2 demonstrates that the obtained model can be effectively employed to predict relative density.

Table 0.5.

Regression Model Summary for relative density

S	**R^2**	**Adjusted R^2**	**Predicted R^2**	**PRESS**
0,218203	99,34%	98,24%	79,81%	4,37751

Fig 2.6 displays the response surface contour plots of relative density with respect to laser power, scan speed, and hatch spacing. These plots highlight the effect of process parameters and their interactions and help to localize the optimum range of processing parameters to obtain full dense material with reasonable precision. As shown in Fig. 2.6(a), increasing scan speed at low energy density led to a significant reduction in relative density. Full dense material can be achieved either at low power and low scan speed or at high laser power and high scan speed. Both conditions can guarantee sufficient energy density to generate overlapping melt pools and high densification behavior. Fig. 2.6(b) and (c) highlight the detrimental effect of large hatch spacing on part density, especially at low laser power and high scanning speed. Therefore, it can be concluded that relative density is significantly influenced by the interactions between the three process parameters, which are combined into the laser energy density. The results are in agreement with the work of Yakout et al. [35]. Many optimum combinations can be obtained in the variation range of this study. Hatch spacing should be in the range of 0.08-0.1mm, whereas laser power and scan speed should be selected such that the resulting energy density is high enough to attain full densification.

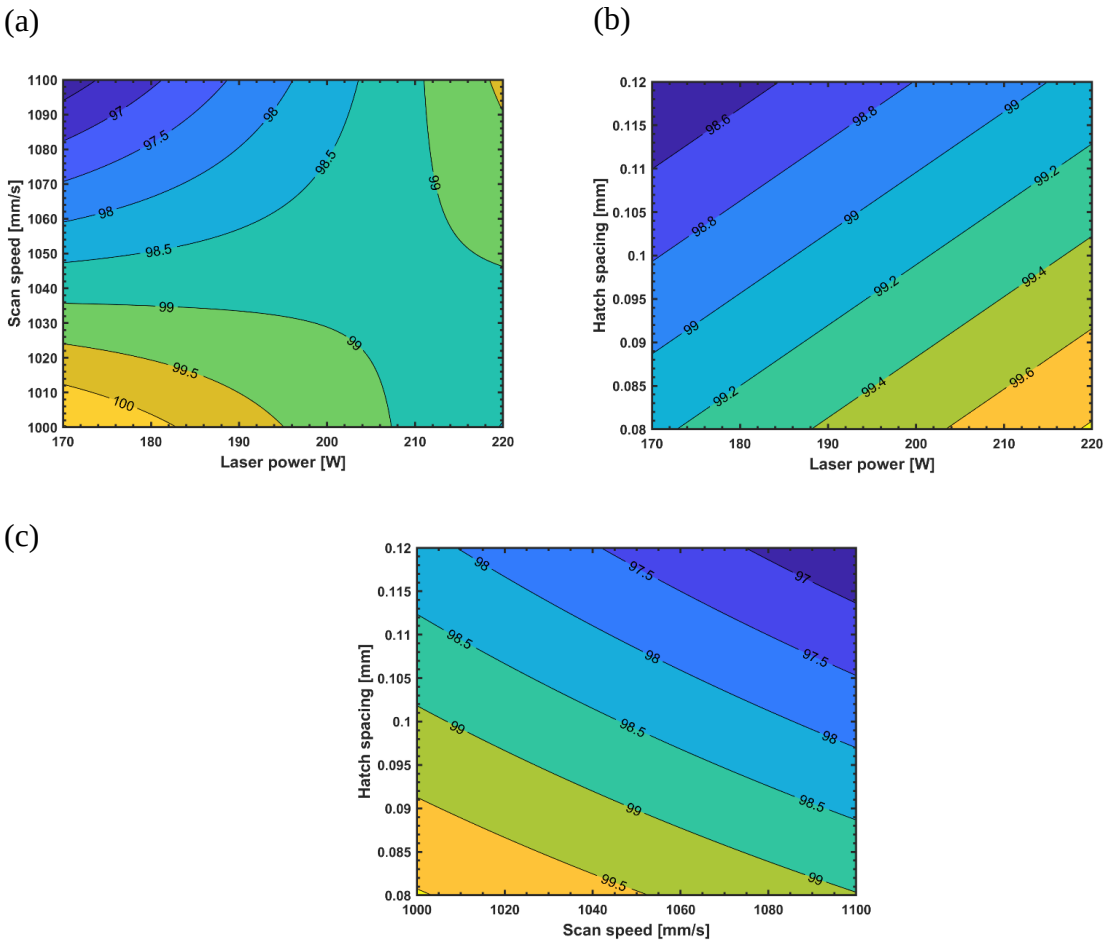

Figure 0.23. Contour plots for the relative density of 316L SS showing the effect of (a) laser power and scan speed at h=0.10 mm, (b) laser power and hatch spacing at v=1050 mm/s, and (c) scan speed and hatch spacing at P=195 W

2.2.4.3 Surface Roughness

Surface roughness measurements were carried out on the side surfaces of tensile specimens. The reported values in table 2.3 are in the range of 4.30-6.47µm. The relatively low surface roughness is due to the fact that samples were sandblasted before measurements. According to ANOVA results presented in table 2.6, the most significant parameters on surface roughness in order are $P \times v, h$, and P. The main effect plots in Fig. 2.7(a) show that increasing scanning speed and hatch spacing is detrimental to the surface finish of SLM-processed 316L. In fact, large hatch spacing is known to increases porosity, and high scan

speed induces balling effect, which results in surface roughness increase [77]. On the other hand, increasing laser power reduced surface roughness due to the higher heat input that properly melted all powder particles and smoothed the surface. At low laser power, the surface tension and viscosity correspond to melt pool decrease, which results in the formation of porosity in the solidifying metal, hence causing higher surface roughness [22]. The effect of energy density on surface roughness is displayed in Fig. 2.7(b). Although the general trend of Ra decreases with the increase in energy density, some fluctuations in surface roughness can be noticed in the range of 45-55 J/mm^3. This fluctuation can explain the relatively high contribution of error in ANOVA results with is 8.67%. The lowest surface roughness was obtained at 48.75 J/mm^3, which corresponds to the optimum process parameters recommended by the machine manufacturer. The observed trends are in good agreement with previous studies [25, 155, 231].

Table 0.6.

ANOVA Results for Surface roughness (Ra)

Factor	**Degree of freedom**	**Sum of squares**	**Contribution**	**Mean squares**	**F-value**	**p-value**
P	1	0,7257	14,05%	2,74895	30,70	0,003
h	1	1,8846	36,48%	2,13912	23,89	0,005
P*V	1	2,1080	40,81%	2,10805	23,54	0,005
Error	5	0,4477	8,67%	0,08954		
Total	8	5,1660	100,00%			

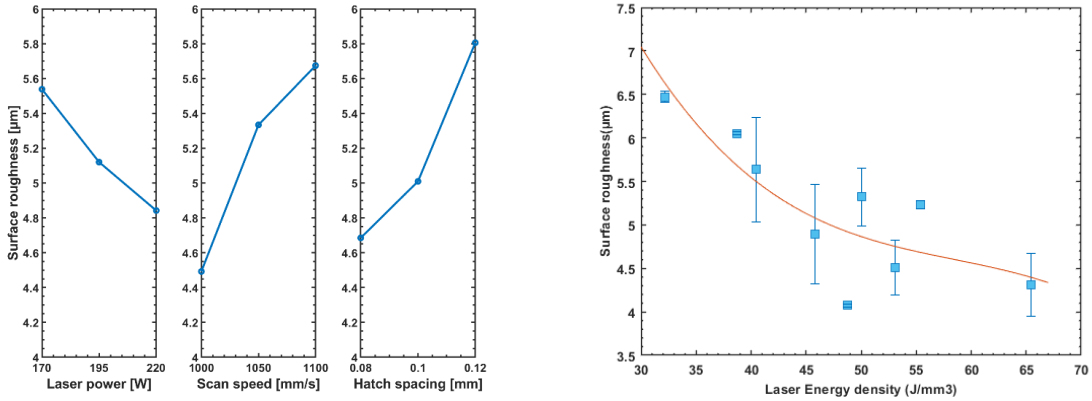

(a) (b)

Figure 0.24. Effect of process parameters (a) and laser energy density (b) on surface roughness

The obtained linear regression model for predicting surface roughness is:

$$Ra = 4.89 - 0.0775\,P + 29.92\,h + 0.000061\,P\,v \quad (3)$$

For $170 < P < 220\,W, 1000 < v < 1100\,mm/s,\ and\ 0.08 < h < 0.12\,mm$

Considering the accuracy measures in table 2.7, the variation of surface roughness with respect to process parameters and their interactions can be well explained and predicted using the fitted regression model. However, a wider variation range with more repetitions should be performed in future work to confirm the robustness of the empirical model.

Table 0.7.

Model Summary for surface roughness

S	R^2	Adjusted R^2	Predicted R^2	PRESS
0,299236	91,33%	86,13%	77,12%	1,18211

The contour plots of the surface roughness of 316L stainless steel are illustrated Fig. 2.8 demonstrate the effect of laser power, scan speed and hatch spacing on the surface finish of SLM processed parts. Although v did not have a significant effect on surface roughness according to ANOVA results, its interaction with laser power was the most influential term

in the model. It is clearly visible that low laser power coupled with high scanning speed tends to rise surface roughness. The negative effect of hatch spacing is also confirmed by RSM analysis. Finally, it can be concluded that the optimum combination to minimize surface roughness is (P= 220W, v= 1000 mm/s, and h= 0.08 mm).

(a) (b)

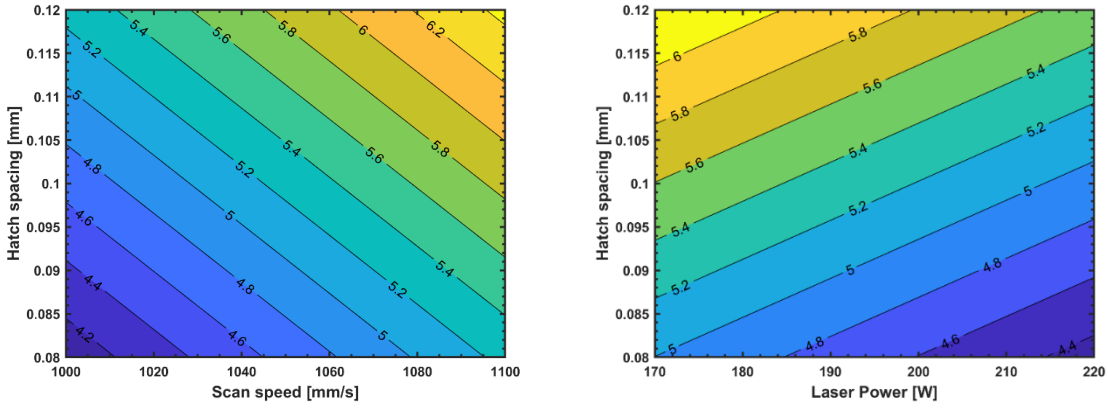

(c)

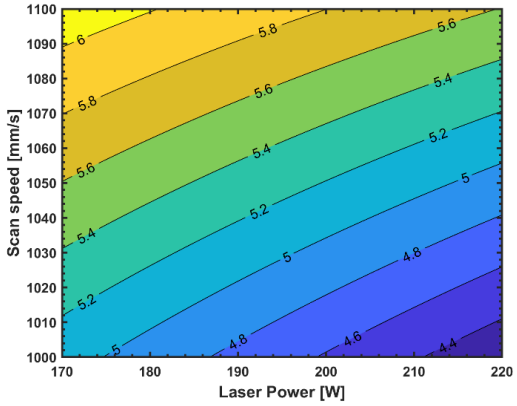

Figure 0.25. Contour plots of surface roughness response as a function of: (a) hatch spacing and scan speed at P= 195 W, (b) hatch spacing and laser power at v= 1050 mm/s, and (c) scan speed and laser power at h= 0.1 mm.

2.2.4.4 Mechanical properties

Experimental results in table 2.3 show that all samples exhibited excellent strength and hardness, exceeding ASTM standard minimum requirements for conventionally processed

material (UTS ≥ 485 MPa and H ≥ 155 HV) [153]. It is commonly reported that the unique hierarchical microstructure is the reason for the enhancement of SLM-processed austenitic stainless steel strength [120, 137, 141]. Elongation at failure values were slightly lower or comparable to the reference value for conventional material (≥ 40%) expect for sample S.3, which showed an elongation at failure of 17.4%. Premature failure could have occurred due to the high amount of porosity and internal defects in this sample, which had the lowest relative density of 94.84%.

Table 0.8.

ANOVA results for Hardness

Factor	**Degree of freedom**	**Sum of squares**	**Contribution**	**Mean Squares**	**F-value**	**p-value**
P*P	1	9,23	0,44%	752,019	175,99	0,000
h*h	1	813,27	38,65%	389,003	91,04	0,001
P*h	1	1184,85	56,32%	725,234	169,73	0,000
V*h	1	79,49	3,78%	79,485	18,60	0,013
Error	4	17,09	0,81%	4,273		
Total	8	2103,93	100,00%			

Table 0.9.

ANOVA results for ultimate yield strength (YS)

Factor	**Degree of freedom**	**Sum of squares**	**Contribution**	**Mean squares**	**F-value**	**p-value**
P	1	80,59	2,54%	820,36	193,89	0,001
V	1	912,42	28,75%	164,90	38,97	0,008
h	1	988,17	31,13%	811,44	191,78	0,001
P*V	1	340,12	10,72%	811,99	191,91	0,001
V*h	1	839,96	26,46%	839,96	198,52	0,001
Error	3	12,69	0,40%	4,23		
Total	8	3173,96	100,00%			

Table 0.10.

ANOVA results for ultimate tensile strength (UTS)

Factor	Degree of freedom	Sum of squares	Contribution	Mean squares	F-value	p-value
P	1	2115,8	14,39%	3324,68	51,76	0,006
V	1	3067,3	20.86%	559,05	8,70	0.060
h	1	4160,7	28,30%	3722,35	57,95	0,005
P*V	1	1315,2	8,94%	3371,37	52,49	0,005
V*h	1	3852,1	26,20%	3852,09	59,97	0,004
Error	3	192,7	1,31%	64,23		
Total	8	14703,6	100,00%			

Table 0.11.

ANOVA results for elongation at failure (El.)

Factor	Degree of freedom	Sum of squares	Contribution	Mean squares	F-value	p-value
P	1	89,012	18,84%	72,023	71,69	0,003
V	1	136,804	28,96%	15,211	15,14	0,030
h	1	131,789	27,90%	78,211	77,85	0,003
P*V	1	29,791	6,31%	74,357	74,01	0,003
V*h	1	81,931	17,35%	81,931	81,55	0,003
Error	3	3,014	0,64%	1,005		
Total	8	472,341	100,00%			

Tables 2.8, 2.9, 2.10, and 2.11 present ANOVA models for hardness, yield strength, tensile strength, and elongation. All tensile proprieties (i.e., YS, UTS, and El.) were significantly influenced by $P, h, v, v \times h$, and $P \times v$ but with different significance orders. For yield strength, the significance order of factors based on their contribution percentage is $h > v > v \times h > P \times v > P$, where laser power had the lowest contribution of 2.54%. For tensile strength, the significance order of factors is $h > v \times h > v > P > P \times v$. For elongation at failure, the parameters are ranked as follows $v > h > P > v \times h > P \times v$. It

can be concluded that tensile properties are mostly affected by hatch spacing and scan speed and their interaction, and less by laser power and its interaction with scan speed. The interaction between hatch spacing and laser power did not show a significant effect. In contrast, a quadratic model was obtained for hardness, where the interaction $P \times h$ was the most significant term, followed by h^2 and $v \times h$. The quadratic term P^2 although retained, had a very low contribution of 0.44%.

To visualize the influence of varying parameter levels on the output responses (H, YS, UTS and El.), the main effect plots are depicted in Fig 2.9. It could be observed that H, YS and UTS had similar trends with respect to the variation of P,v, and h. Fig. 2.9(a) confirms that hatch spacing has a detrimental effect on hardness. Most precisely, the increase of h from 0.1 mm to 0.12 mm resulted in a steep decrease in hardness. Previous studies have demonstrated that hardness is correlated to porosity [129, 155]. In this study, it has been revealed that hatch spacing was the most significant parameter on relative density, leading to a high fraction of lack-of-fusion voids with unmelted powder as observed in sample S.3 in Section 4.1. These findings explain the pronounced effect of hatch spacing on hardness. Similar conclusions can be drawn to the effect of hatch spacing on tensile properties. Elongation at failure is particularly affected by the amount of porosity induced by increased hatch spacing. As shown in Fig. 2.9(c), the variation of hatch spacing from 0.1 mm to 0.12 mm resulted in a 22% decrease in elongation. Internal defects are known to be critical issues for ductility and fatigue as they act as stress concentrators and crack initiation sites [152]. Yakout et al. [35] investigated mechanical properties of 316L with varying energy densities and established a brittle-ductile transition energy density below which the material undergoes a brittle failure due to void formation. The increase of scan speed had also a negative effect on hardness and tensile properties, which is similarly attributed to the decrease in energy density and poor densification. The increase of laser power from 170 W to 195 W resulted in an increase in strength and hardness due to the proper melting. However, a further increase in laser power caused a slight reduction in strength and hardness. This is suggested to arise from the lower cooling rate and thus more coarsened grains at high laser power, as observed

in previous studies [130, 135]. In fact, refined cell size results in Hall-pitch strengthening [127].

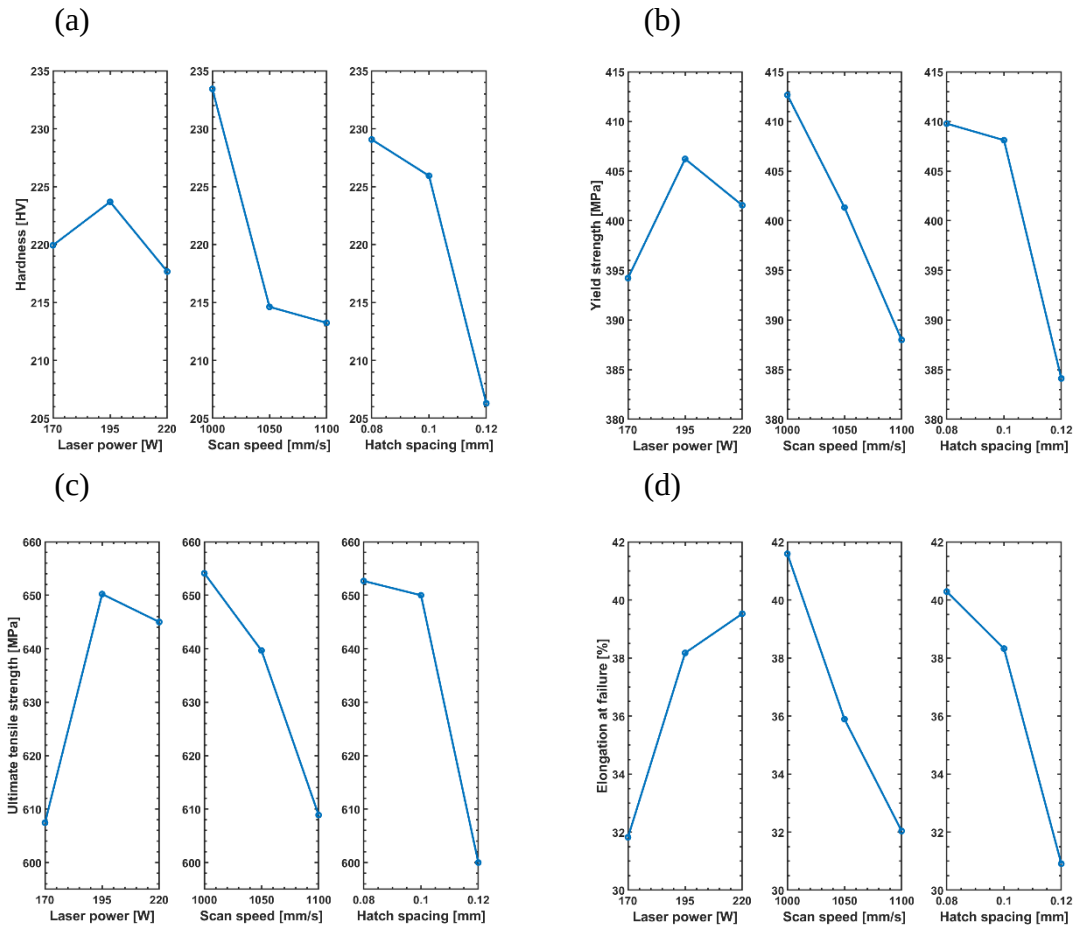

Figure 0.26. Main effect plots for (a) Hardness, (b) yield strength, (c) ultimate strength and (d) elongation at failure

The predictive regression models for hardness, yield strength, ultimate tensile strength, and elongation are given by the following equations:

$$H = 305.1 - 0.006775\,P^2 - 23887\,h^2 + 25.81\,P \times h - 0.783\,v \times h \quad (4)$$

$$UTS = 3227 - 33.76\,P - 2.420\,v + 44656\,h + 0.03205\,P \times v - 42.83\,v \times h \quad (5)$$

$$YS = 1845 - 16.77\,P + 1.314\,v + 20849\,h + 0.01573\,P \times v \quad (6)$$

$$El.\,\% = 458 - 4.969\,P + 0.399\,v + 6473\,h + 0.00476\,P \times v \quad (7)$$

For $170 < P < 220\,W, 1000 < v < 1100\,mm/s,\ and\ 0.08 < h < 0.12\,mm.$

The effectiveness of these fitted models can be assessed through the values of standard deviation (S), R^2, adjusted R^2, predicted R^2 and predicted residual error sum of squares (PRESS) summarized in table 2.12. The displayed results indicate good fit and good prediction abilities for the established models.

Table 0.12.
Summary of regression models for H, YS, UTS and El.

Model	**S**	**R^2**	**Adjusted R^2**	**Predicted R^2**	**PRESS**
Hardness	2.07	99.19%	98.38%	88.83%	235.19
Yield strength	2.06	99.60%	98.93%	94.40%	177.61
Ultimate tensile strength	2.76	99.90%	99.58%	93.55%	948.16
Elongation at failure	1.00	99.36%	98.30%	85.30%	69.42

Based on these regression models, RSM analysis can be carried out through the contour plots shown in Fig. 2.10. The results confirm the main effects of the process parameters discussed previously. Optimal hardness and tensile strength may be obtained at P = 170 W, v = 1000, h = 0.08. This combination corresponds to sample S.1, which showed the highest yield strength, hardness, and ductility among the nine Taguchi combinations (YS = 421.33 MPa, El. = 42.65% and H = 245 HV). However, higher laser power and thus higher energy density would probably increase relative density, improve surface roughness and enhance ductility. On the other hand, the increase in laser power reduces the strength of material due to larger grain and sub-grain sizes. Hence, setting laser power at P = 195 W, scan speed at v = 1000 mm/s and hatch spacing at h = 0.08 would provide a good compromise of enhanced strength and ductility. Validation tests should be performed in future work to validate this optimal combination. Meanwhile, sample S.4 built with P = 195 W, v = 1000 mm/s and h = 0.1 mm, which is close to the optimum combination, already showed comparable tensile

properties (YS = 412 MPa, El. = 40.71% and H = 233 HV). Thus, reducing hatch spacing to 0.08 mm would increase energy density and improve relative density, ductility, and hardness.

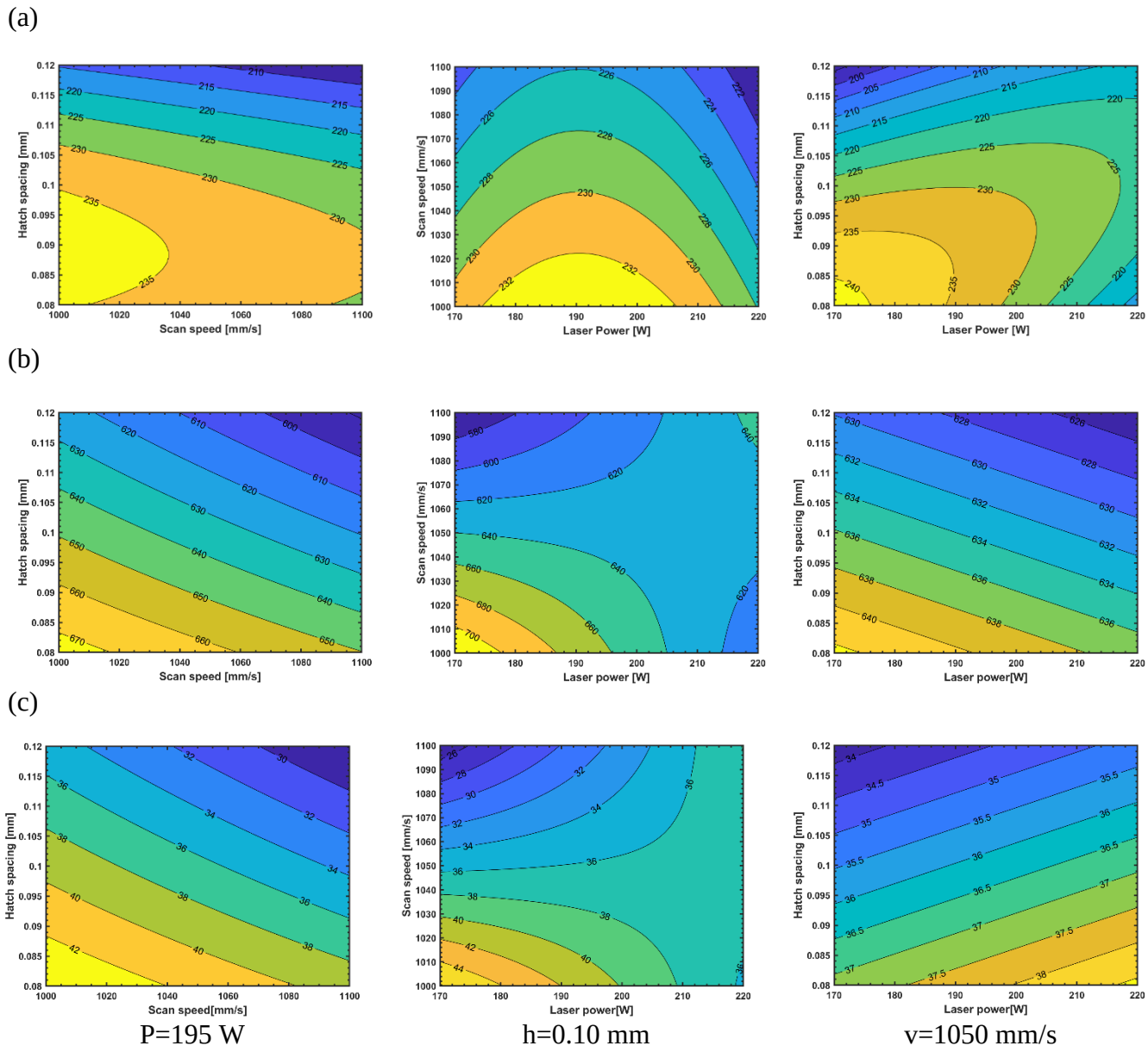

Figure 0.27. Contour plots of response surfaces versus process parameters for (a) hardness, (b) Ultimate tensile strength, and (c) Elongation at failure

2.2.5 Conclusion

This work investigated the effect of process parameters on the relative density, surface roughness, and mechanical behavior of 316L stainless steel fabricated by SLM. The Taguchi method was used for experimental design. Microstructure was also observed using optical microscopy. The typically reported hierarchical features, including melt pool boundaries, high angle grain boundaries, and cellular substructure inside the large columnar austenite grains of SLM-built 316L SS, were clearly visible. Three types of porosities were depicted in samples fabricated with different process parameters. These are poor bonding, lack-of-fusion voids with unmelted powder, and gas pores. Overall, good densification levels (99.97%) and excellent mechanical properties were obtained. ANOVA and RSM were employed as powerful statistical tools to elucidate the influence of process parameters, namely laser power, scan speed, hatch spacing, and their interactions, on response variables; relative density, surface roughness, hardness, tensile strength, and elongation. The parameter levels were set around the optimum combination recommended by the manufacturer. According to ANOVA results, hatch spacing was mainly the most significant factor for all properties. Scan speed also had a significant effect, particularly on tensile properties. All response variables were negatively affected by the increase in hatch spacing and scan speed. This was attributed to the low laser energy density resulting from the increase in hatch spacing and scan speed and, hence, low densification level. Laser power was found to be significant for relative density, surface roughness and elongation. The increase in laser power induces a high energy input that is able to properly melt the powder and reduce the amount of porosity. Therefore, surface finish and ductility are enhanced. Interactions $P \times v$, and $v \times h$ are also effective for most response variables. Empirical predictive models were developed using multiple linear regression, reflecting the complex correlations between response

variables and input parameters. These models allow the prediction and optimization of SLM-processed 316L stainless steel properties with high accuracy.

CHAPITRE 3
EFFET DES PARAMETRES DE TRAITEMENT THERMIQUE SUR LA MICROSTRUCTURE ET LA MICRODURETE DE L'ACIER INOXYDABLE 15-5 PH PRODUIT PAR FUSION LASER SELECTIVE

A. Mansoura[1], M. Houria[2], N. Barka[1], S.S. Kangranroudi[3]

[1] Université du Québec à Rimouski, Québec, Canada

[2] Ecole de Technologie Supérieure, Québec, Canada

[3] Université du Québec à Trois-Rivières, Québec, Canada

3.1 RESUME EN FRANÇAIS DU PREMIER ARTICLE

La fusion sélective au laser (SLM) est une technologie de fabrication additive de pointe permettant la fabrication de géométries complexes qui étaient auparavant irréalisables. Cependant, pour répondre aux exigences les plus strictes des applications industrielles, les performances des composants métalliques fabriqués par SLM doivent être améliorées davantage. Ainsi, il apparaît qu'un post-traitement thermique est nécessaire pour améliorer les propriétés microstructurales et mécaniques des pièces fabriquées de manière additive. L'acier 15-5 PH est un acier inoxydable martensitique à durcissement structural (par précipitation) qui est couramment utilisé dans l'industrie aérospatiale et d'autres applications d'ingénierie grâce à sa haute résistance mécanique, sa dureté élevée et son excellente résistance à la corrosion. Cette étude examine l'influence des paramètres de traitement thermique de durcissement par vieillissement sur la microstructure et la microdureté de l'acier inoxydable 15-5 PH fabriqué par SLM afin de déterminer les réglages optimaux des paramètres. La méthode de Taguchi est utilisée pour définir le plan expérimental. Les facteurs pris en compte sont : la solution de trempe, la température de vieillissement et le temps de vieillissement. Avec trois niveaux pour chaque facteur, neuf combinaisons sont examinées,

et comparées à l'état non vieilli. La microstructure des échantillons est analysée à l'aide de la microscopie optique (OM) et de la microscopie électronique à balayage (SEM) pour comprendre la relation microstructure-propriété. La dureté la plus élevée, atteinte après 1h de vieillissement à 500 °C, était corrélée à la présence de précipités de Cu extrêmement fins uniformément répartis. Les résultats de microdureté sont analysés à l'aide d'une approche statistique. L'analyse de la variance (ANOVA) a été utilisée pour évaluer l'effet de chaque facteur de traitement thermique. La combinaison optimale des paramètres de durcissement par vieillissement a été sélectionnée sur la base de la méthode de surface de réponse (RSM). Il est démontré que la température de vieillissement est le paramètre le plus important pour la dureté de la pièce, tandis que la solution de trempe n'a eu aucun effet. La méthode proposée a conduit au développement d'un modèle de régression fiable qui prédit la dureté de l'acier inoxydable 15-5PH vieilli et fabriqué par SLM en fonction de la température de vieillissement et de la durée de vieillissement. Les tests de traction démontrent que l'optimisation des paramètres de durcissement par précipitation peut également améliorer la résistance à la traction et la ductilité à la fois.

Cet article, intitulé « *Effect of Heat Treatment Parameters on Microstructure and Microhardness of 15-5 PH Stainless Steel produced by Selective Laser Melting* », a été soumis au journal *Additive Manufacturing*. En tant que première auteure, j'ai conduit la recherche de l'état de l'art, réalisé les mesures de dureté, mené l'analyse statistique et l'interprétation des résultats, et rédigé l'essentiel de l'article. Manel Houria, la deuxième auteure, a contribué à la caractérisation et à l'analyse de la microstructure par MEB. Le professeur Noureddine Barka, troisième auteur, a fourni l'idée originale, développé la méthodologie et a révisé l'article. Sasan Sattarpanah Kangranroudi, quatrième auteur, a également contribué au développement de la méthodologie, à la réalisation des traitements thermiques et à la révision de l'article.

3.2 Effect of Heat Treatment Parameters on Microstructure and Microhardness of 15-5 PH Stainless Steel Produced by Selective Laser Melting

3.2.1 Abstract

Selective Laser Melting (SLM) is a cutting-edge additive manufacturing technology that enables the fabrication of complex geometries that were formerly unattainable. However, to satisfy the most stringent requirements of industrial applications, the performance of SLM-fabricated metal components still needs to be enhanced. Thus, it appears that post-processing heat treatment is required to improve the microstructural and mechanical properties of additively manufactured parts. 15-5 PH stainless steel is a martensitic precipitation hardenable stainless steel that is commonly utilized in aerospace and other engineering applications thanks to its high strength, high hardness, and excellent corrosion resistance. This study investigates the influence of precipitation hardening heat treatment parameters on the microstructure and microhardness of 15-5 PH stainless steel fabricated by SLM in order to determine the optimal settings of parameters. The Taguchi method is used to set the experimental plan. The factors under consideration are: quenching solution, aging temperature, and aging time. With three levels for each factor, nine combinations are examined, in addition to the as-built specimen. The microstructure of samples is analyzed using Optical Microscopy (OM) and Scanning Electron Microscopy (SEM) to understand the microstructure-property relationship. The highest hardness, attained after 1h of aging at 500 °C, was correlated to the presence of extremely fine Cu-precipitates uniformly distributed. Microhardness results are assessed using a statistical approach. The Analysis of Variance (ANOVA) was used to evaluate the main effect of each heat treatment factor. The optimal combination of precipitation hardening parameters was selected based on the Response Surface Method (RSM). It is shown that aging temperature is the most significant parameter for part hardness, while quenching solution has no effect. The proposed method led to the development of a reliable regression model that accurately predicts the hardness of

heat-treated 15-5 PH stainless steel manufactured by SLM as a function of aging temperature and aging time. Validation experiments demonstrate that optimizing precipitation-hardening parameters may improve tensile strength and ductility as well.

Keywords: Selective laser melting, Precipitation hardening, 15-5 PH stainless steel, ANOVA, Microhardness.

3.2.2 Introduction

The unprecedented development of additive manufacturing technologies has allowed industry to overcome the constraints associated with conventional manufacturing techniques [232]. As a single-step process, the primary advantages of AM include freedom of design, energy and material savings, and shortened design-to-manufacture time [4]. One of the most promising metal additive manufacturing processes is Selective Laser Melting (SLM), also called Direct Metal Laser Sintering (DMLS), a laser powder-bed fusion process that uses a scanning laser beam to build up parts by selectively melting certain portions of the metal powder-bed, layer by layer, based on computer-aided design (CAD) data. Researchers and manufacturers are becoming increasingly interested in SLM because it can process a broad variety of materials such as steels, aluminum alloys, titanium alloys, nickel alloys, etc., that may be expensive or difficult to produce using traditional techniques [9]. In addition, SLM provides the opportunity to increase functionality and tailor the microstructure and subsequent properties of the manufactured part.

Although SLM has numerous benefits, its full acceptance in the industry is still challenging due to the presence of defects such as porosity, lack of fusion and cracks, as well as anisotropy, inhomogeneous microstructure and high residual stress caused by the complex thermal history and the rapid cooling rate [48, 60].

15-5 PH stainless steel is a martensitic precipitation-hardening stainless steel with high corrosion resistance, good toughness, and good mechanical properties at temperatures up to 300 °C [233]. This makes it suitable for a wide range of applications in aerospace, chemical,

petrochemical, and food processing industries [233, 234]. Due to the low carbon content and the addition of copper as an alloying element, its body-centered cubic (BCC) martensite matrix can be strengthened through the formation of nanometric-sized Cu precipitates [235, 236]. The conventional heat treatment for this type of alloy consists of two steps: (1) solution treatment in the austenite phase field, followed by air or water quenching; (2) aging in a heat treatment furnace at 480-620 °C for a few minutes to several hours [237]. Aging starts with the formation of small and coherent Cu clusters having a BCC structure. With increasing aging temperature and/or aging time, the precipitate size and shape evolve until they transform into incoherent face-centered cubic (FCC) clusters [187, 238]. By selecting proper post-process parameters, the characteristics of this precipitation in terms of volume fraction and size can be tuned to obtain different application-oriented mechanical properties [30, 185]. This combination of characteristics and high-value applications makes the 15-5 PH stainless steel an excellent candidate for additive manufacturing. Recently, SLM has shown promising results for the fabrication of precipitation-hardening stainless steels [18, 190]. Several studies have focused on comparing the performance of SLM-processed 15-5PH and traditionally manufactured 15-5 PH stainless steel. Coffy et al. [239] reported a smaller grain size with a layered microstructure and a significant volume fraction of retained austenite phase in DMLS processed 15-5 PH compared to the conventional alloy. Roberts et al. [240] compared the microstructure, microhardness, and high-temperature mechanical behavior of AM and wrought 15-5 PH steel in the as-built condition. Additively manufactured 15-5 PH showed better performance except for ductility. Some of the researchers investigated the effect of processing parameters such as energy density, scanning strategy, building direction, and powder characteristics on the microstructure and mechanical properties of selective laser-melted 15-5 PH to obtain high-quality final parts [53, 241-243]. However, this approach cannot effectively control anisotropy and heterogeneous microstructure caused by the complex metallurgical interactions during the SLM process, especially for precipitation hardening grade. To address this challenge, recent studies focused on post-process heat treatment to achieve a better tradeoff between microstructure and mechanical properties for 15-5 PH stainless steel. Alafaghani et al. [234] investigated the influence of different solution

annealing treatments on the microstructure and mechanical properties of DMLS 15-5 PH steel. They found that extending the solution treatment time improved microstructure isotropy and tensile strength at the expense of ductility, while increasing the solution treatment temperature adversely affected SLM parts. Nong et al. [188] examined the effect of the standard precipitation hardening heat treatment H900 (i.e., solution heat treatment at 1040 °C for 30 min, followed by water-quenching and subsequent aging at 482 °C for 1 h, followed by air-cooling) on the microstructural and mechanical characteristics of SLM-fabricated 15-5 PH parts. They reported that heat-treated SLM sample demonstrated greater strength and higher hardness than aged wrought 15-5 PH sample and comparable ductility. This was explained by the finer grain structure, the high concentration of dislocations around grain boundaries, and the retained austenite. Mechanical properties, microstructural evolution, and corrosion resistance were evaluated in several conditions (solution annealed, aged at different temperatures and times) [19, 180, 183, 197]. Experimental results showed that different aging processes affect the Cu-rich precipitate characteristics and the amount of retained austenite, resulting in different mechanical behavior and corrosion resistance.

Although existing studies have demonstrated the importance of heat treatment in enhancing the mechanical performance of SLM 15-5 PH steel, the large variation in the results has revealed that standard heat treatments are insufficient to achieve a tailored microstructure. Therefore, efficient experimental design and analysis methods are needed to model, predict and obtain desired mechanical properties by systematically finding optimal heat treatment parameters.

Among optimization techniques, Taguchi method is a powerful and consistent tool for the statistical design of experiments. It provides a simple, efficient, and systematic approach to optimize designs for performance, quality, and cost [229].

Accordingly, this study aims to investigate the influence of precipitation hardening heat treatment parameters on the microstructure and microhardness of 15-5 PH parts processed by SLM based on Taguchi design. A statistical approach based on ANOVA, RSM, and linear regression has been used to identify the significant heat treatment parameters and predict

their effects on 15-5 PH microhardness. Microstructure characterization has been performed and correlated to the obtained hardness.

3.2.3 Material and methods

3.2.3.1 Design of experiment

The Taguchi method is a simple and powerful optimization tool used to evaluate the significance of different process parameters for a target response. It allows reducing the number and cost of experimental tests without affecting accuracy, thanks to the orthogonal array design [244]. The procedure of Taguchi design includes the following steps: (1) identification of the quality characteristics and selection of the design parameters; (2) selection of the appropriate orthogonal array according to the number of parameters and number of levels; (3) conducting of the experiments and statistical analysis of the results; (4) identification of the optimal levels of design parameters [229].

Microhardness of precipitation-hardening stainless steel rely on a complex microstructure developed during a sequence of quenching after austenitization, followed by aging heat treatment [235]. Aging temperature and aging time play a prominent role in the control of the Cu-precipitate characteristics and thus, the alloy's strength. The homogenization step and the subsequent quench are also important in the control of austenite/martensite proportions. Accordingly, quenching solution (A), aging temperature (B), and aging time (C) are selected as design parameters for the Taguchi plan. Three levels for each parameter are set, as shown in table 3.1.

Aging parameters were chosen to cover the typical under-aged, peak-aged and over-aged conditions known in standard precipitation hardening treatments. For quenching, three different aqueous solutions were used in the experiments; distilled water (level 1), NaCl solution at 6% of mass concentration (level 2) and 12 mass% NaCl solution (level 3), allowing to have three different quenching rates as reported in [245]. Based on Taguchi method, the appropriate experimental design for this study is L_9 orthogonal array. This array

has eight degree of freedom and thus, is suitable for three-level design parameters. Therefore, nine unique heat treatment combinations are available as shown in table 3.2.

Table 0.13.

Heat treatment parameters and their levels

Parameters	**Symbols**	**Levels**		
Quenching solution	A	1	2	3
Aging Temperature (°C)	B	400	500	600
Aging time (min)	C	60	120	180

Table 0.14.

Experimental layout using L_9 orthogonal array

Test No.	**Quenching solution**	**Aging temperature [°C]**	**Aging time [min]**
	A	**B**	**C**
1	1	400	60
2	1	500	120
3	1	600	180
4	2	400	120
5	2	500	180
6	2	600	60
7	3	400	180
8	3	500	60
9	3	600	120

3.2.3.2 Specimen fabrication and preparation

The samples were produced on EOS M 290 system using the commercialized Powder Range 155 stainless steel (15-5PH) powder from Carpenter Additive. The particle size distribution ranges from 15 to 45 µm. Table 3.3 lists the chemical composition of the 15-5 PH powder used.

The SLM machine is equipped with an Yb-fiber laser with a beam diameter of 0.1 mm. To avoid oxidation, printing was done in an Argon atmosphere. Specimens were produced using optimized processing parameters recommended by manufacturer, which are listed in table 3.4. Fig. 3.1 depicts the dimensions and building orientation of the specimen. Laser scan paths were rotated at 45° angle between two adjacent layers.

Table 0.15.

Chemical composition of 15-5PH stainless steel powder (wt. %)

Element	C	Cr	Cu	Fe	Mn	Ni	Nb	N	O	P	Si	S
wt%	≤0.04	14.0-14.6	3.5-4.0	Bal.	≤0.3	2.8-4.5	0.20-0.40	≤0.1	≤0.03	≤0.03	≤0.7	≤0.03

Table 0.16.

SLM process parameters for 15-5PH stainless steel

Parameter	**Laser power**	**Scan speed**	**Hatch spacing**	**Layer thickness**
Value	195 W	800 mm/s	0.1 mm	40 µm

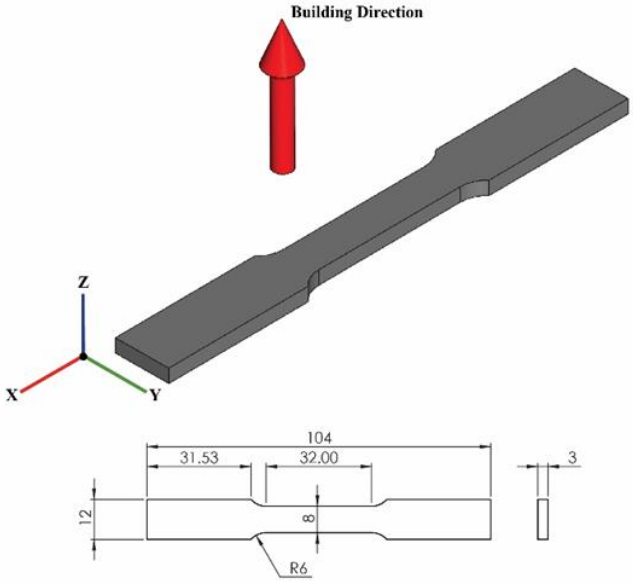

Figure 0.28. Dimensions (in mm) and building direction of samples

For comparison, we kept two samples in their as-built condition. All the remaining samples were solution-treated at 1020°C for 15 minutes, in a first step. Each group of three is then cooled in a different quenching solution (1, 2 and 3). After quenching, samples are individually aged in furnace at different temperatures and holding durations according to the orthogonal array (see table 3.2) and cooled in air, giving rise to precipitation hardening. Two other validation samples were later solution-treated at 1020°C for 15 minutes, water quenched and aged in furnace according to the optimal set of parameters.

3.2.3.3 Microstructure and microhardness measurement

To evaluate the microhardness and microstructure of SLM-fabricated 15-5 PH steel samples at their cross-section parallel to the building direction, samples were mounted in epoxy and polished with diamond suspensions with average diamond particle diameters of 9 µm, 6 µm, 3 µm, and 1 µm. The samples were then chemically etched with Fry's reagent (5g $CuCl_2$ + 40 mL HCl + 30 mL water + 25 mL ethanol) to reveal grain structure. Microstructure characterization was performed using LEXT OLS4100 laser confocal microscope, Hitachi

TM3000 scanning electron microscope (SEM), and Energy Dispersive Spectroscopy (EDS). Rockwell Microhardness measurements were carried out with a testing load of 300 gf and 10 s dwell time using a Clemex machine. For each sample, the hardness value is determined by averaging 20 indentations spaced at 200 µm and performed along the surface's diagonal.

3.2.4 Results and discussion

3.2.4.1 Microstructure Analysis

The complex thermal cycle in the SLM process and subsequent heat treatments induce a complex microstructural evolution in 15-5 PH stainless steel that, in turn, affects its mechanical properties. In order to investigate the structure-property relationship, the as-built sample, in addition to aged samples No. 3, 4, and 9 from the Taguchi array, were subjected to microstructure examination. The specimens are selected according to the microhardness results reported in table 3.4 as they have the lowest, intermediate, and highest hardness, respectively. The as-built sample in Fig. 3.2(a) reveals a typical layered microstructure with well overlapped molten pools formed by the laser beam. The use of alternating scan strategy, in which scanning direction is rotated by 45° between two successive layers, is evident in scan track shapes. High magnification SEM image of the as-built sample in Fig. 3.2(b) displays equiaxed and columnar sub-grain structures grown epitaxially. The boundaries of the melt pools are apparent by dark lines, and fine equiaxed grains are formed around melt pool boundaries, while columnar grains arose parallel to the building direction towards the center of the melt pool. As shown in OM images in Fig. 3.3, after heat treatment, scan track boundaries are eliminated. The heat-treated 15-5 PH stainless steel samples represent a more homogenized microstructure. Pores and defects seem to be reduced but not completely eliminated compared to the as-built specimen. The examination of SEM micrographs in Fig. 3.4 reveals a large proportion of martensite and ferrite phases with retained austenite.

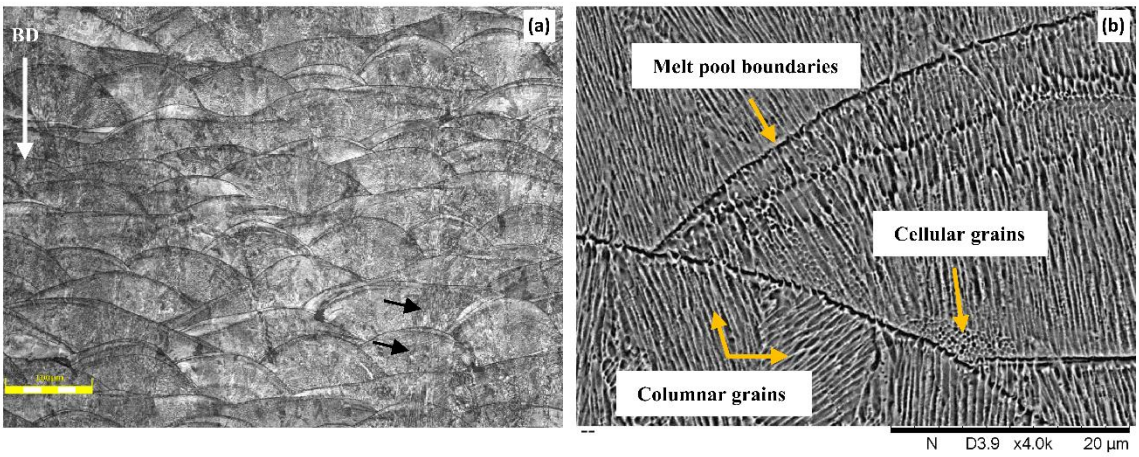

Figure 0.29. Microstructure features of as-built 15-5PH stainless steel: (a) optical microscopy, (b) SEM. The black arrows indicate epitaxial growth.

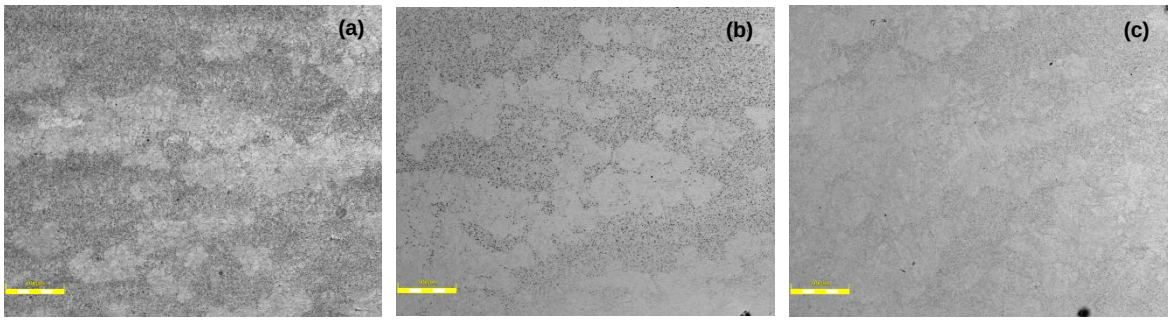

Figure 0.30. Optical micrographs of SLM 15-5PH samples after different heat treatments: (a) S1-600 °C-180 min, (b) S2- 400 °C-120 min and (c) S3- 500 °C-60 min.

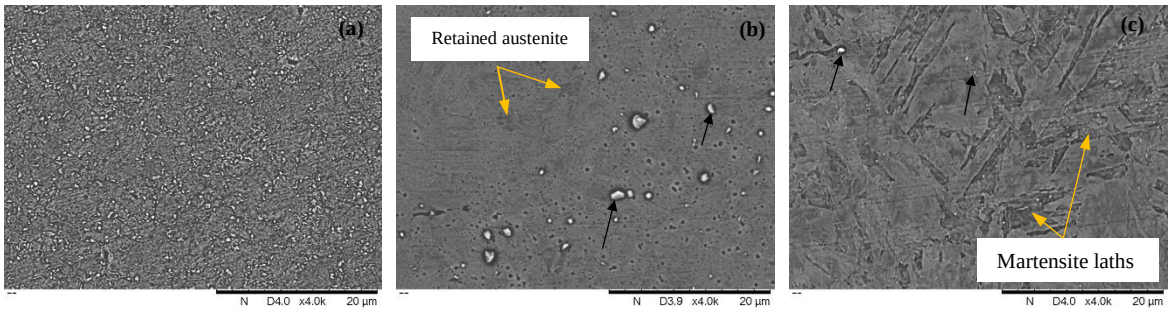

Figure 0.31. SEM micrographs of SLM 15-5PH samples after different heat treatments: (a) S1-600 °C-180 min, (b) S2- 400 °C-120 min and (c) S3- 500 °C-60 min. Black arrows indicate Cu-precipitates.

Although conventional 15-5 PH is a martensitic alloy, the presence of ferrite and retained austenite in the SLM processed 15-5 PH has been widely reported in literature [180, 246]. In fact, the high cooling rate of the SLM process leads to fine grain size with large strain at the grain boundaries, and hence the retention of austenite becomes favorable [192]. The presence of Nitrogen in the initial powder may also promote austenite formation. Additionally, the build chamber temperature during the SLM process may be greater than the martensite finish temperature, leading to incomplete martensitic transformation [239]. Nong et al. [188] declared that the matrix of the as-built 15-5 PH is BCC (martensite and ferrite) with an approximate 10.8% volume fraction of FCC (austenite), which permitted more plastic strain to be accommodated prior to crack initiation and slowed crack propagation but softened the material.

Since SLM process has several common points with welding, basically the fast cooling rate, the phase composition of SLM-fabricated 15-5 PH stainless steel can be effectively predicted using Schaeffler diagram, commonly used for welded stainless steel [247]. The effect of austenite and martensite/ferrite stabilizing elements on the microstructure is quantified using the following equations [180]:

$$Ni_{eq}(wt\%) = \%Ni + 30 \times \%C + 30 \times \%N + 0.5 \times \%Mn \quad (1)$$

$$Cr_{eq}(wt\%) = \%Cr + \%Mo + 1.5 \times \%Si + 0.5 \times \%Nb \quad (2)$$

Based on the chemical composition listed in table 3.3, the calculated values of Ni_{eq} and Cr_{eq} are 15.85 % and 8.85 %, respectively. The point of intersection is used to predict phase constituents of the 15-5 PH microstructure as illustrated in Fig 3.5. This point, marked with an orange dot on the diagram, confirms that our as-built sample's microstructure contains martensite, austenite, and less than 5% of ferrite.

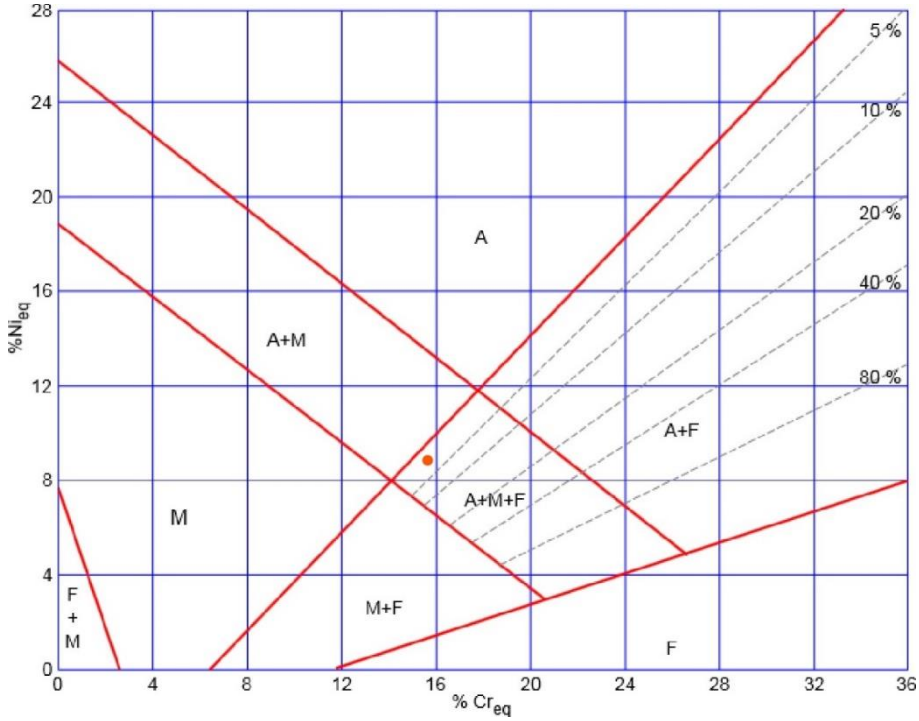

Figure 0.32. Schaeffler diagram [248]. The orange dot represents the phase composition of our as-built sample

After solution treatment of the SLM-fabricated sample, the microstructure transformed into a mostly martensitic matrix with a small amount of residual austenite [197]. During the subsequent quench, martensite laths grow inside the former austenite grains [235]. Upon aging heat treatment, the second phase elements, such as copper, by the diffusion process, are regrouped into clusters and constitute precipitates.

Fig. 3.4a shows the microstructure of Sample No. 3, which was aged at 600 °C for 180 minutes following water-quenching. It indicates a heavily tempered martensitic structure and

abundant Cu-rich particles with different size around the grain boundaries. Fig 3.4b depicts the microstructure of Sample No. 4 that was aged at 400 °C for 120 minutes after being solution-treated and quenched in 6 mass% NaCl solution. The microstructure reveals a higher percentage of austenite compared to as-quenched sample (not presented here). This may be explained by the formation of reverted austenite during the aging treatment as reported by Sarkar et al. [19]. It is also noted that the volume fraction of Cu-precipitates is less than that of sample No. 3 due to the lower aging temperature and aging time. Fig. 3.6 displays the EDS mapping analysis of the second phase precipitates in Sample No. 4. It confirms that these were Cu-enriched particles with varying size (> 100nm). Pasebani et al. [185] reported similar large Cu precipitates non-uniformly distributed in gas-atomized 17-4 PH powder produced by SLM following solutionizing and aging at 482 °C. Fig. 3.4c shows the microstructure of sample No. 8 heat-treated at 500 °C for 60 minutes after quenching in 12 mass% NaCl solution. It reveals less retained austenite and finer Cu-precipitates evenly distributed compared to the two previous samples, which was consistent with the precipitates in traditional 15-5 PH stainless steel after similar aging conditions [249]. Some studies have also reported the formation of carbides and nano-metric oxide inclusions during aging of conventional [187, 235] and additively manufactured 15-5 PH stainless steel [183, 250] that acted as strengthening factors.

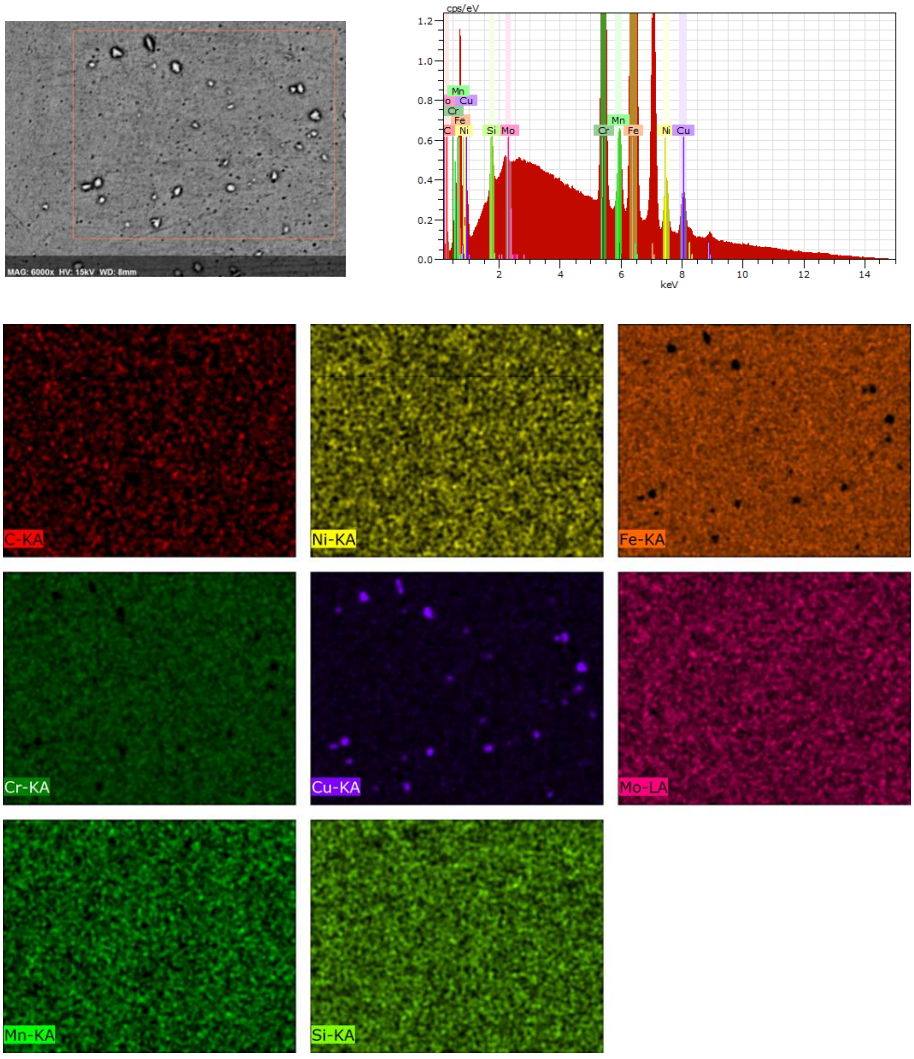

Figure 0.33. EDS mapping of Cu precipitates in Sample N°4 (S 2-400 °C-120 min)

3.2.4.2 Microhardness Results

Microhardness is a significant mechanical property for metallic components, especially when they are used in applications that include friction and contact. Microhardness measurements resulting from the various heat treatment combinations are listed in table 3.4. The hardness values range between 36.3 HRC and 46.5 HRC with 39.5 HRC for the as-built specimen. Considering the orthogonal array combinations, sample No. 8 (S 3, 500 °C, 60 min) exhibited the highest hardness, whereas sample No. 3 exhibited the lowest hardness (S 1, 600 °C, 180 min). The as-quenched samples had the lowest values among all the samples.

These findings show good agreement with literature [19, 28, 183], since our test No. 8 (S 3, 500 °C, 60 min) is comparable to the H900 standard aging treatment, which demonstrated the maximum strength and hardness. Aging at 400 °C brings back hardness to the as-built value after being reduced by solution treatment. Further rise in temperature to 500 °C induces an increase in hardness by ~ 15% compared to the as-built sample and ~24% compared to as-quenched samples. In contrast, after aging at 600 °C, the hardness values decline again. This variation is correlated to the complex microstructural evolution. In fact, the presence of retained and reverted austenite softens the material, while fine Cu-rich precipitates harden it. Primig et al. [237] proved that a significant evolution of 15-5PH chemical composition takes place when aged between 450 °C and 530 °C, leading to a pronounced peak of hardness. Over-aging occurs when the temperature is raised to 600 °C due to the coarsening of copper precipitates [237]. Furthermore, the amount of reverted austenite increases as the heating temperature and duration increase. Consequently, hardness decreases.

Table 0.17.

Microhardness test results

Sample No.	**Factors**			**Response**
	A	**B**	**C**	**H (HRC)**
1	1	400	60	40.0
2	1	500	120	46.3
3	1	600	180	36.8
4	2	400	120	39.5
5	2	500	180	44.2
6	2	600	60	38.1
7	3	400	180	38.9
8	3	500	60	46.5
9	3	600	120	37.1
As-built	-	-	-	39.5
S1-quenched	1	-	-	37.0
S2-quenched	2	-	-	36.3
S3-quenched	3	-	-	36.6

a) Analysis of Variance

ANOVA is a statistical tool that uses the F-test to investigate which design parameters have a significant effect on the target response. In this study, ANOVA was performed to assess the significance of each factor in the quench and aging heat treatment process, namely, quenching solution (A), aging temperature (B), and aging time (C), on the hardness of 15-5 PH stainless steel parts processed by SLM. The analysis presented in table 3.6 is ensured using Minitab 19 statistical analysis software according to the general stepwise method so that only significant factors are kept in the final model. The initial model included independent variables (A, B, C), quadratic variables (A^2, B^2, C^2) and two-way interactions (A × B, A× C, B × C). Statistically significant parameters are determined using the p-value. Comparing p-value with the fixed significance level (α) determines whether the null hypothesis can be rejected or not. The null hypothesis, in this case, states that the effect of studied parameters is not significant on the hardness of 15-5 PH stainless steel produced by SLM. We reject the null hypothesis when the computed p-value is less than the designated significance level. In this study, we used a significance level α = 0.05. The percentage contribution is also a rough but effective guide to the relative importance of each model term [230]. An empirical model for hardness as a function of selected variables was developed by applying the linear regression analysis on the experimental data. The general quadratic equation model is stated by [230]:

$$y = \beta_0 + \sum_{i=1}^{3} \beta_i x_i + \sum_{i=1}^{3} \beta_{ii} x_{ii}^2 + \sum_{i=1}^{2} \sum_{j>1}^{3} \beta_{ij} x_i x_j + \epsilon \qquad (3)$$

Where y represents the hardness, x_i represent the heat treatment parameters, the β's are regression coefficients, and ϵ is the residual error term. According to ANOVA results (table 3.6), hardness is mainly influenced by B^2, B and C variables. It can be observed that aging temperature (B) is the most effective parameter, accounting for 90,1% of the total variability for the quadratic term B^2 and 5,82% for the linear term B. Aging time (C) is less significant, with a contribution of 2,75%. The quenching solution (A) and the remaining

quadratic and interaction terms were omitted from the final model as their p-values were much higher than the significance level $\alpha = 0.05$, meaning that they do not have a significant effect on the hardness.

Table 0.18.

ANOVA for Hardness

Factor	Degree of freedom	Sum of squares	Contribution	Mean Squares	F-value	p-value
B	1	102,191	5,82%	102,191	328,94	0,000
C	1	3,227	2,75%	3,227	10,39	0,023
B^2	1	105,609	90,10%	105,609	339,94	0,000
Error	5	1,553	1,33%	0,311	-	-
Total	8	117,216	100,00%	-	-	-

In order to have a better visual perspective of the impact of each heat treatment parameter on the hardness of SLM-fabricated parts, the main effect plots s are shown in Fig. 3.7. Aging time had a negative effect on hardness. In fact, the decrease of the hardness with prolonged aging time may be ascribed to the coarsening of Cu precipitates and the formation of reverted austenite [184, 251]. The steep variation of mean hardness with respect to aging temperature confirms that this factor is highly significant. It has shown a positive effect between 400°C and 500°C and a negative effect between 500 °C and 600 °C. This variation is in agreement with the chemical and microstructural evolution of 15-5PH stainless steel processed by SLM explained in the previous section. The peak hardness was achieved at 500 °C aging temperature due to the precipitation of fine Cu precipitates uniformly dispersed. Lower aging temperature (400° C) resulted in under-aging characterized by a small volume fraction of Cu precipitates, while higher aging temperature led to over-aging featured by the coarsening of Cu-rich particles and the formation of extensive reverted austenite phase. Both conditions result in a lower hardness compared to the peak value.

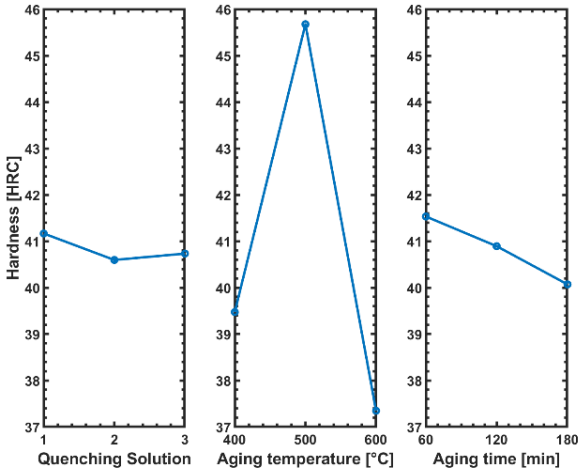

Figure 0.34. Main effect plots

To estimate the hardness of heat-treated SLM parts as a function of the significant factors, a multiple linear regression model was developed using Minitab. The obtained model for predicting hardness is a quadratic model given by equation (4).

$$H = -129.2 + 0.716\,B - 0.01222\,C - 0.000727\,B^2 \quad (4)$$

$For\ 400 < B < 600\ °C\ and\ 60 < C < 180\ min.$

The coefficient of determination R^2 that measures the goodness of fit of the regression model is 98.6%. In other words, the regression model explains 98.6% of the total variation in hardness. The adjusted R^2 (97.88%) and the predicted R^2 (95.72%) are in reasonable agreement, confirming that the predicted model for hardness can be employed. The standard deviation S of the data values around the fitted values is 0,55 meaning that our model describes well the hardness response.

b) Response Surface Model

The ANOVA results led us to the conclusion that aging temperature and aging time are the most influential factors in the heat treatment process that affect the hardness of SLM-fabricated 15-5 PH components. Further investigation into this relationship allows for the

estimation of the optimal set of parameters that provide the highest hardness. For this purpose, Response Surface Method (RSM), a statistical technique for modeling and analysis of such optimization problems, is used. By generating contour plots for response surface analysis, the optimum can be localized with reasonable precision. The response surface contour plot for hardness versus the variation of aging temperature and aging time is presented in Fig. 3.8. The variation of hardness as a function of quenching solution is not considered in the contour plots since ANOVA results show it to be insignificant. Thus, it is taken as a constant parameter at level 2. It can be inferred from this plot that hardness increases with decreasing holding time. The quadratic relationship between aging temperature and hardness is visible through the parabolic curves of the contour plot. The hardness reaches its maximum when the precipitation-hardening temperature ranges between 470 °C and 515 °C approximately and the aging time ranges between 60 and 80 min. Thus, we can consider 490 °C and 70 min as the best set of parameters for precipitation hardening heat treatment.

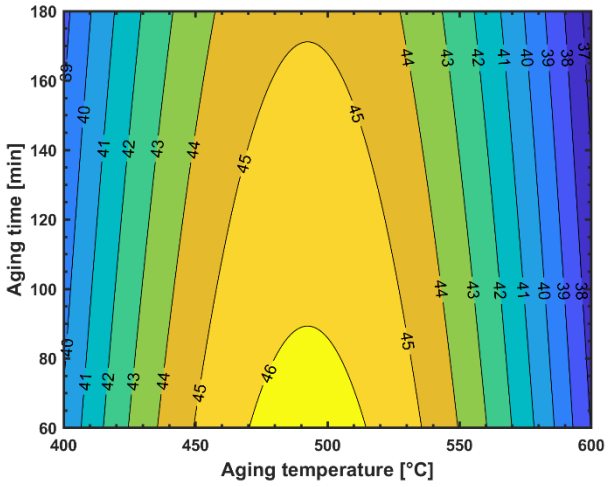

Figure 0.35. Contour plot of hardness versus aging temperature and aging time

c) Tensile properties

Both hardness and tensile strength are important properties of metallic components that are linearly correlated [252]. Achieving maximal hardness implies having the highest tensile strength as well. Therefore, in order to validate the fitted model and assess the mechanical properties of heat-treated 15-5PH stainless steel produced by SLM, tensile tests were conducted on peak-aged and as-built specimens using MTS-810 tensile testing machine. Precipitation hardening was performed at 490 °C for 70 minutes after solution treatment and quenching, to obtain the maximum hardness determined by RSM analysis. Two samples for each testing condition are tested, and the mean values of their tensile properties are summarized in table 3.7. Fig 3.9 illustrates the stress-strain curves. The results of tensile tests indicate that precipitation hardening heat treatment has enhanced the mechanical properties of SLM-fabricated 15-5PH stainless steel. In fact, the yield strength of the heat-treated specimen has increased by approximately 32%, ultimate tensile strength by 26%, and ductility by 89% compared to the as-built specimen. The selected set of parameters enabled the optimal combination of strength, hardness, and ductility to be achieved. This outstanding combination of strength and ductility can be ascribed to (1) grain refinement, (2) high dislocation density, (3) high volume fraction of fine Cu-rich precipitates, and (4) transformation-induced plasticity during tensile deformation due to presence of retained austenite [184, 250, 253].

Table 0.19.

Average tensile properties of 15-5PH stainless steel under as-built and optimal heat-treated conditions

Test	**Yield Strength (MPa)**	**Tensile Strength (MPa)**	**Elongation at break %**
As-built	1190 ± 10	1335 ± 35	4,4 ±0.165
Heat treated	1576 ± 11.5	1692 ± 16	8,3 ± 1.01

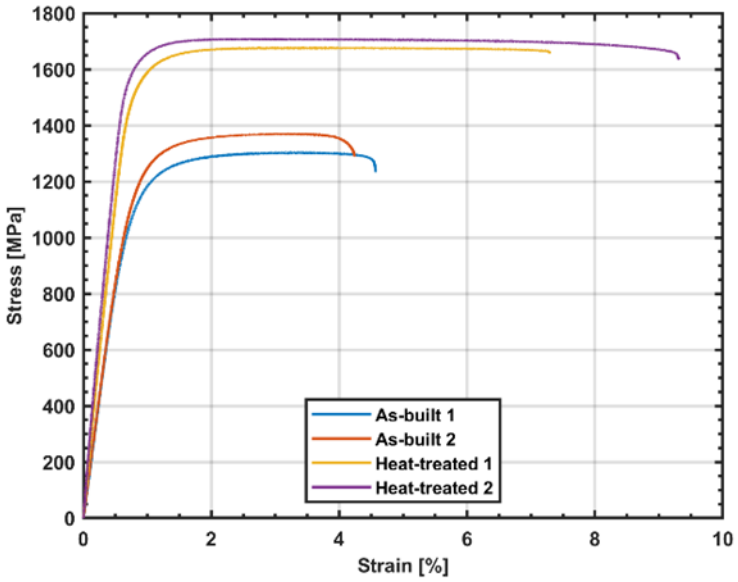

Figure 0.36. Stress-strain curves of as-built and peak-aged 15-5 PH stainless steel

3.2.5 Conclusion

This work investigates the effect of heat treatment parameters on the hardness and microstructure of selective laser-melted 15-5 PH stainless steel. The observation of 15-5PH SS microstructure before and after heat treatment revealed the presence of ferrite, retained/reverted austenite, and copper precipitates. The experimental approach using Taguchi design and Analysis of Variance (ANOVA) allowed a deep understanding of the influence of quenching solution, aging temperature, and aging time on the hardness of samples. The findings reveal that hardness is mainly affected by aging temperature and less by aging time. Predictive regression and RSM models for hardness were developed using the aforementioned heat treatment parameters as independent variables. The optimal set of parameters was then selected and validated by tensile tests. The validation samples were solution treated at 1020°C for 15 min, water-quenched and aged at 490°C for 70 min. The resulting mechanical properties are very promising, with higher hardness (up to 46 HRC), higher mechanical strength (ultimate tensile strength up to 1692 MPa), and improved

ductility (elongation at break up to 8%) compared to the as-built samples. This can be attributed high volume fraction of fine Cu-rich precipitates and transformation-induced plasticity during tensile deformation due to presence of retained austenite. The results of the present study can be used to tailor mechanical properties of the SLM-fabricated 15-5 PH stainless steel by tuning post-process heat treatment parameters. In future work, performing additional tests outside the variation range of parameters presented in this study is needed to improve and confirm the validity of the predictive model. More in-depth analyzes, using more advanced techniques such as high-resolution transmission electron microscopy or atom probe tomography, are also necessary to properly characterize the unique microstructure of SLM-processed 15-5 PH stainless steel and investigate the process-structure-property relationship deeply.

CONCLUSION GÉNÉRALE

Les aciers inoxydables sont très demandés dans presque tous les secteurs industriels en raison de leur chaîne d'approvisionnement étendue, de leur nature non réactive et de leur coût relativement faible. Par conséquent, leur utilisation dans la fabrication additive fait l'objet d'une attention particulière. Le travail de recherche présenté dans ce mémoire a pour but de comprendre, optimiser et prédire les performances des aciers inoxydables fabriqués par fusion sélective au laser, en vue d'étendre leur acceptation en industrie. Pour ce faire, cet objectif est réalisé sur trois phases complémentaires qui sont présentées sous forme d'articles. La première phase faisait l'objet d'une revue de littérature approfondie qui vise à fournir une meilleure compréhension du procédé étudié et de son influence sur la microstructure et les propriétés mécaniques des aciers inoxydables à la lumière des travaux existants. La recension de la littérature a permis d'identifier les lacunes de recherche et les pistes non exploitées. Parmi ces lacunes, l'absence de modèles prédictifs qui décrivent explicitement les corrélations entre les paramètres du procédé et les propriétés résultantes. La seconde phase avait donc pour objectif d'évaluer et prédire systématiquement les effets des paramètres de fusion sélective au laser et leurs interactions sur les propriétés physiques et mécaniques de l'acier 316L. La dernière phase vise à aller encore plus loin dans l'optimisation des performances des aciers inoxydables fabriqués par SLM en agissant sur les paramètres de post-traitement thermique. Elle a pour but de déterminer la relation entre ces paramètres et la microdureté de l'acier inoxydable 15-5PH.

La première phase de ce travail a permis d'avoir une idée détaillée sur les caractéristiques microstructurales et mécaniques des différentes nuances d'aciers fabriquées par SLM. Cette étude a mis en évidence la capacité du procédé SLM à produire des pièces mécaniques en acier inoxydable avec des performances satisfaisantes qui peuvent dépasser celles des pièces fabriquées par des techniques conventionnelles. La résistance à la corrosion,

la dureté, et la résistance mécanique (élastique et à la rupture) sont généralement améliorées grâce à la microstructure hétérogène, les nanoparticules, et la densité de dislocation importante. Cependant, la ductilité et la résistance à la fatigue sont négativement affectées par la présence des différents types de porosités ainsi que par les contraintes résiduelles. De plus, le comportement mécanique des composants fabriqués par SLM est souvent anisotrope. Des stratégies ‘in-situ’ pour minimiser la formation de défauts, réduire les contraintes résiduelles et contrôler l'anisotropie s’avèrent donc essentielles pour la progression du SLM. Pour les aciers inoxydables martensitiques, à durcissement structural et duplex, des changements significatifs sont observés dans la composition de phase de la microstructure construite par SLM par rapport à leur microstructure conventionnelle. Ceci est principalement attribué au refroidissement rapide, qui peut altérer le mode de solidification primaire et rendre les transformations de phase à l'état solide irréalisables ou incomplètes. Dans ce cas, des processus de traitement thermique optimisés sont nécessaires vu que les traitements standards ne sont pas adaptés aux spécificités des aciers inoxydables fabriqués par SLM. De plus, la forte divergence des propriétés des aciers inoxydables produits par SLM, rapportés dans les études existantes, reflète un manque de contrôle sur la microstructure. Enfin, malgré leur popularité dans la fabrication additive, le nombre d'aciers inoxydables couramment imprimés aujourd'hui demeure restreint par rapport à l'immensité des aciers inoxydables actuellement obtenus par les techniques de fabrication traditionnelles.

Dans le but de contribuer à approfondir la compréhension des corrélations entre les paramètres de procédés SLM et les performances des aciers inoxydables et les contrôler, la deuxième phase de ce projet a été consacrée à l’étude des effets des paramètres de procédé sur la densité relative, la rugosité de surface et le comportement mécanique de l'acier inoxydable 316L fabriqué par SLM. La méthode de Taguchi a été utilisée pour la planification expérimentale. Les caractéristiques microstructurales typiquement observées en SLM, y compris les limites des bains de fusion, les joints de grains et la sous-structure cellulaire à l'intérieur des gros grains de l’acier 316L construit par SLM, étaient clairement visibles. Les échantillons présentent des défauts tels que le manque de fusion et les pores de gaz. Globalement, de bons niveaux de densification (99,97%) et d'excellentes propriétés

mécaniques ont été obtenus. L'ANOVA et le RSM ont été utilisés comme outils statistiques pour élucider l'influence des paramètres de processus, à savoir la puissance du laser, la vitesse de balayage, l'espacement des hachures et leurs interactions, sur les variables de réponse ; densité relative, rugosité de surface, dureté, résistance à la traction et allongement. Les niveaux de paramètres ont été fixés autour de la combinaison optimale recommandée par le fabricant. Selon les résultats de l'ANOVA, l'espacement des hachures était principalement le facteur le plus important pour toutes les propriétés. La vitesse de balayage a également eu un effet significatif, en particulier sur les propriétés de traction. Toutes les variables de réponse ont été affectées négativement par l'augmentation de l'espacement des hachures et de la vitesse de balayage. Cela a été attribué à la faible densité d'énergie laser résultant de l'augmentation de l'espacement des hachures et de la vitesse de balayage et, par conséquent, au faible niveau de densification. La puissance laser s'est avérée significative pour la densité relative, la rugosité de surface et l'allongement. L'augmentation de la puissance du laser induit un apport d'énergie élevé capable de fondre correctement la poudre et de réduire la quantité de porosité. Par conséquent, l'état de surface et la ductilité sont améliorés. Les interactions P×v et v×h sont également influents pour la plupart des variables de réponse. Des modèles prédictifs empiriques ont été développés à l'aide d'une régression linéaire multiple, reflétant les corrélations complexes entre les variables de réponse et les paramètres d'entrée. Ces modèles permettent de prédire et d'optimiser les propriétés de l'acier inoxydable 316L traité par SLM avec une bonne précision.

L'optimisation des performances des aciers à durcissement structural fabriqué par SLM est encore plus difficile. Pour y contribuer, la dernière phase de ce travail a porté une attention particulière à l'étude des effets des paramètres de traitement thermique sur la dureté et la microstructure de l'acier inoxydable 15-5 PH produit par fusion sélective. L'observation de la microstructure de l'acier inoxydable 15-5 PH avant et après le traitement thermique a révélé la présence de ferrite, d'austénite résiduelle et de précipités de cuivre au sein de la matrice martensitique. L'approche expérimentale, utilisant la conception de Taguchi et l'analyse de variance (ANOVA), a permis une compréhension approfondie de l'influence de la solution de trempe, de la température de vieillissement et de la durée de vieillissement sur la

microdureté des échantillons. Les résultats révèlent que la dureté est principalement affectée par la température de vieillissement et moins par le temps de vieillissement. Cette approche a permis de développer un modèle de régression prédictif de la microdureté en fonction des paramètres susmentionnés. La combinaison optimale de paramètres a ensuite été sélectionnée par la méthode RSM. La dureté maximale peut être atteinte à la suite d'un durcissement par précipitation à 490 °C pour 70 min. Les propriétés mécaniques résultantes de ce traitement optimal sont très prometteuses, avec une microdureté plus élevée (jusqu'à 46 HRC), une résistance mécanique plus haute (résistance à la traction jusqu'à 1692 MPa) et une ductilité améliorée (allongement à la rupture jusqu'à 8%) par rapport aux échantillons non vieillis. Cela est attribué à une fraction volumique élevée de précipités fins riches en cuivre. Les résultats de la présente étude peuvent être utilisés pour adapter les propriétés mécaniques de l'acier inoxydable 15-5 PH fabriqué par SLM en ajustant les paramètres de post-traitement thermique.

Dans les travaux futurs, la réalisation d'un plus grand nombre de répétitions et des tests de validation en dehors de la plage de variation des paramètres présentés dans cette étude est nécessaire pour améliorer et confirmer la validité des modèles prédictifs. Des techniques d'intelligence artificielle telles que les réseaux neuroniques peuvent être implémentées pour la prédiction et l'optimisation des performances des aciers inoxydables fabriqués par SLM. D'autres paramètres et d'autres performances telles que la corrosion et la résistance à la fatigue peuvent être envisagés, étant donné que ces propriétés sont décisives dans les applications avancées et ne sont pas assez étudié.

RÉFÉRENCES BIBLIOGRAPHIQUES

[1] B. Vayre, F. Vignat, and F. Villeneuve, "Metallic additive manufacturing: State-of-the-art review and prospects," *Mechanics & Industry*, vol. 13, pp. 89-96, 2012, doi: 10.1051/meca/2012003.

[2] C. Zitelli, P. Folgarait, and A. Di Schino, "Laser powder bed fusion of stainless steel grades: a review," *Metals*, vol. 9, no. 7, p. 731, 2019.

[3] T. DebRoy *et al.*, "Additive manufacturing of metallic components–process, structure and properties," *Prog. Mater Sci.*, vol. 92, pp. 112-224, 2018.

[4] A. Katz-Demyanetz, V. V. Popov Jr, A. Kovalevsky, D. Safranchik, and A. Koptioug, "Powder-bed additive manufacturing for aerospace application: Techniques, metallic and metal/ceramic composite materials and trends," *Manuf. Rev.*, vol. 6, 2019.

[5] M. Lodhi, K. Deen, M. Greenlee-Wacker, and W. Haider, "Additively manufactured 316L stainless steel with improved corrosion resistance and biological response for biomedical applications," *Addit. Manuf.*, vol. 27, pp. 8-19, 2019.

[6] M. Peto, E. Ramírez-Cedillo, A. Hernández, and H. R. Siller, "Structural design optimization of knee replacement implants for additive manufacturing," *Procedia Manufacturing*, vol. 34, pp. 574-583, 2019.

[7] R. Leal *et al.*, "Additive manufacturing tooling for the automotive industry," *Int. J. Adv. Manuf. Technol.*, vol. 92, no. 5, pp. 1671-1676, 2017.

[8] W. E. Frazier, "Metal additive manufacturing: a review," *J. Mater. Eng. Perform.*, vol. 23, no. 6, pp. 1917-1928, 2014.

[9] C. Y. Yap *et al.*, "Review of selective laser melting: Materials and applications," *Appl. Phys. Rev.*, vol. 2, no. 4, p. 041101, 2015.

[10] A. Mostafaei *et al.*, "Defects and anomalies in powder bed fusion metal additive manufacturing," *Curr. Opin. Solid State Mater. Sci.*, vol. 26, no. 2, p. 100974, 2022, doi: https://doi.org/10.1016/j.cossms.2021.100974.

[11] I. Yadroitsev and I. Smurov, "Selective laser melting technology: from the single laser melted track stability to 3D parts of complex shape," *Physics Procedia*, vol. 5, pp. 551-560, 2010.

[12] H. Gu, H. Gong, D. Pal, K. Rafi, T. Starr, and B. Stucker, "Influences of energy density on porosity and microstructure of selective laser melted 17-4PH stainless steel," in *2013 International Solid Freeform Fabrication Symposium*, 2013: University of Texas at Austin.

[13] X. Zhao and et al., "Fabrication and Characterization of AISI 420 Stainless Steel Using Selective Laser Melting," (in eng), *Mater. Manuf. Processes*, vol. 30, no. 11, p. 1283, 2015.

[14] M. Ghayoor, K. Lee, Y. He, C.-h. Chang, B. K. Paul, and S. Pasebani, "Selective laser melting of 304L stainless steel: Role of volumetric energy density on the microstructure, texture and mechanical properties," *Addit. Manuf.*, vol. 32, p. 101011, 2020, doi: https://doi.org/10.1016/j.addma.2019.101011.

[15] Z. Sun, X. Tan, S. B. Tor, and C. K. Chua, "Simultaneously enhanced strength and ductility for 3D-printed stainless steel 316L by selective laser melting," *NPG Asia Materials*, Article vol. 10, no. 4, pp. 127-136, 2018, doi: 10.1038/s41427-018-0018-5.

[16] S. Pal, H. R. Tiyyagura, I. Drstvenšek, and C. S. Kumar, "The Effect of Post-processing and Machining Process Parameters on Properties of Stainless Steel PH1 Product Produced by Direct Metal Laser Sintering," *Procedia Eng.*, vol. 149, pp. 359-365, 2016, doi: https://doi.org/10.1016/j.proeng.2016.06.679.

[17] E. Tascioglu, Y. Karabulut, and Y. Kaynak, "Influence of heat treatment temperature on the microstructural, mechanical, and wear behavior of 316L stainless steel fabricated by laser powder bed additive manufacturing," *Int. J. Adv. Manuf. Technol.*, Article vol. 107, no. 5-6, pp. 1947-1956, 2020, doi: 10.1007/s00170-020-04972-0.

[18] A. Yadollahi, N. Shamsaei, S. M. Thompson, A. Elwany, and L. Bian, "Effects of building orientation and heat treatment on fatigue behavior of selective laser melted 17-4 PH stainless steel," *Int. J. Fatigue*, vol. 94, pp. 218-235, 2017, doi: https://doi.org/10.1016/j.ijfatigue.2016.03.014.

[19] S. Sarkar, S. Mukherjee, C. S. Kumar, and A. Kumar Nath, "Effects of heat treatment on microstructure, mechanical and corrosion properties of 15-5 PH stainless steel parts built by selective laser melting process," *J. Manuf. process.*, vol. 50, pp. 279-294, 2020, doi: https://doi.org/10.1016/j.jmapro.2019.12.048.

[20] K. Saeidi, "Stainless steels fabricated by laser melting: Scaled-down structural hierarchies and microstructural heterogeneities," Department of Materials and Environmental Chemistry (MMK), Stockholm University, 2016.

[21] B. Lv *et al.*, "In-situ formed graded microstructure and mechanical property of selective laser melted 15–5 PH stainless steel," *Mater. Sci. Eng., A*, vol. 847, p. 143340, 2022, doi: https://doi.org/10.1016/j.msea.2022.143340.

[22] R. Sheshadri *et al.*, "Experimental investigation of selective laser melting parameters for higher surface quality and microhardness properties: taguchi and super ranking concept approaches," *J. Mater. Res. Technol.*, vol. 14, pp. 2586-2600, 2021, doi: https://doi.org/10.1016/j.jmrt.2021.07.144.

[23] N. Read, W. Wang, K. Essa, and M. M. Attallah, "Selective laser melting of AlSi10Mg alloy: Process optimisation and mechanical properties development," *Mater. Des.*, vol. 65, pp. 417-424, 2015, doi: https://doi.org/10.1016/j.matdes.2014.09.044.

[24] G. Miranda *et al.*, "Predictive models for physical and mechanical properties of 316L stainless steel produced by selective laser melting," *Mater. Sci. Eng., A*, Article vol. 657, pp. 43-56, 2016, doi: 10.1016/j.msea.2016.01.028.

[25] H. Z. Jiang *et al.*, "Factor analysis of selective laser melting process parameters with normalised quantities and Taguchi method," *Opt. Laser Technol.*, Article vol. 119, 2019, Art no. 105592, doi: 10.1016/j.optlastec.2019.105592.

[26] L. Facchini, N. Vicente, I. Lonardelli, E. Magalini, P. Robotti, and A. Molinari, "Metastable Austenite in 17-4 Precipitation-Hardening Stainless Steel Produced by Selective Laser Melting," *Adv. Eng. Mater.*, vol. 12, no. 3, pp. 184-188, 2010, doi: 10.1002/adem.200900259.

[27] M. Alnajjar, F. Christien, K. Wolski, and C. Bosch, "Evidence of austenite by-passing in a stainless steel obtained from laser melting additive manufacturing," *Addit. Manuf.*, vol. 25, pp. 187-195, 2019, doi: https://doi.org/10.1016/j.addma.2018.11.004.

[28] T. LeBrun, T. Nakamoto, K. Horikawa, and H. Kobayashi, "Effect of retained austenite on subsequent thermal processing and resultant mechanical properties of selective laser melted 17–4 PH stainless steel," *Mater. Des.*, vol. 81, pp. 44-53, 2015, doi: https://doi.org/10.1016/j.matdes.2015.05.026.

[29] Y. Sun, R. J. Hebert, and M. Aindow, "Effect of heat treatments on microstructural evolution of additively manufactured and wrought 17-4PH stainless steel," *Mater. Des.*, vol. 156, pp. 429-440, 2018, doi: https://doi.org/10.1016/j.matdes.2018.07.015.

[30] K. Li *et al.*, "Homogenization timing effect on microstructure and precipitation strengthening of 17–4PH stainless steel fabricated by laser powder bed fusion," *Addit. Manuf.*, vol. 52, p. 102672, 2022, doi: https://doi.org/10.1016/j.addma.2022.102672.

[31] D. Herzog, V. Seyda, E. Wycisk, and C. Emmelmann, "Additive manufacturing of metals," *Acta Mater.*, vol. 117, pp. 371-392, 2016, doi: https://doi.org/10.1016/j.actamat.2016.07.019.

[32] T. J. Horn and O. L. A. Harrysson, "Overview of Current Additive Manufacturing Technologies and Selected Applications," *Sci. Prog.*, vol. 95, no. 3, pp. 255-282, 2012, doi: 10.3184/003685012x13420984463047.

[33] J. Spallek and D. Krause, "Process Types of Customisation and Personalisation in Design for Additive Manufacturing Applied to Vascular Models," *Procedia CIRP*, vol. 50, pp. 281-286, 2016, doi: https://doi.org/10.1016/j.procir.2016.05.022.

[34] J. R. Davis, *Stainless steels*. ASM international, 1994.

[35] M. Yakout, M. A. Elbestawi, and S. C. Veldhuis, "Density and mechanical properties in selective laser melting of Invar 36 and stainless steel 316L," *J. Mater. Process. Technol.*, vol. 266, pp. 397-420, 2019, doi: https://doi.org/10.1016/j.jmatprotec.2018.11.006.

[36] R. Rashid, S. H. Masood, D. Ruan, S. Palanisamy, R. A. Rahman Rashid, and M. Brandt, "Effect of scan strategy on density and metallurgical properties of 17-4PH parts printed by Selective Laser Melting (SLM)," *J. Mater. Process. Technol.*, vol. 249, pp. 502-511, 2017, doi: https://doi.org/10.1016/j.jmatprotec.2017.06.023.

[37] E. Liverani and A. Fortunato, "Additive manufacturing of AISI 420 stainless steel: process validation, defect analysis and mechanical characterization in different process and post-process conditions," *Int. J. Adv. Manuf. Technol.*, vol. 117, no. 3-4, pp. 809-821, 2021, doi: 10.1007/s00170-021-07639-6.

[38] J. J. Beaman, D. L. Bourell, C. C. Seepersad, and D. Kovar, "Additive Manufacturing Review: Early Past to Current Practice," *J. Manuf. Sci. Eng.*, vol. 142, no. 11, 2020, doi: 10.1115/1.4048193.

[39] H. Fayazfar *et al.*, "A critical review of powder-based additive manufacturing of ferrous alloys: Process parameters, microstructure and mechanical properties," *Mater. Des.*, vol. 144, pp. 98-128, 2018.
[40] N. Haghdadi, M. Laleh, M. Moyle, and S. Primig, "Additive manufacturing of steels: a review of achievements and challenges," *Journal of Materials Science*, vol. 56, no. 1, pp. 64-107, 2021, doi: 10.1007/s10853-020-05109-0.
[41] P. Bajaj, A. Hariharan, A. Kini, P. Kürnsteiner, D. Raabe, and E. A. Jägle, "Steels in additive manufacturing: A review of their microstructure and properties," *Mater. Sci. Eng., A*, vol. 772, p. 138633, 2020.
[42] *Standard terminology for additive manufacturing technologies : designation F2792-12a*, A. International, West Conshohocken, PA, 2012.
[43] C. K. Chua and K. F. Leong, *3D Printing and additive manufacturing: Principles and applications (with companion media pack)-of rapid prototyping*. World Scientific Publishing Company, 2014.
[44] P. Deng, M. Karadge, R. B. Rebak, V. K. Gupta, B. C. Prorok, and X. Lou, "The origin and formation of oxygen inclusions in austenitic stainless steels manufactured by laser powder bed fusion," *Addit. Manuf.*, vol. 35, p. 101334, 2020, doi: https://doi.org/10.1016/j.addma.2020.101334.
[45] K. Kempen, B. Vrancken, L. Thijs, S. Buls, J. Van Humbeeck, and J.-P. Kruth, "Lowering thermal gradients in selective laser melting by pre-heating the baseplate," in *Solid Freeform Fabrication Symposium Proceedings*, 2013.
[46] EOS. "DMLS Technology for Metal 3D Printer " https://www.eos.info/en/industrial-3d-printing/additive-manufacturing-how-it-works/dmls-metal-3d-printing (accessed 17 March, 2022).
[47] A. Simchi and H. Pohl, "Effects of laser sintering processing parameters on the microstructure and densification of iron powder," *Mater. Sci. Eng., A*, vol. 359, no. 1, pp. 119-128, 2003, doi: https://doi.org/10.1016/S0921-5093(03)00341-1.
[48] S. Sun, M. Brandt, and M. Easton, "Powder bed fusion processes: An overview," in *Laser additive manufacturing: Materials, design, technologies, and applications*, M. Brandt Ed.: Woodhead Publishing, , 2017, pp. 55-77.
[49] J. P. Oliveira, A. LaLonde, and J. Ma, "Processing parameters in laser powder bed fusion metal additive manufacturing," *Mater. Des.*, vol. 193, p. 108762, 2020.
[50] N. T. Aboulkhair, N. M. Everitt, I. Ashcroft, and C. Tuck, "Reducing porosity in AlSi10Mg parts processed by selective laser melting," *Addit. Manuf.*, vol. 1, pp. 77-86, 2014.
[51] M. Letenneur, A. Kreitcberg, and V. Brailovski, "Optimization of Laser Powder Bed Fusion Processing Using a Combination of Melt Pool Modeling and Design of Experiment Approaches: Density Control," *J. Manuf. Mater. Process.*, vol. 3, no. 1, p. 21, 2019, doi: 10.3390/jmmp3010021.
[52] T. Larimian, M. Kannan, D. Grzesiak, B. AlMangour, and T. Borkar, "Effect of energy density and scanning strategy on densification, microstructure and mechanical properties of 316L stainless steel processed via selective laser melting," *Mater. Sci. Eng., A*, Article vol. 770, 2020, Art no. 138455, doi: 10.1016/j.msea.2019.138455.

[53] X. D. Nong and X. L. Zhou, "Effect of scanning strategy on the microstructure, texture, and mechanical properties of 15-5PH stainless steel processed by selective laser melting," *Mater. Charact.,* vol. 174, p. 111012, 2021, doi: https://doi.org/10.1016/j.matchar.2021.111012.
[54] B. AlMangour, D. Grzesiak, and J.-M. Yang, "Scanning strategies for texture and anisotropy tailoring during selective laser melting of TiC/316L stainless steel nanocomposites," *J. Alloys Compd.,* vol. 728, pp. 424-435, 2017, doi: https://doi.org/10.1016/j.jallcom.2017.08.022.
[55] H. Jia, H. Sun, H. Wang, Y. Wu, and H. Wang, "Scanning strategy in selective laser melting (SLM): a review," *Int. J. Adv. Manuf. Technol.,* vol. 113, no. 9, pp. 2413-2435, 2021, doi: 10.1007/s00170-021-06810-3.
[56] J. H. Tan, W. L. E. Wong, and K. W. Dalgarno, "An overview of powder granulometry on feedstock and part performance in the selective laser melting process," *Addit. Manuf.,* vol. 18, pp. 228-255, 2017.
[57] N. Ahmed, I. Barsoum, G. Haidemenopoulos, and R. A. Al-Rub, "Process parameter selection and optimization of laser powder bed fusion for 316L stainless steel: A review," *J. Manuf. process.,* vol. 75, pp. 415-434, 2022.
[58] C. Silbernagel, L. Gargalis, I. Ashcroft, R. Hague, M. Galea, and P. Dickens, "Electrical resistivity of pure copper processed by medium-powered laser powder bed fusion additive manufacturing for use in electromagnetic applications," *Addit. Manuf.,* vol. 29, p. 100831, 2019, doi: https://doi.org/10.1016/j.addma.2019.100831.
[59] M. Anand and A. K. Das, "Issues in fabrication of 3D components through DMLS Technique: A review," *Opt. Laser Technol.,* vol. 139, p. 106914, 2021, doi: https://doi.org/10.1016/j.optlastec.2021.106914.
[60] Z. Snow, A. R. Nassar, and E. W. Reutzel, "Invited Review Article: Review of the formation and impact of flaws in powder bed fusion additive manufacturing," *Addit. Manuf.,* vol. 36, p. 101457, 2020.
[61] S. M. Yusuf, Y. Chen, R. Boardman, S. Yang, and N. Gao, "Investigation on porosity and microhardness of 316L stainless steel fabricated by selective laser melting," *Metals,* Article vol. 7, no. 2, 2017, Art no. 64, doi: 10.3390/met7020064.
[62] E. Liverani, S. Toschi, L. Ceschini, and A. Fortunato, "Effect of selective laser melting (SLM) process parameters on microstructure and mechanical properties of 316L austenitic stainless steel," *J. Mater. Process. Technol.,* Article vol. 249, pp. 255-263, 2017, doi: 10.1016/j.jmatprotec.2017.05.042.
[63] S. A. Khairallah, A. T. Anderson, A. Rubenchik, and W. E. King, "Laser powder-bed fusion additive manufacturing: Physics of complex melt flow and formation mechanisms of pores, spatter, and denudation zones," *Acta Mater.,* vol. 108, pp. 36-45, 2016, doi: https://doi.org/10.1016/j.actamat.2016.02.014.
[64] Y. Kaynak and O. Kitay, "Porosity, surface quality, microhardness and microstructure of selective laser melted 316L stainless steel resulting from finish machining," *Journal of Manufacturing and Materials Processing,* vol. 2, no. 2, p. 36, 2018.
[65] M. Yakout, M. A. Elbestawi, and S. C. Veldhuis, "A study of thermal expansion coefficients and microstructure during selective laser melting of Invar 36 and

stainless steel 316L," *Addit. Manuf.,* vol. 24, pp. 405-418, 2018, doi: https://doi.org/10.1016/j.addma.2018.09.035.
[66] H. Choo *et al.*, "Effect of laser power on defect, texture, and microstructure of a laser powder bed fusion processed 316L stainless steel," *Mater. Des.,* vol. 164, p. 107534, 2019, doi: https://doi.org/10.1016/j.matdes.2018.12.006.
[67] B. Zhang, Y. Li, and Q. Bai, "Defect formation mechanisms in selective laser melting: a review," *Chinese Journal of Mechanical Engineering,* vol. 30, no. 3, pp. 515-527, 2017.
[68] S. R. Narasimharaju *et al.*, "A comprehensive review on laser powder bed fusion of steels: Processing, microstructure, defects and control methods, mechanical properties, current challenges and future trends," *J. Manuf. process.,* vol. 75, pp. 375-414, 2022, doi: https://doi.org/10.1016/j.jmapro.2021.12.033.
[69] M. Tang, P. C. Pistorius, and J. L. Beuth, "Prediction of lack-of-fusion porosity for powder bed fusion," *Addit. Manuf.,* vol. 14, pp. 39-48, 2017.
[70] W. E. King *et al.*, "Observation of keyhole-mode laser melting in laser powder-bed fusion additive manufacturing," *J. Mater. Process. Technol.,* vol. 214, no. 12, pp. 2915-2925, 2014.
[71] A. A. Martin *et al.*, "Dynamics of pore formation during laser powder bed fusion additive manufacturing," *Nature Communications,* vol. 10, no. 1, p. 1987, 2019, doi: 10.1038/s41467-019-10009-2.
[72] H. Zheng, H. Li, L. Lang, S. Gong, and Y. Ge, "Effects of scan speed on vapor plume behavior and spatter generation in laser powder bed fusion additive manufacturing," *J. Manuf. process.,* vol. 36, pp. 60-67, 2018/12/01/ 2018, doi: https://doi.org/10.1016/j.jmapro.2018.09.011.
[73] M. Laleh *et al.*, "Two and three-dimensional characterisation of localised corrosion affected by lack-of-fusion pores in 316L stainless steel produced by selective laser melting," *Corros. Sci.,* vol. 165, p. 108394, 2020, doi: https://doi.org/10.1016/j.corsci.2019.108394.
[74] S. Liu and H. Guo, "Balling Behavior of Selective Laser Melting (SLM) Magnesium Alloy," *Materials,* vol. 13, no. 16, p. 3632, 2020, doi: 10.3390/ma13163632.
[75] U. Scipioni Bertoli, A. J. Wolfer, M. J. Matthews, J. P. R. Delplanque, and J. M. Schoenung, "On the limitations of Volumetric Energy Density as a design parameter for Selective Laser Melting," *Mater. Des.,* Article vol. 113, pp. 331-340, 2017, doi: 10.1016/j.matdes.2016.10.037.
[76] R. Li, J. Liu, Y. Shi, L. Wang, and W. Jiang, "Balling behavior of stainless steel and nickel powder during selective laser melting process," *Int. J. Adv. Manuf. Technol.,* vol. 59, no. 9, pp. 1025-1035, 2012.
[77] D. Gu and Y. Shen, "Balling phenomena in direct laser sintering of stainless steel powder: Metallurgical mechanisms and control methods," *Mater. Des.,* vol. 30, no. 8, pp. 2903-2910, 2009, doi: https://doi.org/10.1016/j.matdes.2009.01.013.
[78] Y. F. Shen, D. D. Gu, and Y. F. Pan, "Balling process in selective laser sintering 316 stainless steel powder," in *Key Engineering Materials*, 2006, vol. 315-316, pp. 357-360, doi: 10.4028/0-87849-999-7.357.

[79] J. P. Kruth, L. Froyen, J. Van Vaerenbergh, P. Mercelis, M. Rombouts, and B. Lauwers, "Selective laser melting of iron-based powder," *J. Mater. Process. Technol.*, vol. 149, no. 1, pp. 616-622, 2004, doi: https://doi.org/10.1016/j.jmatprotec.2003.11.051.
[80] Y. Liu, Y. Yang, and D. Wang, "A study on the residual stress during selective laser melting (SLM) of metallic powder," *Int. J. Adv. Manuf. Technol.*, Article vol. 87, no. 1-4, pp. 647-656, 2016, doi: 10.1007/s00170-016-8466-y.
[81] C. Li, J. F. Liu, and Y. B. Guo, "Prediction of Residual Stress and Part Distortion in Selective Laser Melting," *Procedia CIRP*, vol. 45, pp. 171-174, 2016, doi: https://doi.org/10.1016/j.procir.2016.02.058.
[82] P. Mercelis and J.-P. Kruth, "Residual stresses in selective laser sintering and selective laser melting," (in English), *Rapid Prototyp. J.*, vol. 12, no. 5, pp. 254-265, 2006, doi: https://doi.org/10.1108/13552540610707013.
[83] M. F. Zaeh and G. Branner, "Investigations on residual stresses and deformations in selective laser melting," *Production Engineering*, vol. 4, no. 1, pp. 35-45, 2010, doi: 10.1007/s11740-009-0192-y.
[84] A. S. Wu, D. W. Brown, M. Kumar, G. F. Gallegos, and W. E. King, "An Experimental Investigation into Additive Manufacturing-Induced Residual Stresses in 316L Stainless Steel," *Metallurgical and Materials Transactions A*, vol. 45, no. 13, pp. 6260-6270, 2014, doi: 10.1007/s11661-014-2549-x.
[85] M. Ghasri-Khouzani *et al.*, "Experimental measurement of residual stress and distortion in additively manufactured stainless steel components with various dimensions," *Mater. Sci. Eng., A*, vol. 707, pp. 689-700, 2017.
[86] J.-P. Kruth, J. Deckers, E. Yasa, and R. Wauthlé, "Assessing and comparing influencing factors of residual stresses in selective laser melting using a novel analysis method," *Proceedings of the institution of mechanical engineers, Part B: Journal of Engineering Manufacture*, vol. 226, no. 6, pp. 980-991, 2012.
[87] C. Li, Z. Y. Liu, X. Y. Fang, and Y. B. Guo, "Residual Stress in Metal Additive Manufacturing," *Procedia CIRP*, vol. 71, pp. 348-353, 2018, doi: https://doi.org/10.1016/j.procir.2018.05.039.
[88] H. Anandan Kumar and S. Kumaraguru, "Distortion in metal additive manufactured parts," in *3D Printing and Additive Manufacturing Technologies*: Springer, 2019, pp. 281-295.
[89] D. Xie *et al.*, "Towards a comprehensive understanding of distortion in additive manufacturing based on assumption of constraining force," *Virtual and Physical Prototyping*, vol. 16, no. sup1, pp. S85-S97, 2021.
[90] F. Neugebauer, N. Keller, V. Ploshikhin, F. Feuerhahn, and H. Köhler, "Multi scale FEM simulation for distortion calculation in additive manufacturing of hardening stainless steel," in *international workshop on thermal forming and welding distortion, Bremen, Germany*, 2014.
[91] B. M. Colosimo and M. Grasso, "On-machine measurement, monitoring and control," in *Precision Metal Additive Manufacturing*: CRC Press, 2020, pp. 347-391.
[92] R. Li, Y. Shi, Z. Wang, L. Wang, J. Liu, and W. Jiang, "Densification behavior of gas and water atomized 316L stainless steel powder during selective laser melting," *Appl.*

Surf. Sci., vol. 256, no. 13, pp. 4350-4356, 2010, doi: https://doi.org/10.1016/j.apsusc.2010.02.030.
[93] A. Mostafaei *et al.*, "Defects and anomalies in powder bed fusion metal additive manufacturing," *Curr. Opin. Solid State Mater. Sci.,* vol. 26, no. 2, p. 100974, 2022.
[94] S. Waqar, K. Guo, and J. Sun, "Evolution of residual stress behavior in selective laser melting (SLM) of 316L stainless steel through preheating and in-situ re-scanning techniques," *Opt. Laser Technol.,* vol. 149, p. 107806, 2022, doi: https://doi.org/10.1016/j.optlastec.2021.107806.
[95] M. Shiomi, K. Osakada, K. Nakamura, T. Yamashita, and F. Abe, "Residual Stress within Metallic Model Made by Selective Laser Melting Process," *CIRP Annals,* vol. 53, no. 1, pp. 195-198, 2004, doi: https://doi.org/10.1016/S0007-8506(07)60677-5.
[96] Y. Liu, Y. Yang, and D. Wang, "A study on the residual stress during selective laser melting (SLM) of metallic powder," *The International Journal of Advanced Manufacturing Technology,* vol. 87, no. 1, pp. 647-656, 2016.
[97] P. Bian, J. Shi, Y. Liu, and Y. Xie, "Influence of laser power and scanning strategy on residual stress distribution in additively manufactured 316L steel," *Opt. Laser Technol.,* vol. 132, p. 106477, 2020.
[98] T. Mukherjee, V. Manvatkar, A. De, and T. DebRoy, "Mitigation of thermal distortion during additive manufacturing," *Scripta Mater.,* vol. 127, pp. 79-83, 2017, doi: https://doi.org/10.1016/j.scriptamat.2016.09.001.
[99] T. Simson, A. Emmel, A. Dwars, and J. Böhm, "Residual stress measurements on AISI 316L samples manufactured by selective laser melting," *Addit. Manuf.,* vol. 17, pp. 183-189, 2017, doi: https://doi.org/10.1016/j.addma.2017.07.007.
[100] B. Blinn, F. Krebs, M. Ley, R. Teutsch, and T. Beck, "Determination of the influence of a stress-relief heat treatment and additively manufactured surface on the fatigue behavior of selectively laser melted AISI 316L by using efficient short-time procedures," *Int. J. Fatigue,* vol. 131, p. 105301, 2020, doi: https://doi.org/10.1016/j.ijfatigue.2019.105301.
[101] A. Riemer, S. Leuders, M. Thöne, H. A. Richard, T. Tröster, and T. Niendorf, "On the fatigue crack growth behavior in 316L stainless steel manufactured by selective laser melting," *Engineering Fracture Mechanics,* Article vol. 120, pp. 15-25, 2014, doi: 10.1016/j.engfracmech.2014.03.008.
[102] L. Mugwagwa, I. Yadroitsava, N. Makoana, and I. Yadroitsev, "Residual stress in laser powder bed fusion," 2021, pp. 245-276.
[103] A. Saha Podder and A. Bhanja, "Applications of stainless steel in automobile industry," in *Advanced Materials Research*, 2013, vol. 794: Trans Tech Publ, pp. 731-740.
[104] N. Baddoo, "Stainless steel in construction: A review of research, applications, challenges and opportunities," *Journal of constructional steel research,* vol. 64, no. 11, pp. 1199-1206, 2008.
[105] P. Kangas and G. C. Chai, "Use of advanced austenitic and duplex stainless steels for applications in Oil & Gas and Process industry," in *Advanced Materials Research*, 2013, vol. 794: Trans Tech Publ, pp. 645-669.

[106] A. Peter, A. H. Lutey, S. Faas, L. Romoli, V. Onuseit, and T. Graf, "Direct laser interference patterning of stainless steel by ultrashort pulses for antibacterial surfaces," *Opt. Laser Technol.*, vol. 123, p. 105954, 2020.
[107] M. F. McGuire, *Stainless steels for design engineers*. Asm International, 2008.
[108] D. Kong *et al.*, "Bio-functional and anti-corrosive 3D printing 316L stainless steel fabricated by selective laser melting," *Mater. Des.*, Article vol. 152, pp. 88-101, 2018, doi: 10.1016/j.matdes.2018.04.058.
[109] S. Anandan *et al.*, "Failure in metal honeycombs manufactured by selective laser melting of 304 L stainless steel under compression," *Virtual and Physical Prototyping*, vol. 14, no. 2, pp. 114-122, 2019.
[110] A. Kumar, Y. Balaji, N. E. Prasad, G. Gouda, and K. Tamilmani, "Indigenous development and airworthiness certification of 15–5 PH precipitation hardenable stainless steel for aircraft applications," *Sadhana*, vol. 38, no. 1, pp. 3-23, 2013.
[111] SANDVIK. "Stainless Steels " https://www.metalpowder.sandvik/en/products/metal-powder-alloys/stainless-steels/ (accessed 17/03/2022, 2022).
[112] K. Abd-Elghany and D. Bourell, "Property evaluation of 304L stainless steel fabricated by selective laser melting," *Rapid Prototyp. J.*, 2012.
[113] H. Yu, J. Yang, J. Yin, Z. Wang, and X. Zeng, "Comparison on mechanical anisotropies of selective laser melted Ti-6Al-4V alloy and 304 stainless steel," *Mater. Sci. Eng., A*, vol. 695, pp. 92-100, 2017, doi: https://doi.org/10.1016/j.msea.2017.04.031.
[114] N. Jeyaprakash, C.-H. Yang, and K. R. Ramkumar, "Correlation of Microstructural Evolution with Mechanical and Tribological Behaviour of SS 304 Specimens Developed Through SLM Technique," *Met. Mater. Int.*, vol. 27, no. 12, pp. 5179-5190, 2021, doi: 10.1007/s12540-020-00933-0.
[115] B. Zhang, L. Dembinski, and C. Coddet, "The study of the laser parameters and environment variables effect on mechanical properties of high compact parts elaborated by selective laser melting 316L powder," *Mater. Sci. Eng., A*, Article vol. 584, pp. 21-31, 2013, doi: 10.1016/j.msea.2013.06.055.
[116] C. Qiu, M. A. Kindi, A. S. Aladawi, and I. A. Hatmi, "A comprehensive study on microstructure and tensile behaviour of a selectively laser melted stainless steel," *Scientific Reports*, Article vol. 8, no. 1, 2018, Art no. 7785, doi: 10.1038/s41598-018-26136-7.
[117] D. Wang, C. Song, Y. Yang, and Y. Bai, "Investigation of crystal growth mechanism during selective laser melting and mechanical property characterization of 316L stainless steel parts," *Mater. Des.*, Article vol. 100, pp. 291-299, 2016, doi: 10.1016/j.matdes.2016.03.111.
[118] N. Diaz Vallejo, C. Lucas, N. Ayers, K. Graydon, H. Hyer, and Y. Sohn, "Process Optimization and Microstructure Analysis to Understand Laser Powder Bed Fusion of 316L Stainless Steel," *Metals*, vol. 11, no. 5, p. 832, 2021.
[119] Y. Zhong, L. Liu, S. Wikman, D. Cui, and Z. Shen, "Intragranular cellular segregation network structure strengthening 316L stainless steel prepared by selective laser melting," *J. Nucl. Mater.*, vol. 470, pp. 170-178, 2016/03/01/ 2016, doi: https://doi.org/10.1016/j.jnucmat.2015.12.034.

[120] T. Kurzynowski, K. Gruber, W. Stopyra, B. Kuźnicka, and E. Chlebus, "Correlation between process parameters, microstructure and properties of 316 L stainless steel processed by selective laser melting," *Mater. Sci. Eng., A*, vol. 718, pp. 64-73, 2018.
[121] Z. Sun, X. Tan, S. B. Tor, and W. Y. Yeong, "Selective laser melting of stainless steel 316L with low porosity and high build rates," *Mater. Des.*, Article vol. 104, pp. 197-204, 2016, doi: 10.1016/j.matdes.2016.05.035.
[122] J. Hou, W. Chen, Z. Chen, K. Zhang, and A. Huang, "Microstructure, tensile properties and mechanical anisotropy of selective laser melted 304L stainless steel," *Mater. Sci. Technol.*, vol. 48, pp. 63-71, 2020, doi: https://doi.org/10.1016/j.jmst.2020.01.011.
[123] Z. Zhu *et al.*, "Enhanced strength–ductility synergy and transformation-induced plasticity of the selective laser melting fabricated 304L stainless steel," *Addit. Manuf.*, vol. 35, p. 101300, 2020, doi: https://doi.org/10.1016/j.addma.2020.101300.
[124] S. Astafurov and E. Astafurova, "Phase composition of austenitic stainless steels in additive manufacturing: A review," *Metals*, vol. 11, no. 7, p. 1052, 2021.
[125] J. W. Fu and Y. S. Yang, "Origin of the lathy ferrite in AISI 304 stainless steel during directional solidification," *J. Alloys Compd.*, vol. 580, pp. 191-194, 2013, doi: https://doi.org/10.1016/j.jallcom.2013.05.107.
[126] K. Saeidi, X. Gao, Y. Zhong, and Z. J. Shen, "Hardened austenite steel with columnar sub-grain structure formed by laser melting," *Mater. Sci. Eng., A*, vol. 625, pp. 221-229, 2015, doi: https://doi.org/10.1016/j.msea.2014.12.018.
[127] A. Röttger *et al.*, "Microstructure and mechanical properties of 316L austenitic stainless steel processed by different SLM devices," *Int. J. Adv. Manuf. Technol.*, Article vol. 108, no. 3, pp. 769-783, 2020, doi: 10.1007/s00170-020-05371-1.
[128] Y. M. Wang *et al.*, "Additively manufactured hierarchical stainless steels with high strength and ductility," *Nature materials*, vol. 17, no. 1, pp. 63-71, 2018.
[129] W. M. Tucho, V. H. Lysne, H. Austbø, A. Sjolyst-Kverneland, and V. Hansen, "Investigation of effects of process parameters on microstructure and hardness of SLM manufactured SS316L," *J. Alloys Compd.*, Article vol. 740, pp. 910-925, 2018, doi: 10.1016/j.jallcom.2018.01.098.
[130] A. Leicht, M. Rashidi, U. Klement, and E. Hryha, "Effect of process parameters on the microstructure, tensile strength and productivity of 316L parts produced by laser powder bed fusion," *Mater. Charact.*, vol. 159, p. 110016, 2020, doi: https://doi.org/10.1016/j.matchar.2019.110016.
[131] F. Yan, W. Xiong, and E. J. Faierson, "Grain structure control of additively manufactured metallic materials," *Materials*, vol. 10, no. 11, p. 1260, 2017.
[132] M. S. Pham, B. Dovgyy, and P. A. Hooper, "Twinning induced plasticity in austenitic stainless steel 316L made by additive manufacturing," *Mater. Sci. Eng., A*, vol. 704, pp. 102-111, 2017, doi: https://doi.org/10.1016/j.msea.2017.07.082.
[133] P. Krakhmalev *et al.*, "Microstructure, Solidification Texture, and Thermal Stability of 316 L Stainless Steel Manufactured by Laser Powder Bed Fusion," *Metals*, vol. 8, no. 8, p. 643, 2018, doi: 10.3390/met8080643.
[134] H.-Z. Jiang *et al.*, "Effect of Process Parameters on Defects, Melt Pool Shape, Microstructure, and Tensile Behavior of 316L Stainless Steel Produced by Selective

Laser Melting," *Acta Metallurgica Sinica (English Letters),* vol. 34, no. 4, pp. 495-510, 2021, doi: 10.1007/s40195-020-01143-8.

[135] M. L. Montero-Sistiaga, M. Godino-Martinez, K. Boschmans, J.-P. Kruth, J. Van Humbeeck, and K. Vanmeensel, "Microstructure evolution of 316L produced by HP-SLM (high power selective laser melting)," *Addit. Manuf.,* vol. 23, pp. 402-410, 2018, doi: 10.1016/j.addma.2018.08.028.

[136] T. Niendorf, S. Leuders, A. Riemer, H. A. Richard, T. Tröster, and D. Schwarze, "Highly Anisotropic Steel Processed by Selective Laser Melting," *Metallurgical and Materials Transactions B,* vol. 44, no. 4, pp. 794-796, 2013, doi: 10.1007/s11663-013-9875-z.

[137] R. Casati, J. Lemke, and M. Vedani, "Microstructure and Fracture Behavior of 316L Austenitic Stainless Steel Produced by Selective Laser Melting," *Mater. Sci. Technol.,* vol. 32, no. 8, pp. 738-744, 2016, doi: https://doi.org/10.1016/j.jmst.2016.06.016.

[138] J. Liu and A. C. To, "Quantitative texture prediction of epitaxial columnar grains in additive manufacturing using selective laser melting," *Addit. Manuf.,* vol. 16, pp. 58-64, 2017, doi: https://doi.org/10.1016/j.addma.2017.05.005.

[139] J. J. Marattukalam *et al.,* "The effect of laser scanning strategies on texture, mechanical properties, and site-specific grain orientation in selective laser melted 316L SS," *Mater. Des.,* vol. 193, p. 108852, 2020, doi: https://doi.org/10.1016/j.matdes.2020.108852.

[140] S.-H. Sun, T. Ishimoto, K. Hagihara, Y. Tsutsumi, T. Hanawa, and T. Nakano, "Excellent mechanical and corrosion properties of austenitic stainless steel with a unique crystallographic lamellar microstructure via selective laser melting," *Scripta Mater.,* vol. 159, pp. 89-93, 2019, doi: https://doi.org/10.1016/j.scriptamat.2018.09.017.

[141] S. Bahl, S. Mishra, K. U. Yazar, I. R. Kola, K. Chatterjee, and S. Suwas, "Non-equilibrium microstructure, crystallographic texture and morphological texture synergistically result in unusual mechanical properties of 3D printed 316L stainless steel," *Addit. Manuf.,* vol. 28, pp. 65-77, 2019, doi: https://doi.org/10.1016/j.addma.2019.04.016.

[142] K. Saeidi, X. Gao, F. Lofaj, L. Kvetková, and Z. J. Shen, "Transformation of austenite to duplex austenite-ferrite assembly in annealed stainless steel 316L consolidated by laser melting," *J. Alloys Compd.,* vol. 633, pp. 463-469, 2015, doi: https://doi.org/10.1016/j.jallcom.2015.01.249.

[143] D. Kong *et al.,* "Heat treatment effect on the microstructure and corrosion behavior of 316L stainless steel fabricated by selective laser melting for proton exchange membrane fuel cells," *Electrochim. Acta,* Article vol. 276, pp. 293-303, 2018, doi: 10.1016/j.electacta.2018.04.188.

[144] M. Montero Sistiaga, S. Nardone, C. Hautfenne, and J. Van Humbeeck, "Effect of heat treatment of 316L stainless steel produced by selective laser melting (SLM)," in *Proceedings of the 27th Annual International Solid Freeform Fabrication Symposium-An Additive Manufacturing Conference*, 2016: Solid Freeform Fabrication, pp. 558-565.

[145] E. Liverani, A. H. Lutey, A. Ascari, and A. Fortunato, "The effects of hot isostatic pressing (HIP) and solubilization heat treatment on the density, mechanical properties, and microstructure of austenitic stainless steel parts produced by selective laser melting (SLM)," *Int. J. Adv. Manuf. Technol.,* vol. 107, no. 1, pp. 109-122, 2020.
[146] H. D. Carlton, A. Haboub, G. F. Gallegos, D. Y. Parkinson, and A. A. MacDowell, "Damage evolution and failure mechanisms in additively manufactured stainless steel," *Mater. Sci. Eng., A,* vol. 651, pp. 406-414, 2016, doi: https://doi.org/10.1016/j.msea.2015.10.073.
[147] I. Tolosa, F. Garciandía, F. Zubiri, F. Zapirain, and A. Esnaola, "Study of mechanical properties of AISI 316 stainless steel processed by "selective laser melting", following different manufacturing strategies," *Int. J. Adv. Manuf. Technol.,* vol. 51, no. 5, pp. 639-647, 2010.
[148] K. Guan, Z. Wang, M. Gao, X. Li, and X. Zeng, "Effects of processing parameters on tensile properties of selective laser melted 304 stainless steel," *Mater. Des.,* vol. 50, pp. 581-586, 2013.
[149] Q. B. Nguyen, Z. Zhu, F. L. Ng, B. W. Chua, S. M. L. Nai, and J. Wei, "High mechanical strengths and ductility of stainless steel 304L fabricated using selective laser melting," *Mater. Sci. Technol.,* vol. 35, no. 2, pp. 388-394, 2019, doi: https://doi.org/10.1016/j.jmst.2018.10.013.
[150] H. H. Alsalla, C. Smith, and L. Hao, "Effect of build orientation on the surface quality, microstructure and mechanical properties of selective laser melting 316L stainless steel," *Rapid Prototyp. J.,* Article vol. 24, no. 1, pp. 9-17, 2018, doi: 10.1108/RPJ-04-2016-0068.
[151] L. Hitzler, J. Hirsch, B. Heine, M. Merkel, W. Hall, and A. Öchsner, "On the anisotropic mechanical properties of selective laser-melted stainless steel," *Materials,* Article vol. 10, no. 10, 2017, Art no. 1136, doi: 10.3390/ma10101136.
[152] J. Suryawanshi, K. G. Prashanth, and U. Ramamurty, "Mechanical behavior of selective laser melted 316L stainless steel," *Mater. Sci. Eng., A,* Article vol. 696, pp. 113-121, 2017, doi: 10.1016/j.msea.2017.04.058.
[153] *ASTM A240/A240M-11 Standard Specification for Chromium and Chromium-Nickel Stainless Steel Plate, Sheet, and Strip for Pressure Vessels and for General Applications*, West Conshohocken, PA, 2011.
[154] E. Polatidis, J. Čapek, A. Arabi-Hashemi, C. Leinenbach, and M. Strobl, "High ductility and transformation-induced-plasticity in metastable stainless steel processed by selective laser melting with low power," *Scripta Mater.,* vol. 176, pp. 53-57, 2020, doi: https://doi.org/10.1016/j.scriptamat.2019.09.035.
[155] J. A. Cherry, H. M. Davies, S. Mehmood, N. P. Lavery, S. G. R. Brown, and J. Sienz, "Investigation into the effect of process parameters on microstructural and physical properties of 316L stainless steel parts by selective laser melting," *Int. J. Adv. Manuf. Technol.,* Article vol. 76, no. 5-8, pp. 869-879, 2015, doi: 10.1007/s00170-014-6297-2.
[156] J. Kluczyński *et al.,* "Comparison of different heat treatment processes of selective laser melted 316L steel based on analysis of mechanical properties," *Materials,* vol. 13, no. 17, p. 3805, 2020.

[157] O. O. Salman, C. Gammer, A. K. Chaubey, J. Eckert, and S. Scudino, "Effect of heat treatment on microstructure and mechanical properties of 316L steel synthesized by selective laser melting," *Mater. Sci. Eng., A*, vol. 748, pp. 205-212, 2019, doi: https://doi.org/10.1016/j.msea.2019.01.110.
[158] J. J. Lewandowski and M. Seifi, "Metal Additive Manufacturing: A Review of Mechanical Properties," *Annual Review of Materials Research*, vol. 46, no. 1, pp. 151-186, 2016, doi: 10.1146/annurev-matsci-070115-032024.
[159] T. M. Mower and M. J. Long, "Mechanical behavior of additive manufactured, powder-bed laser-fused materials," *Mater. Sci. Eng., A*, vol. 651, pp. 198-213, 2016, doi: https://doi.org/10.1016/j.msea.2015.10.068.
[160] A. B. Spierings, T. L. Starr, and K. Wegener, "Fatigue performance of additive manufactured metallic parts," (in English), *Rapid Prototyp. J.*, vol. 19, no. 2, pp. 88-94, 2013, doi: https://doi.org/10.1108/13552541311302932.
[161] M. Zhang *et al.*, "Fatigue and fracture behaviour of laser powder bed fusion stainless steel 316L: Influence of processing parameters," *Mater. Sci. Eng., A*, vol. 703, pp. 251-261, 2017, doi: https://doi.org/10.1016/j.msea.2017.07.071.
[162] H. Zhang *et al.*, "The fatigue performance evaluation of additively manufactured 304L austenitic stainless steels," *Mater. Sci. Eng., A*, vol. 802, p. 140640, 2021, doi: https://doi.org/10.1016/j.msea.2020.140640.
[163] J. W. Pegues, M. D. Roach, and N. Shamsaei, "Additive manufacturing of fatigue resistant austenitic stainless steels by understanding process-structure–property relationships," *Materials Research Letters*, vol. 8, no. 1, pp. 8-15, 2020, doi: 10.1080/21663831.2019.1678202.
[164] J. R. Trelewicz, G. P. Halada, O. K. Donaldson, and G. Manogharan, "Microstructure and Corrosion Resistance of Laser Additively Manufactured 316L Stainless Steel," *JOM*, vol. 68, no. 3, pp. 850-859, 2016, doi: 10.1007/s11837-016-1822-4.
[165] Q. Chao *et al.*, "On the enhanced corrosion resistance of a selective laser melted austenitic stainless steel," *Scripta Mater.*, vol. 141, pp. 94-98, 2017, doi: https://doi.org/10.1016/j.scriptamat.2017.07.037.
[166] J. Stewart and D. E. Williams, "The initiation of pitting corrosion on austenitic stainless steel: on the role and importance of sulphide inclusions," *Corros. Sci.*, vol. 33, no. 3, pp. 457-474, 1992, doi: https://doi.org/10.1016/0010-938X(92)90074-D.
[167] G. Sander *et al.*, "On The Corrosion and Metastable Pitting Characteristics of 316L Stainless Steel Produced by Selective Laser Melting," *J. Electrochem. Soc.*, vol. 164, no. 6, pp. C250-C257, 2017, doi: 10.1149/2.0551706jes.
[168] M. Kazemipour, M. Mohammadi, E. Mfoumou, and A. Nasiri, "Microstructure and corrosion characteristics of selective laser-melted 316L stainless steel: the impact of process-induced porosities," *JOM*, vol. 71, no. 9, pp. 3230-3240, 2019.
[169] Y. Sun, A. Moroz, and K. Alrbaey, "Sliding wear characteristics and corrosion behaviour of selective laser melted 316L stainless steel," *J. Mater. Eng. Perform.*, vol. 23, no. 2, pp. 518-526, 2014.
[170] M. Laleh *et al.*, "On the unusual intergranular corrosion resistance of 316L stainless steel additively manufactured by selective laser melting," *Corros. Sci.*, vol. 161, p. 108189, 2019, doi: https://doi.org/10.1016/j.corsci.2019.108189.

[171] W. M. Garrison and M. O. H. Amuda, "Stainless Steels: Martensitic," in *Reference Module in Materials Science and Materials Engineering*: Elsevier, 2017.
[172] A. Candelaria and C. Pinedo, "Influence of the heat treatment on the corrosion resistance of the martensitic stainless steel type AISI 420," *J. Mater. Sci. Lett.*, vol. 22, no. 16, pp. 1151-1153, 2003.
[173] L. Zai *et al.*, "Laser powder bed fusion of precipitation-hardened martensitic stainless steels: a review," *Metals*, vol. 10, no. 2, p. 255, 2020.
[174] I. Kartikeya Sarma, N. Selvraj, and A. Kumar, "A Review on Microstructure and Mechanical Properties of L-PBF 17-4PH and 15-5PH SS," *Recent Advances in Manufacturing Processes and Systems*, pp. 37-53, 2022.
[175] S. D. Nath, H. Irrinki, G. Gupta, M. Kearns, O. Gulsoy, and S. Atre, "Microstructure-property relationships of 420 stainless steel fabricated by laser-powder bed fusion," *Powder Technol.*, vol. 343, pp. 738-746, 2019, doi: https://doi.org/10.1016/j.powtec.2018.11.075.
[176] X. Yan *et al.*, "Study of the microstructure and mechanical performance of C-X stainless steel processed by selective laser melting (SLM)," *Mater. Sci. Eng., A*, vol. 781, p. 139227, 2020, doi: https://doi.org/10.1016/j.msea.2020.139227.
[177] S. Cheruvathur, E. A. Lass, and C. E. Campbell, "Additive manufacturing of 17-4 PH stainless steel: post-processing heat treatment to achieve uniform reproducible microstructure," *JOM*, vol. 68, no. 3, pp. 930-942, 2016.
[178] B. AlMangour and J.-M. Yang, "Understanding the deformation behavior of 17-4 precipitate hardenable stainless steel produced by direct metal laser sintering using micropillar compression and TEM," *Int. J. Adv. Manuf. Technol.*, vol. 90, no. 1, pp. 119-126, 2017.
[179] H. K. Rafi, D. Pal, N. Patil, T. L. Starr, and B. E. Stucker, "Microstructure and mechanical behavior of 17-4 precipitation hardenable steel processed by selective laser melting," *J. Mater. Eng. Perform.*, vol. 23, no. 12, pp. 4421-4428, 2014.
[180] J.-R. Lee *et al.*, "Effects of building direction and heat treatment on the local mechanical properties of direct metal laser sintered 15-5 PH stainless steel," *Mater. Charact.*, vol. 167, p. 110468, 2020, doi: https://doi.org/10.1016/j.matchar.2020.110468.
[181] T.-H. Hsu *et al.*, "Microstructure and property of a selective laser melting process induced oxide dispersion strengthened 17-4 PH stainless steel," *J. Alloys Compd.*, vol. 803, pp. 30-41, 2019, doi: https://doi.org/10.1016/j.jallcom.2019.06.289.
[182] S. Vunnam, A. Saboo, C. Sudbrack, and T. L. Starr, "Effect of powder chemical composition on the as-built microstructure of 17-4 PH stainless steel processed by selective laser melting," *Addit. Manuf.*, vol. 30, p. 100876, 2019, doi: https://doi.org/10.1016/j.addma.2019.100876.
[183] L. F. Kultz Unti *et al.*, "Microstructural characterization of 15-5PH stainless steel processed by laser powder-bed fusion," *Mater. Charact.*, vol. 181, p. 111485, 2021, doi: https://doi.org/10.1016/j.matchar.2021.111485.
[184] S. Sabooni *et al.*, "Laser powder bed fusion of 17–4 PH stainless steel: A comparative study on the effect of heat treatment on the microstructure evolution and mechanical

properties," *Addit. Manuf.,* vol. 46, p. 102176, 2021, doi: https://doi.org/10.1016/j.addma.2021.102176.
[185] S. Pasebani, M. Ghayoor, S. Badwe, H. Irrinki, and S. V. Atre, "Effects of atomizing media and post processing on mechanical properties of 17-4 PH stainless steel manufactured via selective laser melting," *Addit. Manuf.,* vol. 22, pp. 127-137, 2018, doi: https://doi.org/10.1016/j.addma.2018.05.011.
[186] L. E. Murr *et al.*, "Microstructures and Properties of 17-4 PH Stainless Steel Fabricated by Selective Laser Melting," *J. Mater. Res. Technol.,* vol. 1, no. 3, pp. 167-177, 2012, doi: https://doi.org/10.1016/S2238-7854(12)70029-7.
[187] H. R. Habibi Bajguirani, "The effect of ageing upon the microstructure and mechanical properties of type 15-5 PH stainless steel," *Mater. Sci. Eng., A,* vol. 338, no. 1, pp. 142-159, 2002, doi: https://doi.org/10.1016/S0921-5093(02)00062-X.
[188] X. D. Nong, X. L. Zhou, J. H. Li, Y. D. Wang, Y. F. Zhao, and M. Brochu, "Selective laser melting and heat treatment of precipitation hardening stainless steel with a refined microstructure and excellent mechanical properties," *Scripta Mater.,* vol. 178, pp. 7-12, 2020, doi: https://doi.org/10.1016/j.scriptamat.2019.10.040.
[189] S. Sarkar, C. S. Kumar, and A. K. Nath, "Effect of Different Heat Treatments on Mechanical Properties of Laser Sintered Additive Manufactured Parts," *J. Manuf. Sci. Eng.,* vol. 139, no. 11, p. 111010, 2017, doi: 10.1115/1.4037437.
[190] H. K. Rafi, T. L. Starr, and B. E. Stucker, "A comparison of the tensile, fatigue, and fracture behavior of Ti–6Al–4V and 15-5 PH stainless steel parts made by selective laser melting," *Int. J. Adv. Manuf. Technol.,* vol. 69, no. 5, pp. 1299-1309, 2013, doi: 10.1007/s00170-013-5106-7.
[191] *ASTM A564/A564M-19a Standard Specification for Hot-Rolled and Cold-Finished Age-Hardening Stainless Steel Bars and Shapes,* West Conshohocken, 2019.
[192] S. Sarkar, C. S. Kumar, and A. K. Nath, "Effects of heat treatment and build orientations on the fatigue life of selective laser melted 15-5 PH stainless steel," *Mater. Sci. Eng., A,* vol. 755, pp. 235-245, 2019.
[193] P. D. Nezhadfar, K. Anderson-Wedge, S. R. Daniewicz, N. Phan, S. Shao, and N. Shamsaei, "Improved high cycle fatigue performance of additively manufactured 17-4 PH stainless steel via in-process refining micro-/defect-structure," *Addit. Manuf.,* vol. 36, p. 101604, 2020, doi: https://doi.org/10.1016/j.addma.2020.101604.
[194] M. R. Stoudt, R. E. Ricker, E. A. Lass, and L. E. Levine, "Influence of Postbuild Microstructure on the Electrochemical Behavior of Additively Manufactured 17-4 PH Stainless Steel," *JOM,* vol. 69, no. 3, pp. 506-515, 2017, doi: 10.1007/s11837-016-2237-y.
[195] C. Garcia-Cabezon, M. A. Castro-Sastre, A. I. Fernandez-Abia, M. L. Rodriguez-Mendez, and F. Martin-Pedrosa, "Microstructure–Hardness–Corrosion Performance of 17–4 Precipitation Hardening Stainless Steels Processed by Selective Laser Melting in Comparison with Commercial Alloy," *Met. Mater. Int.,* 2022, doi: 10.1007/s12540-021-01155-8.
[196] H. Irrinki *et al.*, "Effects of powder characteristics and processing conditions on the corrosion performance of 17-4 PH stainless steel fabricated by laser-powder bed

fusion," *Prog. Addit. Manuf.,* vol. 3, no. 1-2, pp. 39-49, 2018, doi: 10.1007/s40964-018-0048-0.
[197] L. Wang, C. Dong, C. Man, D. Kong, K. Xiao, and X. Li, "Enhancing the corrosion resistance of selective laser melted 15-5PH martensite stainless steel via heat treatment," *Corros. Sci.,* vol. 166, p. 108427, 2020, doi: https://doi.org/10.1016/j.corsci.2019.108427.
[198] P. Krakhmalev, I. Yadroitsava, G. Fredriksson, and I. Yadroitsev, "In situ heat treatment in selective laser melted martensitic AISI 420 stainless steels," *Mater. Des.,* vol. 87, pp. 380-385, 2015, doi: https://doi.org/10.1016/j.matdes.2015.08.045.
[199] K. Saeidi *et al.,* "Ultra-high strength martensitic 420 stainless steel with high ductility," *Addit. Manuf.,* vol. 29, p. 100803, 2019, doi: https://doi.org/10.1016/j.addma.2019.100803.
[200] M. Liljas, P. Johansson, H. P. Liu, and C. O. A. Olsson, "Development of a lean duplex stainless steel," *Steel Res. Int.,* vol. 79, no. 6, pp. 466-473, 2008.
[201] K. Saeidi, L. Kevetkova, F. Lofaj, and Z. Shen, "Novel ferritic stainless steel formed by laser melting from duplex stainless steel powder with advanced mechanical properties and high ductility," *Mater. Sci. Eng., A,* vol. 665, pp. 59-65, 2016.
[202] H. Tan, Y. Jiang, B. Deng, T. Sun, J. Xu, and J. Li, "Effect of annealing temperature on the pitting corrosion resistance of super duplex stainless steel UNS S32750," *Mater. Charact.,* vol. 60, no. 9, pp. 1049-1054, 2009.
[203] M. Knyazeva and M. Pohl, "Duplex steels: part I: genesis, formation, structure," *Metallography, Microstructure, and Analysis,* vol. 2, no. 2, pp. 113-121, 2013.
[204] F. Hengsbach *et al.,* "Duplex stainless steel fabricated by selective laser melting - Microstructural and mechanical properties," *Mater. Des.,* vol. 133, pp. 136-142, 2017, doi: https://doi.org/10.1016/j.matdes.2017.07.046.
[205] O. Andreau *et al.,* "Texture control of 316L parts by modulation of the melt pool morphology in selective laser melting," *J. Mater. Process. Technol.,* vol. 264, pp. 21-31, 2019.
[206] S. Papula *et al.,* "Selective laser melting of duplex stainless Steel 2205: Effect of post-processing heat treatment on microstructure, mechanical properties, and corrosion resistance," *Materials,* vol. 12, no. 15, p. 2468, 2019.
[207] E. B. Fonseca, A. H. Gabriel, L. C. Araújo, P. L. Santos, K. N. Campo, and E. S. Lopes, "Assessment of laser power and scan speed influence on microstructural features and consolidation of AISI H13 tool steel processed by additive manufacturing," *Addit. Manuf.,* vol. 34, p. 101250, 2020.
[208] M. Mirz, S. Herzog, C. Broeckmann, and A. Kaletsch, "Influence of the L-PBF Process Atmosphere on the Microstructure and Tensile Properties of AISI 318LN Duplex Stainless Steel," *J. Manuf. Mater. Process.,* vol. 6, no. 2, p. 32, 2022.
[209] K. Bertsch, G. M. De Bellefon, B. Kuehl, and D. Thoma, "Origin of dislocation structures in an additively manufactured austenitic stainless steel 316L," *Acta Mater.,* vol. 199, pp. 19-33, 2020.
[210] H. Miura, M. Kobayashi, C. Watanabe, N. Sugiura, and N. Yoshinaga, "Static recrystallization behavior and mechanical properties of heterogeneous nanostructured

duplex phase stainless steel," *Materials transactions,* vol. 61, no. 2, pp. 416-419, 2020.
[211] R. Mondal *et al.*, "Dynamic Recrystallization and Phase-Specific Corrosion Performance in a Super Duplex Stainless Steel," *J. Mater. Eng. Perform.*, vol. 31, no. 2, pp. 1478-1492, 2022.
[212] Y. Yang *et al.*, "Effect of annealing temperature on the pitting corrosion behavior of UNS S82441 duplex stainless steel," *Corrosion,* vol. 69, no. 2, pp. 167-173, 2013.
[213] G. N. Nigon, O. B. Isgor, and S. Pasebani, "Effect of build orientation and annealing on corrosion resistance of additively manufactured duplex stainless steel in 3.5% NaCl," *J. Electrochem. Soc.*, vol. 167, no. 14, p. 141508, 2020.
[214] S. Jeffs *et al.*, "Characterising the high temperature tensile behaviour of laser powder bed fused duplex stainless steel 2205 using the small punch test," *Mater. Charact.*, p. 111953, 2022.
[215] K. Davidson and S. Singamneni, "Selective laser melting of duplex stainless steel powders: an investigation," *Mater. Manuf. Processes,* vol. 31, no. 12, pp. 1543-1555, 2016.
[216] M. Knyazeva and M. Pohl, "Duplex Steels. Part II: Carbides and Nitrides," *Metallography, Microstructure, and Analysis,* vol. 2, no. 5, pp. 343-351, 2013, doi: 10.1007/s13632-013-0088-2.
[217] F. Shang *et al.*, "The microstructure, mechanical properties, and corrosion resistance of UNS S32707 hyper-duplex stainless steel processed by selective laser melting," *Metals,* vol. 9, no. 9, p. 1012, 2019.
[218] P. Jiang, C. Zhang, S. Zhang, J. Zhang, J. Chen, and H. Chen, "Additive manufacturing of novel ferritic stainless steel by selective laser melting: Role of laser scanning speed on the formability, microstructure and properties," *Opt. Laser Technol.*, vol. 140, p. 107055, 2021.
[219] E. Vasquez *et al.*, "Elaboration of oxide dispersion strengthened Fe-14Cr stainless steel by selective laser melting," *J. Mater. Process. Technol.*, vol. 267, pp. 403-413, 2019, doi: https://doi.org/10.1016/j.jmatprotec.2018.12.034.
[220] A. Wasilkowska, M. Bartsch, U. Messerschmidt, R. Herzog, and A. Czyrska-Filemonowicz, "Creep mechanisms of ferritic oxide dispersion strengthened alloys," *J. Mater. Process. Technol.*, vol. 133, no. 1, pp. 218-224, 2003, doi: https://doi.org/10.1016/S0924-0136(02)00237-6.
[221] D. Karlsson *et al.*, "Additive manufacturing of the ferritic stainless steel SS441," *Addit. Manuf.*, vol. 36, p. 101580, 2020.
[222] J. C. Walker, K. M. Berggreen, A. R. Jones, and C. J. Sutcliffe, "Fabrication of Fe-Cr-Al Oxide Dispersion Strengthened PM2000 Alloy Using Selective Laser Melting," *Adv. Eng. Mater.*, vol. 11, no. 7, pp. 541-546, 2009, doi: 10.1002/adem.200800407.
[223] T. Boegelein, S. N. Dryepondt, A. Pandey, K. Dawson, and G. J. Tatlock, "Mechanical response and deformation mechanisms of ferritic oxide dispersion strengthened steel structures produced by selective laser melting," *Acta Mater.*, vol. 87, pp. 201-215, 2015, doi: https://doi.org/10.1016/j.actamat.2014.12.047.

[224] M. Brandt, *Laser additive manufacturing : Materials, design, technologies, and applications* (Woodhead publishing series in electronic and optical materials ; 88). Woodhead Publishing, (in English), 2017.
[225] P. Konda Gokuldoss, S. Kolla, and J. Eckert, "Additive manufacturing processes: Selective laser melting, electron beam melting and binder jetting—Selection guidelines," *materials*, vol. 10, no. 6, p. 672, 2017.
[226] Y. Liu, J. Zhang, and Z. Pang, "Numerical and experimental investigation into the subsequent thermal cycling during selective laser melting of multi-layer 316L stainless steel," *Opt. Laser Technol.*, Article vol. 98, pp. 23-32, 2018, doi: 10.1016/j.optlastec.2017.07.034.
[227] L. Cui, S. Jiang, J. Xu, R. L. Peng, R. T. Mousavian, and J. Moverare, "Revealing relationships between microstructure and hardening nature of additively manufactured 316L stainless steel," *Mater. Des.*, vol. 198, p. 109385, 2021, doi: https://doi.org/10.1016/j.matdes.2020.109385.
[228] S. Greco, K. Gutzeit, H. Hotz, B. Kirsch, and J. C. Aurich, "Selective laser melting (SLM) of AISI 316L—impact of laser power, layer thickness, and hatch spacing on roughness, density, and microhardness at constant input energy density," *Int. J. Adv. Manuf. Technol.*, Article vol. 108, no. 5-6, pp. 1551-1562, 2020, doi: 10.1007/s00170-020-05510-8.
[229] W. H. Yang and Y. S. Tarng, "Design optimization of cutting parameters for turning operations based on the Taguchi method," *J. Mater. Process. Technol.*, vol. 84, no. 1, pp. 122-129, 1998, doi: https://doi.org/10.1016/S0924-0136(98)00079-X.
[230] D. Mongomery, "Montgomery: design and analysis of experiments," *John Willy & Sons*, 2017.
[231] D. Wang, Y. Liu, Y. Yang, and D. Xiao, "Theoretical and experimental study on surface roughness of 316L stainless steel metal parts obtained through selective laser melting," *Rapid Prototyp. J.*, 2016.
[232] M. Brandt, "The role of lasers in additive manufacturing," in *Laser additive manufacturing : Materials, design, technologies, and applications*, M. Brandt Ed., (Woodhead publishing series in electronic and optical materials ; 88: Woodhead Publishing,, 2017, pp. 1-18.
[233] "Carpenter Additive, PowderRange 15-5PH datasheet." https://www.carpenteradditive.com/hubfs/Resources/Data%20Sheets/PowderRange_15-5PH_Datasheet.pdf (accessed 05 August, 2022).
[234] A. a. Alafaghani, A. Qattawi, M. S. Jaman, and M. A. Ablat, "Microstructure and mechanical properties of direct metal laser–sintered 15-5PH steel with different solution annealing heat treatments," *Int. J. Adv. Manuf. Technol.*, vol. 105, no. 7, pp. 3499-3520, 2019.
[235] L. Couturier, F. De Geuser, M. Descoins, and A. Deschamps, "Evolution of the microstructure of a 15-5PH martensitic stainless steel during precipitation hardening heat treatment," *Mater. Des.*, vol. 107, pp. 416-425, 2016, doi: https://doi.org/10.1016/j.matdes.2016.06.068.

[236] X.-y. Peng, X.-l. Zhou, X.-z. Hua, Z.-w. Wei, and H.-y. Liu, "Effect of aging on hardening behavior of 15-5 PH stainless steel," *J. Iron Steel Res. Int.*, vol. 22, no. 7, pp. 607-614, 2015.
[237] S. Primig, G. Stechauner, and E. Kozeschnik, "Early Stages of Cu Precipitation in 15-5 PH Maraging Steel Revisited − Part I: Experimental Analysis," *Steel Res. Int.*, vol. 88, no. 1, p. 1600084, 2017, doi: 10.1002/srin.201600084.
[238] V. Anil Kumar, M. Karthikeyan, R. K. Gupta, F. Gino Prakash, and P. Ram Kumar, "Aging behavior in 15-5 PH precipitation hardening martensitic stainless steel," in *Materials Science Forum*, 2012, vol. 710: Trans Tech Publ, pp. 483-488.
[239] K. Coffy, "Microstructure and chemistry evaluation of direct metal laser sintered 15-5 PH stainless steel," 2014.
[240] D. Roberts, Y. Zhang, I. Charit, and J. Zhang, "A comparative study of microstructure and high-temperature mechanical properties of 15-5 PH stainless steel processed via additive manufacturing and traditional manufacturing," *Prog. Addit. Manuf.*, vol. 3, no. 3, pp. 183-190, 2018, doi: 10.1007/s40964-018-0051-5.
[241] A. a. Alafaghani, A. Qattawi, and M. A. G. Castañón, "Effect of manufacturing parameters on the microstructure and mechanical properties of metal laser sintering parts of precipitate hardenable metals," *Int. J. Adv. Manuf. Technol.*, vol. 99, no. 9, pp. 2491-2507, 2018.
[242] L. Wang *et al.*, "Effect of manufacturing parameters on the mechanical and corrosion behavior of selective laser-melted 15-5PH stainless steel," *Steel Res. Int.*, vol. 91, no. 2, p. 1900447, 2020.
[243] E. A. Lass, F. Zhang, and C. E. Campbell, "Nitrogen effects in additively manufactured martensitic stainless steels: Conventional thermal processing and comparison with wrought," *Metall. Mater. Trans. A*, vol. 51, no. 5, pp. 2318-2332, 2020.
[244] O. Agboola *et al.*, "Optimization of heat treatment parameters of medium carbon steel quenched in different media using Taguchi method and grey relational analysis," *Heliyon*, vol. 6, no. 7, p. e04444, 2020.
[245] L. H. P. Zordão, V. A. Oliveira, G. E. Totten, and L. C. Canale, "Quenching power of aqueous salt solution," *Int. J. Heat Mass Transfer*, vol. 140, pp. 807-818, 2019.
[246] V. Contaldi, F. Del Re, B. Palumbo, A. Squillace, P. Corrado, and P. Di Petta, "Mechanical characterisation of stainless steel parts produced by direct metal laser sintering with virgin and reused powder," *Int. J. Adv. Manuf. Technol.*, vol. 105, no. 7, pp. 3337-3351, 2019.
[247] G. Jacob and G. Jacob, *Prediction of solidification phases in Cr-Ni stainless steel alloys manufactured by laser based powder bed fusion process*. US Department of Commerce, National Institute of Standards and Technology, 2018.
[248] Cdang. "Schaeffler diagram: structure of steel according to the nickel and chrome equivalent percentages " Wikimedia Commons, the free media repository. https://commons.wikimedia.org/w/index.php?title=File:Diagramme_schaeffler.svg&oldid=466484688 (accessed.

[249] H. Luo *et al.*, "Influence of the aging time on the microstructure and electrochemical behaviour of a 15-5PH ultra-high strength stainless steel," *Corros. Sci.*, vol. 139, pp. 185-196, 2018, doi: https://doi.org/10.1016/j.corsci.2018.04.032.
[250] H. Chae *et al.*, "Unearthing principal strengthening factors tuning the additive manufactured 15-5 PH stainless steel," *Mater. Charact.*, vol. 184, p. 111645, 2022, doi: https://doi.org/10.1016/j.matchar.2021.111645.
[251] C. Hsiao, C. Chiou, and J. Yang, "Aging reactions in a 17-4 PH stainless steel," *Mater. Chem. Phys.*, vol. 74, no. 2, pp. 134-142, 2002.
[252] E. Pavlina and C. Van Tyne, "Correlation of yield strength and tensile strength with hardness for steels," *J. Mater. Eng. Perform.*, vol. 17, no. 6, pp. 888-893, 2008.
[253] H. Chae *et al.*, "Plastic anisotropy and deformation-induced phase transformation of additive manufactured stainless steel," *Mater. Sci. Eng., A*, vol. 762, p. 138065, 2019, doi: https://doi.org/10.1016/j.msea.2019.138065.